UNIVERSITÉ DE SHERBROOKE
Faculté de génie
Département de génie civil

BEHAVIOUR OF REINFORCED CFFT COLUMNS UNDER AXIAL COMPRESSION LOADING

COMPORTEMENT AXIAL DE COLONNES EN BÉTON ARMÉ RENFORCÉES DE TUBES EN MATÉRIAUX COMPOSITES

Mémoire de maîtrise ès sciences appliquées
Spécialité: génie civil

Asmaa Abd El daim Ibrahim Ahmed

A dissertation submitted in partial fulfillment
of the requirements for the degree of
Master of Science
(Civil Engineering)

Jury: Prof. Radhouane MASMOUDI, Université de Sherbrooke (Directeur de recherche)
Prof. Josée BASTIEN, Université de Laval (Examinateur)
Prof. Richard GAGNÉ, Université de Sherbrooke (Rapporteur)

Sherbrooke (Québec) Canada **January 2016**

ABSTRACT

The construction industry is expressing great demand for innovative and durable structural members such as bridge decks and piers, piling, and poles. Many steel-reinforced concrete structures subjected to de-icing salts and marine environments require extensive and expensive maintenance. Fiber-reinforced polymers (FRPs) have recently gained wide acceptance as a viable construction material for repair, rehabilitation, or new construction of the aging infrastructures particularly those exposed to harsh environment conditions. The promising concept of concrete-filled FRP tube (CFFT) system, that may be further reinforced with steel or FRP bars, has raised great interest amongst researchers in the last decade. The CFFT technique has been used successfully in different concrete structure elements such as pier column and girder for bridges and also as fender piles in marine structures. The FRP tube acts as a stay-in-place structural formwork, a noncorrosive reinforcement for the concrete for flexure and shear, provides confinement to the concrete in compression, and the contained concrete is protected from intrusion of moisture with corrosive agents that could otherwise deteriorate the concrete core. Using FRP bars instead of conventional steel bars in the CFFT columns can provide a step forward to develop a promising totally corrosion-free new structural system. Nonetheless, the axial behaviour of FRP bars as longitudinal reinforcement in compression members has yet to be explored, especially for the CFFT columns.

To date, most of the experimental investigations performed on FRP confined concrete columns have considered short, unreinforced, small-scale concrete cylinders, tested under concentric, monotonic, and axial load. The slenderness ratio, internal longitudinal reinforcement type (steel or FRP bars), and axial cyclic loading effects on the behaviour of FRP confined concrete long columns, however, have received only limited research attention. To address such knowledge gaps, this study aimed at investigating the behaviour of the CFFT long columns internally reinforced with steel or FRP bars tested under monotonic and cyclic axial loading. A total of ten reinforced concrete (RC) and CFFT columns were constructed and tested until failure. All columns had 1900-mm in height and 213-mm in diameter. The investigated parameters were: i) the effect of internal reinforcement type (steel, glass FRP

(GFRP), or carbon FRP (CFRP)) and amount, ii) GFRP tube thicknesses, and iii) nature of loading (i.e. monotonic and cyclic). The effect of the different parameters on the axial behaviour of the tested columns is presented and discussed. The research work presented in this dissertation has resulted in one paper submitted to the *Elsevier Journal of Engineering Structures* (manuscript ID: ENGSTRUCT-D-15-01381) and one accepted conference paper submitted to the *5 th International Structural Specialty Conference* (*CSCE 2016*), London, Ontario, June 1st - 4th, 2016.

The experimental test results showed that the CFFT columns reinforced with GFRP bars exhibited similar responses compared to their counterparts reinforced with steel bars with no significant difference in terms of ultimate axial strength and strain capacities. The GFRP tubes provided significant confinement of the tested specimens attributing to shift the mode of failure from axially dominated material failure to flexural-dominated instability failure. The results also indicated that the plastic strains of the FRP-reinforced CFFT columns was linearly proportional to the envelop unloading strains ($\varepsilon_{un,env}$). The relationship depended little on level of confinement, but strongly on the longitudinal reinforcement amount and type, particularly when $\varepsilon_{un,env} > 0.0035$. On the other hand, an analytical investigation was conducted to examine the validity of the available design provisions for predicting the ultimate load capacity of tested columns. The results of the analysis were compared with the experimental values. It was found that the ACI 440.R1 (2015), CSA S806 (2012), and CSA S6-06 (2010) design provisions provided higher conservative results for the GFRP-reinforced control specimens than that of steel-reinforced specimen. This might be due to neglecting the contribution of the compressive resistance of the GFRP bars to the axial carrying capacity. Furthermore, for FRP-reinforced CFFT columns, the ACI 440.2R (2008), CSA S806 (2012), and CSA S6-06 (2010) provisions results over the experimental results were an average of 1.68±0.31, 1.57±0.18, and 1.72±0.35 with a COV of 18.4%, 11.3%, and 20.5%, respectively. By considering the confinement codes limits, the CSA S806 (2012) showed better correlation for the ultimate carrying capacity based on the average than the CSA S6-06 (2010) and ACI 440.2R (2008), particularly for specimens cast with tube Type B.

Keywords: Columns; FRP; CFFT, Tube; Cyclic loading; Confinement; Slender; and Plastic Strain.

RÉSUMÉ

L'industrie de la construction exprime une grande demande pour les structures innovantes et durables tels que les tabliers de ponts et les quais, les pieux et les poteaux. Plusieurs structures en béton armé sont soumises à des sels de déglaçage et à des environnements marins qui exigent un entretien coûteux. Les polymères renforcés de fibres (PRF) ont récemment été reconnus en tant que matériau de construction viable pour la réparation, la réhabilitation ou la construction de nouvelles infrastructures vieillissantes en particulier celles exposées à des conditions d'environnement sévères. Le concept prometteur du système de tube rempli de béton PRF (CFFT), qui peut être encore renforcé avec de l'acier ou des barres en PRF, a amorcé un grand intérêt parmi les chercheurs durant la dernière décennie. La technique CFFT a été utilisée avec succès dans les différents éléments de structure en béton tels que les colonnes et les poutres de ponts et aussi comme des pieux pour les structures marines. Le tube en PRF agit comme un coffrage structural sur place, un renforcement non corrosif pour le béton en flexion et au cisaillement en utilisant l'orientation des fibres multidirectionnelle, fournit un confinement au béton en compression, et le béton est protégé de toute intrusion d'humidité des agents corrosifs qui, autrement, pourraient détériorer le noyau de béton (ACI 440. R-07 (2007)). L'utilisation des barres de PRF au lieu de barres d'acier conventionnelles dans les colonnes CFFT peut fournir un pas en avant pour développer un nouveau système structurel. Néanmoins, le comportement axial des barres en PRF comme armatures longitudinales dans les membrures en compression n'a pas encore été exploré, en particulier pour les colonnes CFFT.

À ce jour, la plupart des études expérimentales effectuées sur les colonnes en béton confinés de PRF, ont considéré des cylindres en béton, courts, à petite échelle non armés, et testés sous un charge concentrique, monotone, et axiale. Le rapport d'élancement, le renfort longitudinal interne (acier ou barres en PRF), et les effets du chargement axial cyclique sur le comportement des colonnes élancées de béton confinés et en PRF, ont connu une recherche limitée. Pour combler ce manque de connaissance, cette étude vise à étudier le comportement des colonnes élancées CFFT armé en acier ou en barres de PRF testées sous charges axiales monotones et cycliques. Un total de dix colonnes en béton armé (RC) et CFFT été fabriquées

et testées jusqu'à la rupture. Toutes les colonnes ont 1900 mm de hauteur et 213 mm de diamètre. Les paramètres étudiés sont les suivants: i) l'effet de type de renforcement interne et la quantité de renforcement, ii) les épaisseurs de tubes PRV, et iii) le type de chargement (monotone et cyclique). L'effet des variables considérées sur le comportement axial des colonnes testées dans le travail expérimental est présenté et discuté. Le travail de recherche présenté dans cette analyse a fait l'objet d'un article scientifique soumis à *Elsevier Journal of Engineering Structures* (manuscrit ID: ENGSTRUCT-D-15-01381) et un article lors d'une conférence acceptée soumis à la *5ième International Structural Specialty Conference (CSCE 2016)*, London, Ontario, Juin 1er - 4ième, 2016.

Les résultats des essais expérimentaux ont montré que les colonnes CFFT renforcées de barres en PRFV présentaient des réponses similaires par rapport à leurs homologues renforcées avec des barres d'acier sans différence significative en termes de capacité ultime de résistance axiale et de déformation. Les tubes en PRFV fournissent un confinement significatif des échantillons testés attribuant à changer le mode de rupture, c'est-à-dire d'une rupture des matériaux axialement à une rupture d'instabilité en flexion. En outre, l'augmentation de l'épaisseur du tube en PRFV de 2,9 à 6,4 mm améliore les rapports de résistance et de déformation de 25 % et 12 %, respectivement. Les résultats indiquent également que les déformations plastiques des colonnes renforcées de PRF sont linéairement proportionnelles aux enveloppes de tension de déchargement ($\varepsilon_{de,env}$). La relation dépend un peu du niveau de confinement, mais fortement de la quantité et du type de renfort longitudinal, en particulier lorsque $\varepsilon_{de,env} > 0,0035$. D'autre part, une investigation a été menée pour examiner la validité des dispositions de conception disponibles pour prédire la capacité de la charge ultime des colonnes testées. Les résultats de l'analyse ont été comparés avec les valeurs expérimentales. Il a été constaté que les prévisions de l'ACI 440.R1 (2015), CSA S806 (2012), et CSA S6-06 (2010) ont fourni des résultats conservateurs plus élevés pour les échantillons de contrôle en PRFV que celui de l'échantillon d'acier. Cela peut être dû à la négligence de la contribution de la résistance à la compression des barres de PRFV à la capacité de charge axiale. En outre, pour les colonnes de CFFT renforcées de PRF, les prévisions de l'ACI 440.2R (2008), du CSA S806 (2012), et du CSA S6-06 (2010) étaient de 1,68 ± 0,31, 1,57 ± 0,18 et 1,72 ± 0,35 avec un COV de 18,4 %, 11,3%, et 20,5%, respectivement. En considérant les limites des codes de confinement, le code CSA S806 (2012) a révélé les meilleures prévisions pour la capacité de

charge ultime basée sur la moyenne que celui du code CSA S6-06 (2010) et de l'ACI 440.2R (2008), en particulier pour les échantillons réalisés avec des tubes de Type B.

Mots-clés: Colonnes; PRF; CFFT, Tube; Chargement cyclique; Confinement; Élancement; et déformation plastique.

ACKNOWLEDGEMENT

Praise be to Allah Almighty and Peace be upon His Prophet Muhammad.

The author would like to express her profound gratitude and appreciation to her supervisor, Prof. Radhouane MASMOUDI, not only for his support and patience throughout the course of this study but also for giving an opportunity to conduct this research.

The author would like to express her faithful appreciation to Dr. Mohamed HASSAN, postdoctoral researcher, for his technical support and guidance throughout this research program and writing this dissertation. Sincere words of thanks must also go to Prof. Josée BASTIEN, Université de Laval, and Prof. Richard GAGNÉ, Université de Sherbrooke, for their appreciation on this work and valuable comments and suggestions on the dissertation.

Sincere words of thanks must be extended to Dr. Mohamed HAMDY, postdoctoral researcher, for his valuable contribution in fabricating the specimens and Ahmed SOLIMAN, PhD Candidate, for his help in testing the specimens. Thanks are due to the technical staff of the Civil Engineering Department at the Université de Sherbrooke, in particular Mr. Nicolas Simard and Mr. Éric Beaudoin.

The financial support received from the Natural Sciences and Engineering Research Council of Canada (NSERC) and contribution of the Canadian Foundation for Innovation (CFI) for the infrastructure is deeply appreciated. Special thanks to the manufacturer (FRE Composites, QC, Canada) for providing FRP tubes.

The author would like to express her deepest appreciation and thanks to her parents and her sisters for their endless love, support, encouragement, duas, and prayers. The spiritual support of all of them cannot be praised enough. The author is indebted to her father, who sacrificed his life for her family when she was growing up. I have a great believe that he is the real reason of my accomplishments in my life.

Words stand helpless and cannot express my deepest love and appreciation to my husband (Mohamed) for his faithful encouragement, for his endless support and his prominent role in helping me to achieve one of the greatest accomplishments in my life; his selflessness will always be remembered. I cannot present this work without expressing my love to my sweetie son (Omar) and my little baby girl (Aseel), who enlightened my life with their smile; to them this thesis is dedicated.

Asmaa Abdeldaim Ahmed

January 2016

Dedication

To the memory of my father "Abd el daim"

To my mother and sisters

To my dear husband "Mohamed" and my sweetie kids "Omar" and "Aseel"

with all my love and respect

TABLE OF CONTENTS

LIST OF TABLES

LIST OF FIGURES

LIST OF SYMBOLS

SI units are used throughout the study presented herein. Unless otherwise stated, the symbols most frequently used have the following meanings:

Symbol	Definition
Ac	cross-sectional area of concrete in compression member;
A_f	area of FRP external reinforcement;
A_g	gross area of concrete section;
A_s	area of nonprestressed steel reinforcement;
A_f	area of nonprestressed FRP reinforcement;
D	internal diameter of the FRP tubes;
Ec	modulus of elasticity of concrete
Es	steel elastic modulus;
E_f	FRP elastic modulus;
E_{11}	primary modulus of elasticity;
Ex	tubes Young's modulus in the axial direction;
E_{FRPU}	tubes Young's modulus in the hoop direction;
$f_c^{/}$	unconfined cylinder compressive strength of concrete;
$f_{cc}^{/}$	confined concrete compressive strength;
f_{lFRP}	lateral confinement pressure of FRP;
f_{lu}	ultimate lateral confinement stress;
$f_{lu,a}$	actual lateral confinement stress;
$f_{lu,a} / f_{cc}^{'}$	actual confinement ratio;
f_{FRPU}	tubes ultimate strength in the hoop direction;
fx	tubes ultimate strength in the axial direction;
$f_{ul,env}$	envelop unloading stress;

f_{new}	stress where the first reloading path reaches to the point corresponding to the maximum axial strain in the envelop unloading path;
f_t	split cylinder tensile strength of concrete;
f_u	ultimate tensile strength of steel bars;
f_y	yield strength of steel bars;
f_{fu}	ultimate tensile strength of FRP bars;
G_{12}	shear modulus;
K_a	efficiency factor accounts for the geometry of the section, circular, and noncircular;
k_c	factor accounts for the shape of the cross section, which is equal to 1.0 for circular section and 0.4 for square and rectangular section;
k_e	strength reduction factor applied for unexpected eccentricities;
K_ε	strain efficiency factor =0.55;
M	Bending moment;
N	axial compression force;
n_f	modular ratio of elasticity between FRP and concrete = E_f/E_c;
n_s	modular ratio of elasticity between steel and concrete = E_s/E_c;
P_{11}	resultant axial force;
P_m	resultant forces in the matrix;
P_f	resultant forces in the fibers;
P_u	experimental ultimate load;
P_r	factored axial load resistance of the confined columns;
Q_{ij}	denote the reduced stiffness of an orthotropic lamina;
t_{frp}	FRP tubes thickness;
V	volume fraction;
ε_{co}'	corresponding axial strain of unconfined concrete;
$\varepsilon_{h,\,min}$	minimum hoop strain for the tested specimen;
$\varepsilon_{h,\,aver}$	average hoop strain for the tested specimen;
$\varepsilon_{h,\,max}$	maximum hoop strain for the tested specimen;
ε_{fe}	effective strain level in the FRP at failure;

ε_{FRPU}	tubes ultimate tensile strain in the hoop direction;
εx	tubes ultimate tensile strain in the axial direction;
ε_{pl}	plastic strain (is defined as the residual axial strain when the stress unloaded to zero stress of each unloading path);
$\varepsilon_{ul,max}$	maximum axial strain in the envelop unloading path;
ϕ_c	material resistance factor for concrete;
ϕ_s	material resistance factor for steel;
ϕ_{FRP}	material resistance factor for FRP;
$\varepsilon_{un,env}$	envelop unloading strains;
ρ_L	longitudinal reinforcement ratio;
ρ_s	Steel reinforcement ratio;
ρ_f	FRP reinforcement ratio;
α_1	multiplier on *fc′* to determine intensity of an equivalent rectangular stress distribution for concrete;
$\beta 1$	stress deterioration ratio;
ν_m	poisson's rations for the matrix;
ν_f	poisson's rations for the fibers;
Ψ_f	FRP strength reduction factor =0.95;

CHAPTER 1
INTRODUCTION

1.1 Context and Problem Definition

Concrete-filled steel tubes (CFST) have been used as alternative to typical reinforced concrete (RC) columns, due to the full confinement effects for concrete and the construction efficiency of the tube as permanent formwork. The tube interacts with the core in three ways: i) it confines the core, thereby enhancing its compressive strength and ductility; ii) it provides additional shear strength for the core; and iii) depending on its bond strength with concrete and its stiffness in the axial direction, it develops some level of composite action, thereby also enhancing the flexural strength of concrete (Mirmiran and Shahawy 1997). Since steel is an isotropic material, its resistance in the axial and hoop directions cannot be uncoupled nor optimized. Steel high modulus of elasticity causes a large portion of axial loads to be carried by the tube, resulting in premature buckling. In addition, its Poisson's ratio is higher than that of concrete at early stages of loading. This differential expansion results in partial separation of the two materials, delaying the activation of confinement mechanism (Fam and Rizkalla, 2001). In cold regions or Canadian climates in an aging highway and marine infrastructure, steel tubes are exposed to harsh environment conditions such as significant temperature fluctuations, freeze-thaw cycles, marine sea spray, and chlorides accelerating the corrosion of steel tubes, which typically lead to significant deterioration and rehabilitation needs. These problems can be eliminated by using fiber-reinforced-polymer (FRP) tubes as an alternative to the steel tubes particularly where steel corrosion is a major concern.

The FRP tube provides lightweight structural component, permanent formwork, non-corrosive characteristics, protected the contained concrete from intrusion of moisture with corrosive agents that could otherwise deteriorate the concrete core and saving of construction time and effort. Furthermore, the laminate structure of FRP tubes could be optimized by controlling the proportions of fibers in the axial and hoop directions to suit the application

(Rizkalla and Fam, 2002). For instance the axial members, larger stiffness is required in the hoop direction as well as a minimum Poisson's ratio in order to produce the maximum confinement of concrete. The composite system thus formed is commonly referred to as concrete-filled FRP tubes (CFFTs), and is found to be a viable alternative and has showed superior performance to RC or CFST for use as columns, piles, and beams. The promising concept of concrete-filled FRP tube (CFFT) system, that may be further reinforced with steel or FRP bars, has raised great interest amongst researchers in the last decade. The CFFT technique has been used successfully in different concrete structure elements such as pier column and girder for bridges and also as fender piles in marine structures (Fam et al 2003b).

Using FRP bars instead of conventional steel bars in the CFFT columns can provide a step forward to develop a promising totally corrosion-free new structural system. Nonetheless, investigation of the axial behaviour of FRP bars as longitudinal reinforcement in CFFT columns has been quite limited. To date, most of the experimental investigations performed on FRP confined concrete columns have considered short, unreinforced, small-scale concrete cylinders, tested under concentric, monotonic, and axial load (Mirmiran et al. 2001; Fam et al 2003a; Lam and Teng 2009; Ozbakkaloglu et al 2013; Vincent and Ozbakkaloglu 2014). The slenderness ratio and internal longitudinal reinforcement type (steel or FRP bars) effects on the behaviour of FRP confined concrete long columns have received only limited research attention. Thus, this experimental study is designed to investigate the axial behaviour of CFFT long columns reinforced with longitudinal steel and FRP bars under monotonic and axial cyclic compression loading.

1.2 Research Significance

This study, which presents experimental test results of circular CFFT long columns reinforced with steel or FRP bars, contributes to expand the knowledge in the area of CFFT, used as structural members, by addressing new parameters intended to simulate practical applications. Using FRP bars in the CFFT columns can provide a step forward to develop a totally corrosion-free new structural system. The effect of glass FRP (GFRP) tubes wall thicknesses, internal reinforcement type and amount, and nature of loading (monotonic and cyclic) on the strength and mode of failure of CFFT long columns is investigated.

1.3 Objectives

The main objectives of this research project can be summarized as follows:

1. Evaluate the axial behaviour of reinforced concrete and GFRP-CFFT long columns reinforced with steel and FRP bars.
2. Investigate the influencing of internal reinforcement type and amount, GFRP tubes thicknesses, axial monotonic and cyclic loading of the strength, strain capacity, and mode of failure of the tested columns.
3. Investigate the influencing of the investigated parameters on the shape of unloading/reloading paths, the ultimate axial strain, and plastic strain values of steel and FRP-reinforced CFFT columns.
4. Evaluate the accuracy of the existing design equations as provided in ACI and CSA codes and design guidelines to predicate the axial compression capacity of the test specimens.

1.4 Methodology

In order to achieve these objectives, an experimental program is designed. The experimental program focuses on axial behaviour of RC and CFFT circular columns internally reinforced with steel and FRP bars. The test specimens included construction and testing of ten fixed-fixed columns measuring 1900 mm in-height and 203 mm-in diameter. The test specimens were divided into two series denoted as Series I and II. Series I included three control RC specimens reinforced with a longitudinal reinforcement ratio (ρ_L) equals to (3.4%), one specimen reinforced with steel bars and two identical specimens reinforced with GFRP bars. Steel spiral stirrups (pitch = 50.6 mm) were used as transverse reinforcement to have approximately similar hoop stiffness of the GFRP tube (Type A). Series II consisted of seven reinforced CFFT columns laterally confined with GFRP tubes (Type A or B). One specimen reinforced steel bars and laterally confined with tube type (A). Four specimens reinforced with GFRP bars (ρ_L = 1.2 and 3.4%) and laterally confined with tubes type (A and B). In addition, two identical specimens reinforced with CFRP bars (ρ_L = 1.2 %) and laterally confined with tube type (A). All specimens were tested under single complete unloading/reloading cyclic axial compression loading, except for one specimen, which was tested under monotonic axial

compression loading. The investigated test parameters were: (i) GFRP tubes thicknesses (2.9 and 6.4 mm); (ii) internal reinforcement type (steel; GFRP; or CFRP bars) and amount; and (iii) nature of loading (i.e. monotonic and cyclic).

1.5 Organization of the Dissertation

This dissertation consists of five chapters. The following is a brief description of each:

Chapter 1: This chapter defines the problem and summarizes the main objectives and originality of the research program. The methodology undertaken to achieve these objectives is also emphasized.

Chapter 2: This chapter provides general information on the FRP composites materials and their characteristics. The chapter also presents background and review on modeling FRP tubes and test methods to evaluate the mechanical properties of FRP tubes. An overview of the background literature carried out to investigate the structural behaviour of CFFT column with different parameters is reviewed. Furthermore, design guide (recently published in Canada and USA) of the concrete infill columns structures are also covered.

Chapter 3: This chapter describes the experimental program conducted at the University of Sherbrooke to test 10 RC and CFFT columns internally reinforced with (steel and FRP bars). In this chapter, the details of test specimens, test setup, and instrumentation are given. The chapter provides detailed characteristics of the materials used in the research program.

Chapter 4: This chapter presents the results obtained from the experimental investigation. The influence of each test parameter on the axial behaviour of the tested columns is also discussed. The behaviour of the tested columns in each series is discussed in terms of failure mode, axial and lateral stress strain responses, the plastic strains and stress deterioration. Furthermore, the effect of the GFRP tube thickness on confinements, internal longitudinal reinforcement steel or FRP bar and loading pattern (monotonic and cyclic) are discussed as well. The accuracy of the existing design equations as provided in ACI and CSA codes and design guidelines to predicate the axial compression capacity of the test specimens is also highlighted.

Chapter 5: A summary of this investigation is given in this chapter. The chapter also presents the general conclusions drawn from the work presented in this dissertation. Recommendations for future research are also given.

CHAPTER 2
LITERATURE REVIEW

2.1 General

Harsh environmental effects, such as significant temperature fluctuations, freeze-thaw cycles, and high concentrations of chlorides, on concrete bridge pier columns and piles have resulted in their steady deterioration that shortens their long-term durability and structural integrity. The key problems are permeability of concrete and corrosion of the embedded steel reinforcement. One promising innovative structural system is concrete filled fiber-reinforced polymer (FRP) tubes, which provide many unique advantages (Seible 1996). The FRP tube acts as a stay-in-place structural formwork to contain the fresh concrete, which may save the costs of formwork and labor used by the cast-in-place or precast industries. At the same time, the FRP tube acts as non-corrosive reinforcement for the concrete for flexure and shear. More importantly, the FRP tube provides confinement to the concrete in compression, which significantly improves the strength and ductility. The contained concrete is protected from severe environmental effects and deterioration resulting from moisture intrusion (Mirmiran 1995).

This chapter provides brief information on the FRP materials and their characteristics compared to steel reinforcement, modeling FRP tubes and test methods to evaluate the mechanical properties of FRP tubes. An overview of the background literature carried out to investigate the structural behaviour of CFFT column with different parameters is reviewed. Furthermore, codes design guides (recently published in Canada and USA) of the concrete infill columns structures are also examined.

2.2 FRP Composite Materials

“FRP” is an acronym for fiber-reinforced polymers. The term composite material is a generic term used to describe combination of two or more materials, which yield a product that is more efficient from its strength. The fibers provide the tensile strength, which are

embedded in the matrix. The matrix provides protection and support for the sensitive fibers as well as local stress transfer from one fiber to another. The matrix, such as a cured resin-like epoxy, polyester, vinyl ester, or other matrix acts as a binder and holds the fibers in the intended position, giving the composite material its structural integrity by providing shear transfer capability. Three FRPs are commonly used (among others): composites containing glass fibers are called glass fiber reinforced polymers (GFRP); those containing carbon fibers are called carbon fiber reinforced polymers (CFRP); and those reinforced with aramid fibers are referred to as aramid fiber reinforced polymers (AFRP). GFRPs are the most inexpensive compared to the other commercially available FRPs, consequently the most commonly used fibers in structural engineering applications. Moreover, the latest FRP composite is namely Basalt FRP (BFRP), which has developed within the last ten years and has higher tensile strength than E-glass fibers but lower than S-glass; however, its cost is near the cost of E-glass (Zhishen et al., 2012).

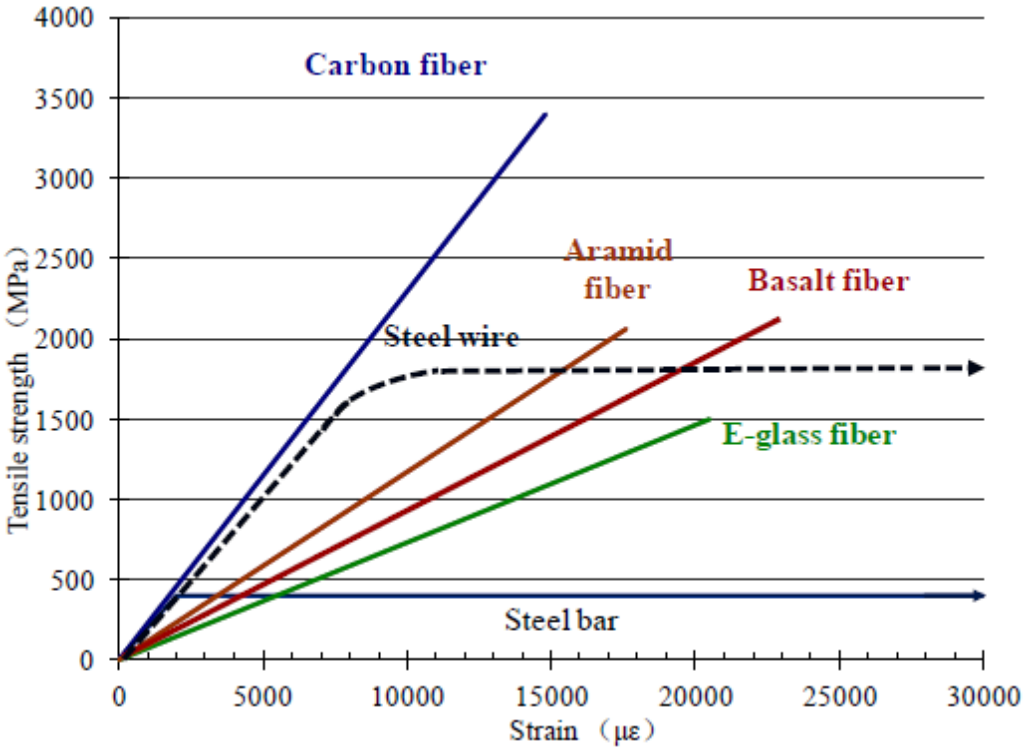

Figure 2.1: Typical stress-strain relationships of different FRPs compared to steel bars (Zhishen et al., 2012)

Typical stress-strain relationships of different FRPs compared to steel bars relationship are shown in Figure 2.1. FRP is linear elastic up to final brittle rupture when subject to tension while steel shows an elastic-plastic region. These curves give a clear contrast between the brittle behaviour of FRP composite and the ductile behaviour of steel. The fundamental difference between steel and FRP materials is due to the stress-strain behaviour of steel, which after the initial linearly elastic phase displays the yielding plateau. Therefore, after reaching the maximum value corresponding to the yielding stress the confinement pressure remains constant (neglecting strain hardening).

2.3 Modeling of FRP Tubes

Mechanical properties of FRP materials depend on the fabrication technique, type and properties of its components, particularly the fibers, and the volume fraction of the fibers in the overall mix. Pressure or vacuum molding generally results in a higher fiber volume fraction as compared to hand lay-up. While the ultimate strength of FRP materials depends on the strength and modulus of the fibers, its in-service properties are functions of the matrix. Fibers generally exhibit linear elastic behaviour, while resins are visco-elastic or visco-plastic. As such, linear elastic behaviour of fibers is generally the dominant factor in the response of unidirectional FRP materials loaded in the direction of the fibers. However, a nonlinear behaviour is often observed in the off-axis direction, under certain fiber orientations and fiber volume ratios, as the matrix resists the pull out of broken fibers in shear.

FRP materials are laminate structures made up of a stack of lamina with various fiber orientations. Bonding of the plies or layers of a laminate is often made with the same matrix used in the lamina. In the filament-winding of a tube, for example, each fiber orientation represents a ply, and the entire laminate is made with the same matrix in a single batch. Figure 2.2 shows the different modes of failure in laminate structures, including fiber rupture, transverse or longitudinal cracking of the matrix, debonding at the fiber-matrix interface, and delamination between different layers.

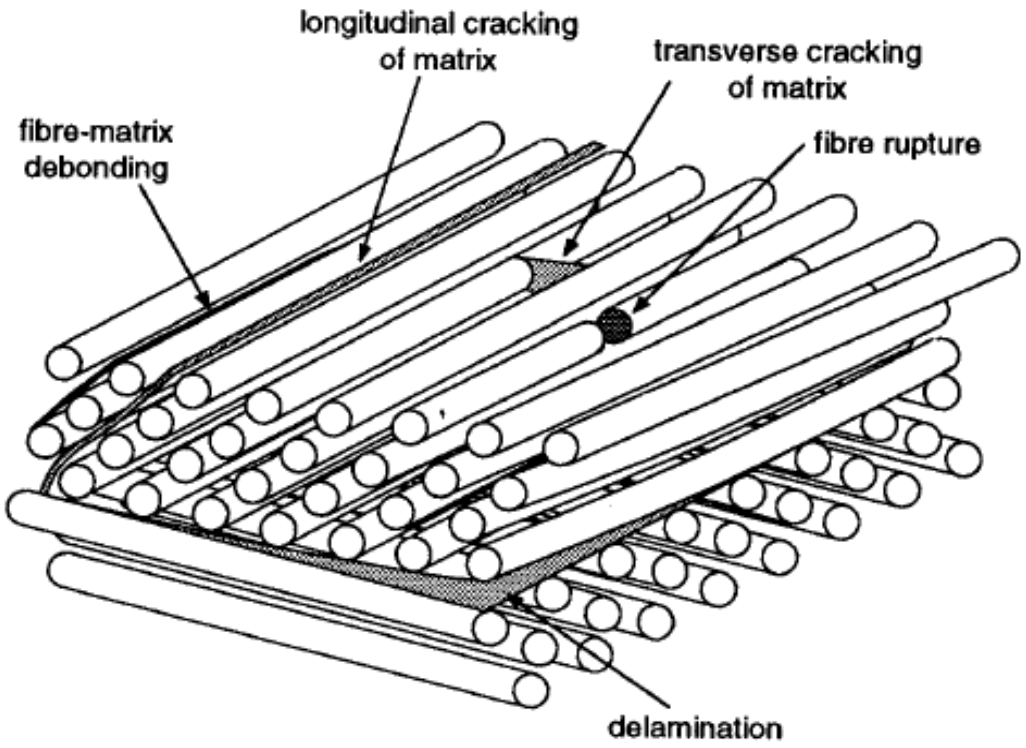

Figure 2.2: Modes of failure in a laminate (Berthlot 1995)

Because of their inherent heterogeneous and anisotropic nature, FRP materials are studied from two points of view: micromechanics and macro-mechanics. The former is a study of FRP at the level of its constituent materials and their interaction at a microscopic scale, whereas the latter is a study of FRP materials at a macroscopic scale, assuming homogeneity along with the average properties of the constituent materials. On the other hand, FRP materials are more advantageous than their isotropic counterparts, because they can be engineered or tailored for optimum properties in different directions. The tailoring process includes selecting appropriate constituents, fiber volume fraction, fiber orientation, and the stacking sequence of layers.

Figure 2.3 shows fibers uniformly dispersed within a matrix in a unidirectional lamina. Perfect bond is assumed at the interface between fibers and the matrix. The lamina, therefore, has orthotropic properties with the greatest stiffness and strength in the direction of fibers. The primary modulus of elasticity E_{11} can be calculated as

$$E_{11} = E_f V_f + E_m V_m \tag{2.1}$$

where E and V are the elastic modulus and volume fraction, respectively, and subscripts f and m denote fibers and the matrix, respectively. The above equation, known as the "law of mixture," can be derived from the resultant axial force P_{11} in the lamina, as given by

$$P_{11} = P_m + P_f \tag{2.2}$$

where P_m and P_f are the resultant forces in the matrix and the fibers, respectively. The equation can be written in terms of stresses as

$$\sigma_{11} A_{11} = \sigma_m A_m + \sigma_f A_f \tag{2.3}$$

where σ and A are the stress and area identified with subscripts for each phase, and therefore, in terms of volume fractions, it can be written as

$$\sigma_{11} = \sigma_m V_m + \sigma_f V_f \tag{2.4}$$

from which, one can derive Equation (2.1), assuming strain compatibility. Similarly, the Poisson's ratio ν_{12} of the lamina can also be written as

$$\nu_{12} = \nu_m V_m + \nu_f V_f \tag{2.5}$$

where ν_m and ν_f are the Poisson's rations for the matrix and the fibers, respectively. The transverse modulus of elasticity $E22$ can be written as

$$E_{22} = E_f E_m / \left(E_m V_f + E_f V_m \right) \tag{2.6}$$

Finally, the shear modulus G_{12} is expressed as

$$G_{22} = G_f G_m / \left(G_m V_f + G_f V_m \right) \tag{2.7}$$

At the macromechanics level, the stress-strain relationship of uni-directional lamina can be sufficiently described using the generalized Hooke's law, as

$$\begin{bmatrix}\sigma_1\\ \sigma_2\\ \sigma_3\\ \tau_{23}\\ \tau_{31}\\ \tau_{12}\end{bmatrix}=\begin{bmatrix}C_{11} & C_{12} & C_{13} & 0 & 0 & 0\\ C_{12} & C_{22} & C_{23} & 0 & 0 & 0\\ C_{13} & C_{23} & C_{33} & 0 & 0 & 0\\ 0 & 0 & 0 & C_{44} & 0 & 0\\ 0 & 0 & 0 & 0 & C_{55} & 0\\ 0 & 0 & 0 & 0 & 0 & C_{66}\end{bmatrix}\begin{bmatrix}\varepsilon_1\\ \varepsilon_2\\ \varepsilon_3\\ \gamma_{23}\\ \gamma_{31}\\ \gamma_{12}\end{bmatrix} \tag{2.8}$$

where σ_i ($i = 1, 2, 3$) and ε_i ($i = 1, 2, 3$) are the normal stresses and strains in the three principal material directions (see Figure 2.3), respectively, and τ_{ij} ($i,j = 1, 2, 3$) and γ_{ij} ($i,j = 1, 2, 3$) are the shear stresses and strains, respectively, and C_{ij} are stiffness coefficients. For a thin orthotropic shell, transverse strains are negligible, and therefore, it can be shown that

$$\begin{aligned}&\gamma_{13} = 0 \Rightarrow \tau_{13} \neq 0\\ &\gamma_{23} = 0 \Rightarrow \tau_{23} \neq 0\\ &\varepsilon_3 = 0 \Rightarrow \sigma_3 = 0\end{aligned} \tag{2.9}$$

As such, the constitutive equations can be simplified in the principal material directions of the orthotropic material as

$$\begin{bmatrix}\sigma_1\\ \sigma_2\\ \sigma_3\end{bmatrix}=\begin{bmatrix}Q_{11} & Q_{12} & 0\\ Q_{12} & Q_{22} & 0\\ 0 & 0 & Q_{66}\end{bmatrix}\begin{bmatrix}\varepsilon_1\\ \varepsilon_2\\ \gamma_{12}\end{bmatrix} \tag{2.10}$$

where Q_{ij} denote the reduced stiffness of an orthotropic lamina, and are related to the engineering properties measured along the principal directions, as given by

$$Q_{11}=\frac{E_1}{1-\nu_{12}\nu_{21}};Q_{12}=\frac{\nu_{12}E_2}{1-\nu_{12}\nu_{21}};Q_{11}=\frac{E_2}{1-\nu_{12}\nu_{21}};Q_{66}=G_{12} \tag{2.11}$$

The above relations were developed for the principal materials directions in an orthotropic material. However, the principal directions of orthotropy often do not coincide with the geometric coordinate system, as evident in a helically wound glass FRP tube (see Figure 2.4). Transformation from the principal materials direction to an arbitrary coordinate system can easily be done, as shown in Figure 2.5, using the following equation:

$$\begin{bmatrix} \sigma_x \\ \sigma_\theta \\ \sigma_{x\theta} \end{bmatrix} = \begin{bmatrix} \cos^2\varphi & \sin^2\varphi & -2\sin\varphi.\cos\varphi \\ \sin^2\varphi & \cos^2\varphi & 2\sin\varphi.\cos\varphi \\ \sin\varphi.\cos\varphi & -\sin\varphi.\cos\varphi & \cos^2\varphi - \sin^2\varphi \end{bmatrix} \begin{bmatrix} \sigma_1 \\ \sigma_2 \\ \tau_{12} \end{bmatrix} \tag{2.12}$$

where φ is the angle of rotation. Similar transformations can be applied to the strains and material properties of the shell.

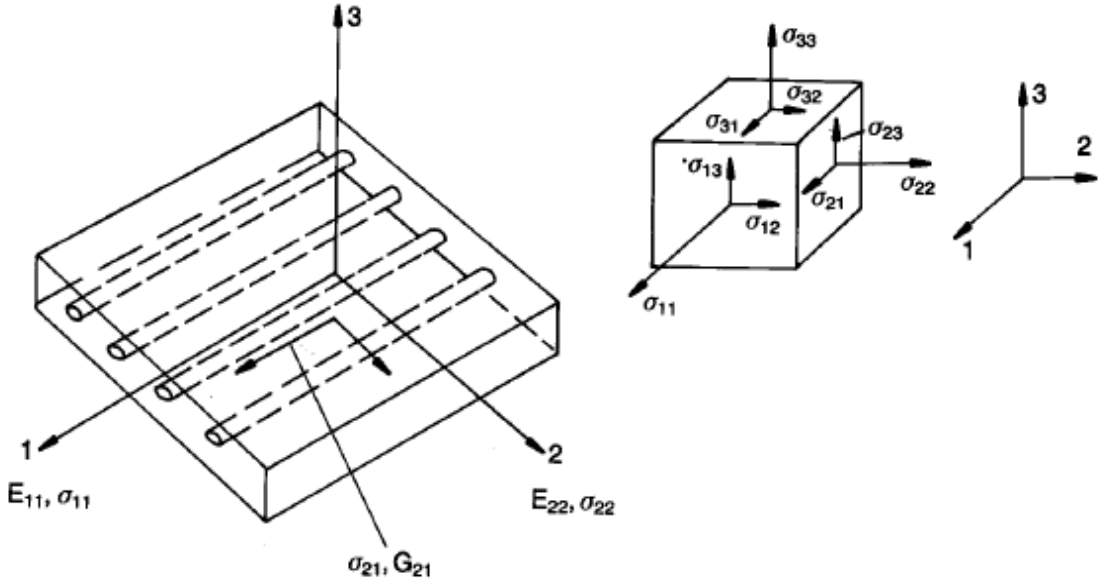

Figure 2.3: Macromechanics of FRP composites (Hollaway 1990)

As stated earlier, nonlinearity in the off-axis direction could be significant. Hahn and Tsai (1973) used a complementary energy density function to derive nonlinear relations for in-plane shear. Hahn (1973) extended the nonlinear theory of unidirectional lamina to that of laminated composites. Lifshitz (1998) studied the shear modulus of T300-934 graphite/epoxy lamina with four layers at fiber orientations of ±45º. Hu (1993) reported that unidirectional FRP may exhibit severe nonlinearity in its in-plane shear stress-strain relation. Also, some deviation from linearity may be observed under in-plane transverse loading, but the degree of nonlinearity is not comparable to that of the in-plane shear.

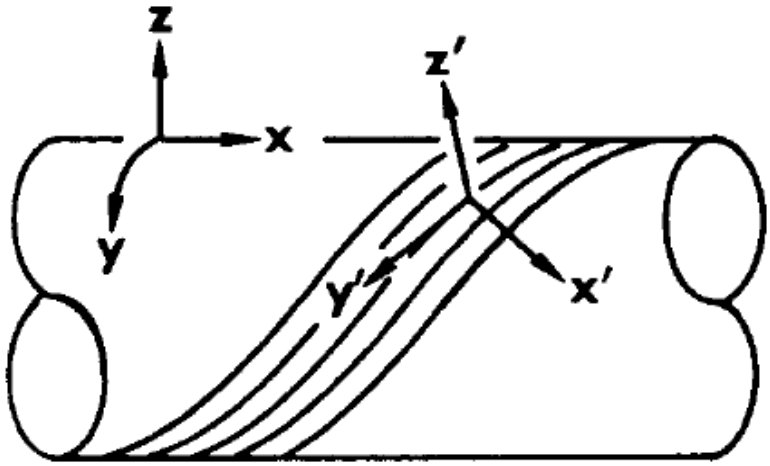

Figure 2.4: Helically wound fiber reinforced cylindrical shell (Jones 1975)

Haj-Ali and Kilic (2002) made coupon tests to calibrate three-dimensional micromechanical models for E-glass/vinyl-ester pultruded FRP. Tension, compression, and shear tests were performed on off-axis coupons cut at different angles of 0°, 15°, 30°, 45°, 60°, and 90°. The overall linear elastic properties were identified along with the nonlinear stress-strain behaviour under in-plane multi-axial tension and compression loading. The material had a lower ultimate tensile stress and initial stiffness in tension compared to the corresponding values from compression tests, regardless of thickness and orientation. This was attributed to the existing voids and micro-cracks that are more pronounced in matrix mode tensile loading. The difference between the compressive and tensile properties increased for off-axis angles approaching 90°.

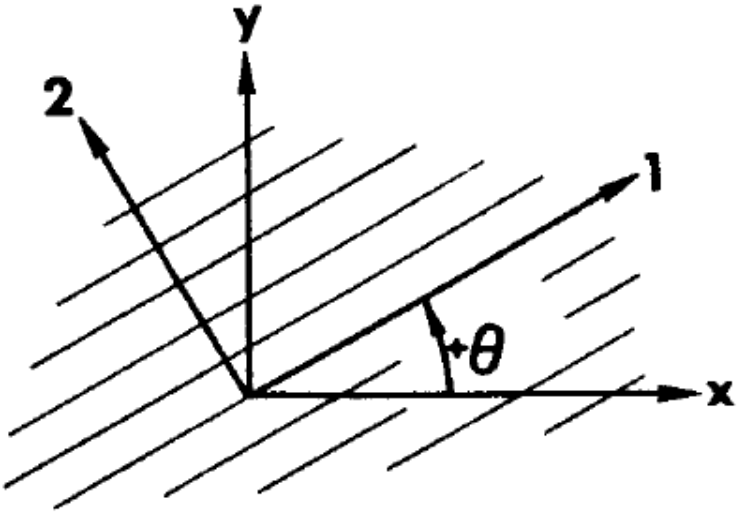

Figure 2.5: Positive rotation of principal material axes from arbitrary XY axes (Jones 1975)

2.3.1 Test Methods

The classical lamination theory provides a feasible method to evaluate the mechanical properties of FRP tubes. This theory, however, involves complicated calculations for FRP laminates, practically those with asymmetric unbalanced laminate structures. In addition, non-linear behaviour may be dominated for FRP tubes with angle-ply laminate structures, which cannot be predicted by lamination theory. Moreover, some previous research (e.g. Fam 2000) showed that the error of predications of the lamination theory may be up to 40% for the ultimate strength up to 25% for the elastic modulus and up to 50% for Poisson's ratio. Thus, standard tests are important for more accurate evaluation of the mechanical properties of FRP tubes.

The most popular test standards for tensile properties of FRP appear to be ASTM D638–10 (2010) and ASTM D2290–12 (2012) which provide test methods for the determination of the tensile properties for FRP tubes using a flat coupon test and split disk test, respectively. On the other hand, the most popular test standard for the compressive properties of FRP includes ASTM D3410/D3410M-08 (2008) which provides a test method for the compressive properties of FRP through shear loading tests. Typical test samples of this standard are shown in Figure 2.6. Figure 2.7 presents the axial tensile stress-strain responses resulted from the coupon tests and Figure 2.8 shows the average stress-strain relationships for the split-disk test in the hoop direction. Lam and Teng (2004) concluded that the ultimate strength obtained by the ring-splitting test is in general lower than that obtained from the corresponding flat coupon test, mainly due to the effect of curvature. Despite the difference in the ultimate strength, Lam and Teng (2004) also found that the elastic modules obtained from these two test methods are almost the same.

(a) Dimension of ring specimens, (b) Ring specimens after test, (c) Coupons specimens after test

Figure 2.6: Specimens of FRP tubes for the split-disk test and coupon tensile test (Masmoudi and Mohamed 2011)


Test setup

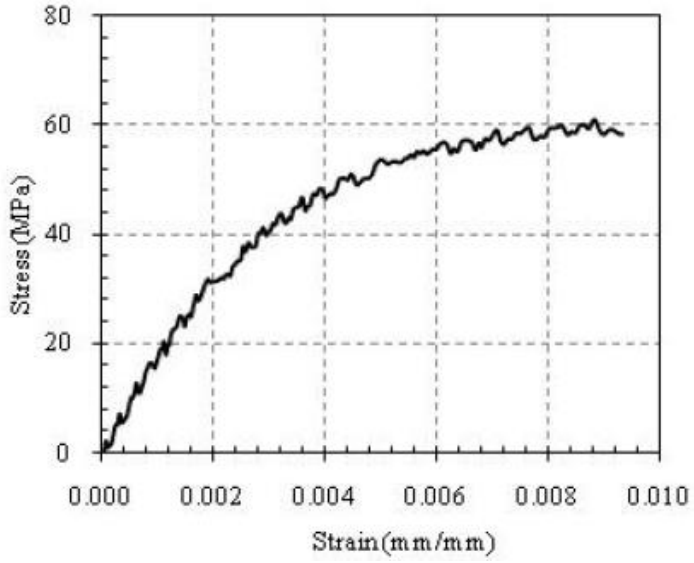

Figure 2.7: Test setup and load-strain curve for the FRP tubes for coupon tensile test (Masmoudi and Mohamed 2011)


Test Setup

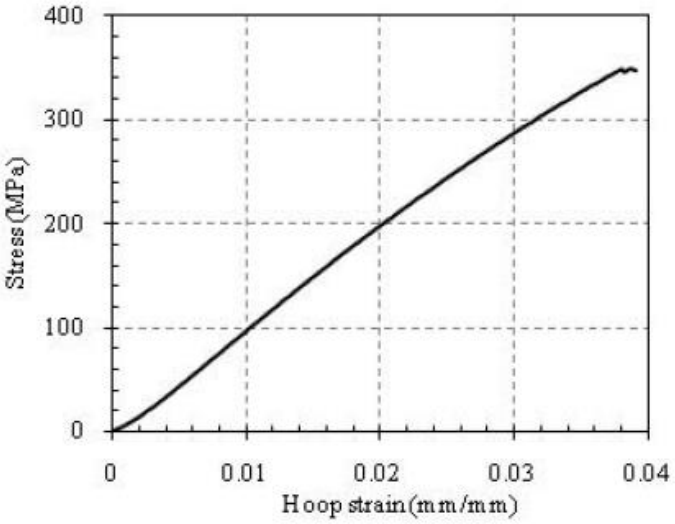

Figure 2.8: Test setup and stress-hoop strain behaviour of the FRP tubes for split-disk test (Masmoudi and Mohamed 2011)

2.4 Confinement of Concrete

Concrete is one of the most commonly analyzed structural civil engineering materials in use today. The difficulty in characterizing the mechanical behaviour of concrete is due to its highly nonhomogeneous structure. In addition, the interaction between the cement paste and

aggregate causes the nonlinearity of the concrete stress-stain response. At relatively low stress levels, the development and propagation of micro-cracks at the aggregate-paste interfaces soften the concrete, resulting in a somewhat parabolic stress-strain curve (Collins and Mitchell 1997). It was demonstrated that with the increase in concrete strength, the ductility decreases, whereas initial stiffness and linearity of the curve increase (see Figure 2.9). Once the maximum stress ($f'c$) is reached at a strain ε_o, concrete cannot support this high level of stress with increasing deformation. For concrete strengths less than about 41MPa, the stress-strain relationship can be reasonably described by a simple parabola (Collins and Mitchell 1997).

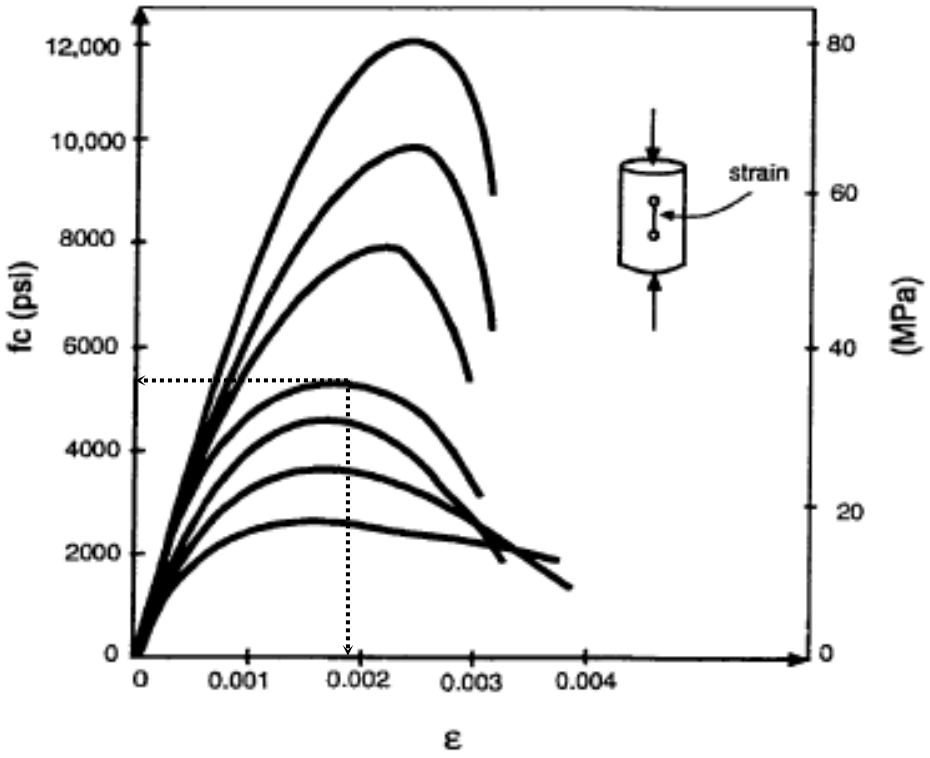

Figure 2.9: Typical compressive stress-strain curves (Collins and Mitchell 1997)

The basic principle of confinement, which adds another dimension to columns analysis, consists of imposing a restriction on the lateral expansion of the concrete, and its corresponding crack growth, due to axial stress. When properly confined, the concrete can sustain plastic deformation with axial strains and stresses higher than its unconfined failure values (Considere 1903; Richart et al. 1928; Mirmiran et al. 1998; Saafi et al. 1999; Fam and Rizkalla 2001; Hong and Kim 2004; Fam et al. 2005; Ozbakkaloglu and Oehlers 2008 a, b; Mohamed and Masmoudi 2010; Park et al. 2011; and Ozbakkaloglu 2013a, b, c, etc.). Figure

2.10 shows the effect of hydraulic confining pressure on stress-strain response. Confinement considerably increases the energy absorption capacity of concrete. Thus, in seismic regions, appropriately detailed transverse reinforcement and/or wrapped with FRP or encasing concrete in tubes (steel or FRP) is provided to confine the concrete and hence increase the ductility of columns and beams (Kent and Park 1971; Sheikh 1978; Sheikh and Uzumeri 1980; Seible et al. 1996; Yamakawa et al. 2003; Zhu et al. 2006; Ozbakkaloglu and Saatcioglu 2006, 2007; Saatcioglu et al. 2008; and Idris and Ozbakkaloglu 2013).

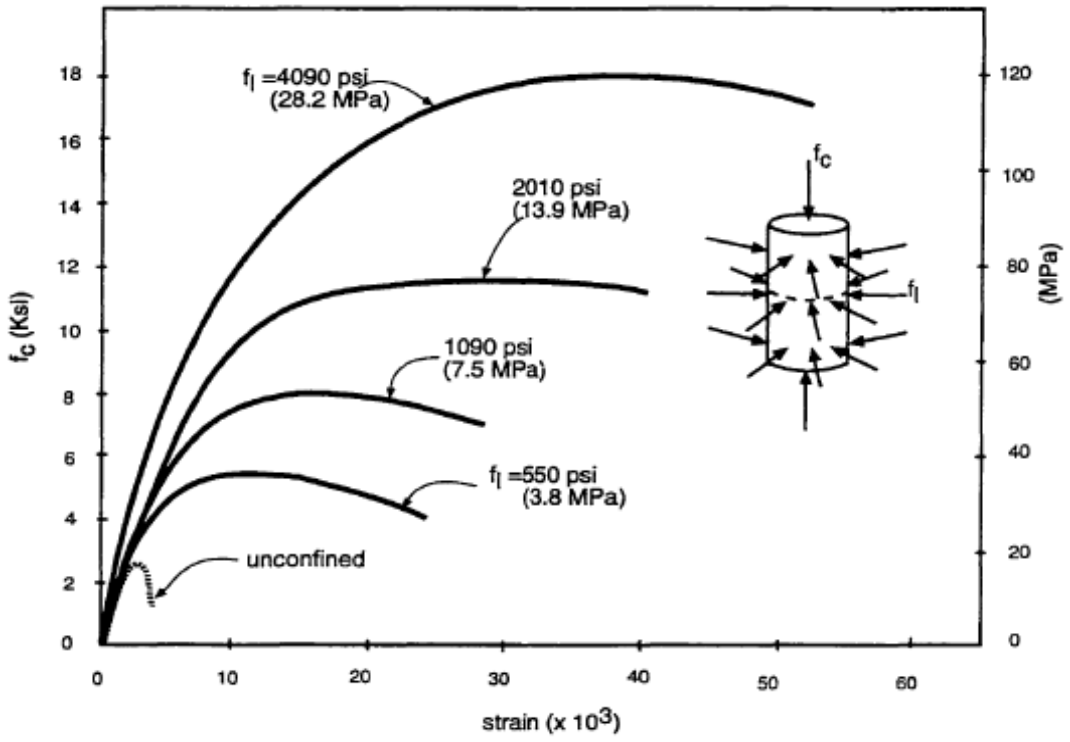

Figure 2.10: Effect of lateral pressure on stress-strain response (Richart et al. 1928)

2.5 Confinement Mechanism

2.5.1 Confinement by lateral steel reinforcement

In practice, columns are confined by lateral reinforcement, commonly in the form of closely spaced steel spirals or hoops. At low levels of stress in the concrete, the lateral reinforcement is hardly stressed, thus the concrete exhibits unconfined behaviour. When stresses approach the uniaxial strength, the progressive internal cracking cause high lateral

strains. The concrete bears out against the lateral reinforcement, which then apply a confining reaction to the concrete and hence the concrete exhibits a confined behaviour (Park and Paulay 1975). Confinement of different column shapes is presented in the following:

(a) *Circular columns*: Circular spirals, because of their shape, are in axial hoop tension and provide continuous confining pressure around the circumference. The pressure provided by closely spaced circular spirals and vertical column reinforcement can be considered to be uniform around the perimeter of the core (Saatcioglu and Razvi 1992). Figure 2.11 shows the lateral pressure of circular column.

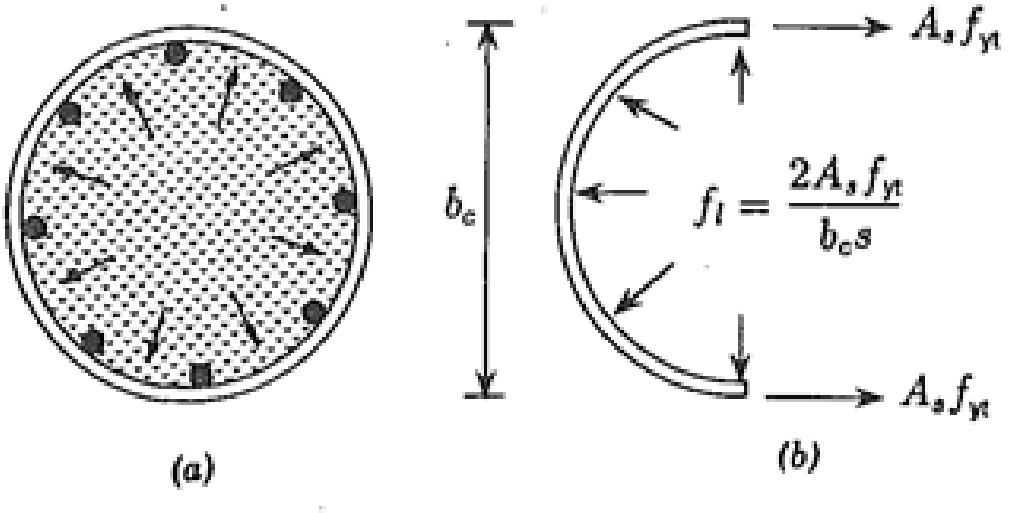

Figure 2.11: Lateral pressure in circular columns: (a) uniform buildup of pressure; and (b) computation of lateral pressure from hoop tension (Saatcioglu and Razvi 1992)

(b) Square columns: Square and rectangular hoops can apply confining pressure only at the corners of the ties, thus causing a portion of the core concrete to remain unconfined (See Figure 2.12). Passive confinement pressure exerted by a square hoop is dependent on the restraining force developed in the hoop steel. The hoop steel can develop high restraining forces at the corners, where it is supported laterally by transverse legs, and low restraining action between the laterally supported corners. The restraining force at the corners depends on the force that can be developed in the transverse legs, which, in turn, is related to the area and strength of the hoop steel. The restraining action of the hoop, between the corners is related to the flexural rigidity of the hoop steel, which depends on the size and unsupported length of the bar. This restraining action is proportional to the elastic rigidity of the hoop steel until

yielding. Beyond yielding, the restraining action remains approximately constant until the strain hardening of steel produces additional restraining action. However, the flexural rigidity of the hoop between the laterally supported nodal points and the resulting restraining action is very small as compared to the restraining action of the corners and the other nodal points. Therefore, as the concrete expands laterally under axial compression, there will be higher reactive pressures building up at the nodal points than at locations away from the nodes. Figure 2.13 (a) illustrates the buildup of passive confinement pressure in a square column. If cross ties or inside hoops are used to support the middle bars, additional points of high lateral restraint are generated. It is clear that the shape of the pressure distribution is a function of the reinforcement arrangement. Shapes of pressure distributions for various tie arrangements are shown in Figure 2.13 (b).

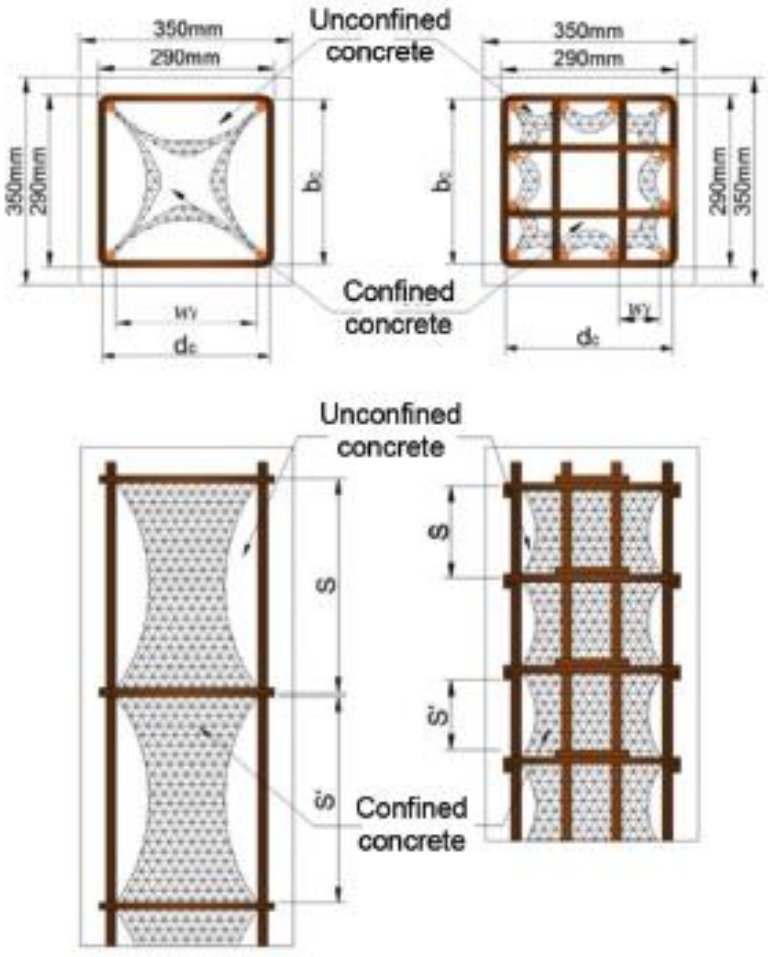

Figure 2.12: Arching action and confined concrete core shape for poorly and well-detailed transverse reinforcement (Adopted from Tobbi et al. 2012)

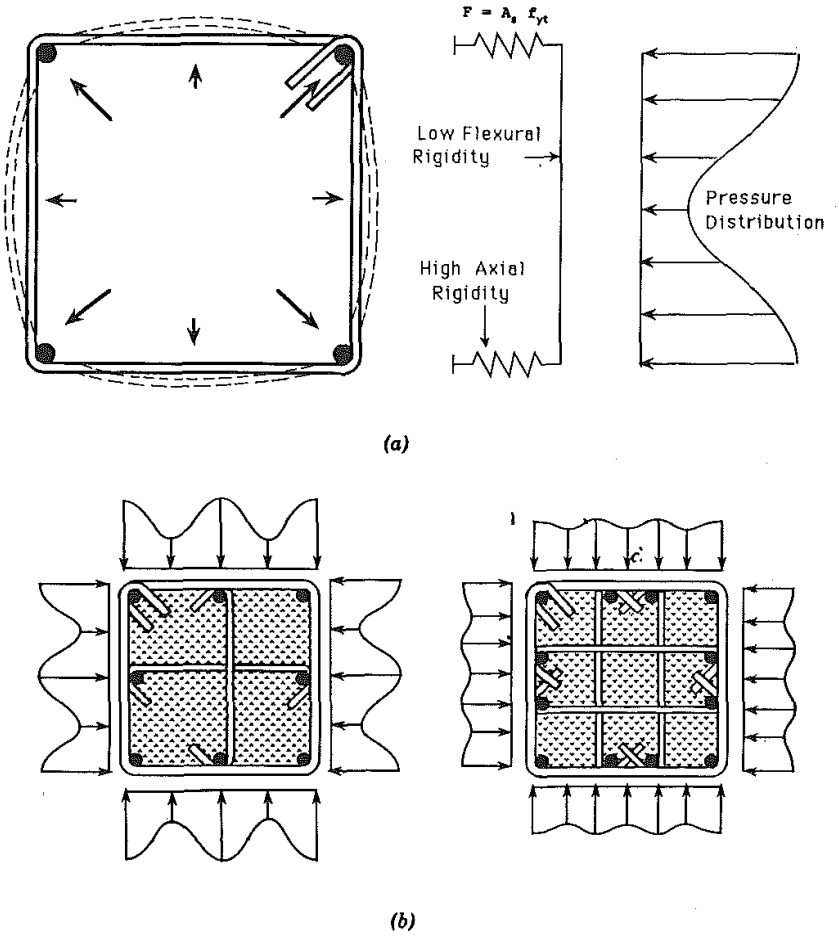

Figure 2.13: Lateral pressure in square columns: (a) Lateral pressure buildup in square columns; and (b) pressure distributions resulting from different reinforcement arrangements (Saatcioglu and Razvi 1992)

(c) Rectangular columns: Rectangular columns may have different confinement reinforcement in two orthogonal directions. This may lead to different levels of confinement pressure along the long and short sides of the section. Figure 2.14 illustrates lateral pressure distributions along the long and short sides of a rectangular-column section. Confinement pressure along the long side plays a more dominant role on concrete strength than that along the short side. Examination of experimental data indicates that the effects of confinement pressures along the long and short sides can be considered to be proportional to the cross sectional dimensions.

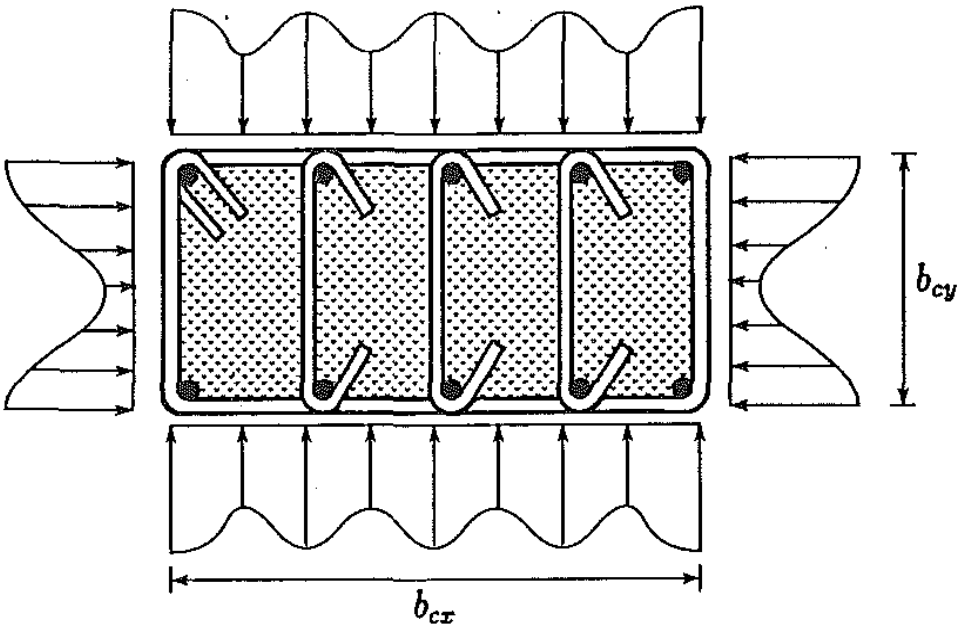

Figure 2.14: Lateral pressure in distribution in rectangular columns (Saatcioglu and Razvi 1992)

2.5.2 Confinement by steel tubes

Another form of concrete confinement is by encasing concrete in a steel tube (Kloppel and Goder 1957). The steel tube acts as longitudinal, transversal, and shear reinforcement; formwork; and as a continuous confining jacket, which provides a tri-axial state of stress for concrete under compression. In return, concrete delays local buckling of the tube (Gardner and Jacobson 1967). Moreover, circular sections provide uniform flexural strength and stiffness in all directions. Due to the large shear capacity of concrete-filled steel tubular members, they predominantly fail in flexure in a ductile manner (Fam 2000).

It should be noted, however, that in addition to the corrosion problems of steel tubes, the confinement effectiveness is reduced at low levels of loading if the tube is also loaded in the axial direction. This is attributed to the fact that Poisson's ratio of concrete at low levels of loading, 0.15 to 0.2, is smaller than the 0.3 value of steel, which rather tends to separate (Prion and Boehme 1994; Wei, Mau, and Mantrala 1995). As loading increases, lateral expansion of unconfined concrete approaches that of steel as micro cracking of the concrete increases and Poisson's ratio reaches up to 0.6. Consequently, a radial pressure develops at the steel-concrete interface, thereby, restraining the concrete core and setting up hoop tension in the tube.

Normally, after the unconfined cylinder strength is attained, concrete would tend to spall and disintegrate in the absence of the confining jacket. However, if the jacket buckles before strains are large enough to develop the unconfined cylinder strength; the full strength of concrete cannot be utilized. It was reported that concrete begins to increase in volume at a strain level of about 0.002 (Knowles and Park 1969) and confinement is activated at stress level of 95 percent of the concrete strength (Prion and Boehme 1994). At this stage, the concrete is stressed tri-axially and the tube bi-axially. The interaction between the tube and the core results in a synergistic effect where the capacity of the composite column exceeds the sum of the individual strengths of steel and concrete (Kilpatrick and Rangan 1997). Prion and Boehme (1994) reported that the confining level is higher if the axial load is applied to the concrete only as the steel shell will not expand laterally and keep in contact with concrete. However, in practice, bond stresses and friction cause longitudinal strain in steel, which also reduces the yield strength in both directions.

2.5.3 Confinement by FRP tubes

Concrete filled FRP tubes (CFFTs) are a simple system comprised of filling prefabricated hollow FRP tubes with concrete. The FRP tubes are fabricated in a number of different ways, which include pultrusion, filament winding, spin casting or hand lay-up. The layers of fibre may also be oriented in a number of different directions, including longitudinal, circumferential or at angles, depending on the desired structural requirements. These CFFTs may or may not be further strengthened with the addition of conventional internal reinforcing steel bars and/or prestressing steel strands. CFFTs are particularly advantageous because the prefabricated hollow FRP tube serves as stay-in-place formwork, which greatly simplifies construction. In addition, these FRP tubes provide confinement for the inner concrete core, which not only increases its compressive strength, but also protects the core from the aggressive environmental conditions.

FRP jackets, other than being much lighter than steel jackets and non-corrosive, provide other advantages from the structural point of view. FRP-confined concrete is insensitive to small lateral expansion due to its lower Young's modulus which forces concrete to carry most of the axial load, therefore, allowing the shell to be more solicitude in the hoop direction rather than failing prematurely by outward local buckling in the axial direction (Rizkalla and Fam

2002). As the unconfined strength is approached, high lateral expansion occurs due to major microcracking, which activates the FRP jacket. Passive confining pressure, continuously increasing due to the linear characteristics of the FRP, is induced. Once the jacket reaches its hoop strength, it ruptures, and the concrete fails. Unlike steel jackets, the FRP expansion in the hoop direction due to axial load is less than that of concrete at the early stage of loading for most laminates. This results in eliminating any separation of the FRP tube with the concrete or delay of the confinement process. In addition, the orthotropic laminate structure of FRP shells allows uncoupling of the two fiber orientations for design optimization as reported by Shahawy and Mirmiran (1998).

The fundamental difference between FRP and steel tubes is that the stress-strain behaviour of steel, which after the initial linearly elastic phase, displays the yielding plateau. Therefore, after reaching the maximum value corresponding to the yielding stress, the confinement pressure remains constant (neglecting strain hardening). Another difference is the greater stiffness of steel when compared to FRP (especially to GFRP, whereas CFRP may reach even higher values of elastic modulus). Both differences are reflected in the typical axial stress-strain behaviour of steel-confined and FRP-confined concrete, illustrated in Figure 2.15. Stresses and strains are normalized with respect to the unconfined concrete strength and peak strain. The steel-confined concrete follows an approximately linear trend before reaching the peak stress (f'_{cc}) after which it follows a gradual post-peak descending branch, therefore, the ultimate stress (f_{cu}) is lower than the peak stress.

The FRP confined concrete displays a distinct bilinear response with a sharp softening and a transition zone at the level of its unconfined strength (f'_{co}), after which the tangent stiffness stabilizes at a constant value until reaching the ultimate strength. Thus, the peak point coincides with the ultimate point and they both correspond to tensile rupture of the FRP confining device. It has been noted that the strain measured in the confining FRP at rupture is in most cases lower than the ultimate strain of the FRP tested in uniaxial tension (see, for example, Matthys et al. 1999; Lorenzis and Tepfers 2003). The ever-increasing response is associated to the absence of yielding. The decrease in stiffness at the level of the concrete unconfined strength is due to the lower stiffness of the FRP confining device with respect to steel (in Figure 2.15 it can be seen that it is more pronounced for GFRP than for CFRP

confinement, the latter being very close to the response of the steel-confined column). From the observed behaviour, it has been noted that the value of the confined strength is essentially dependent on the maximum confining pressure that the FRP may apply, whereas the slope of the second branch of the stress-strain relationship (and, as a consequence, the value of the strain at peak stress) is mainly related to the confinement stiffness.

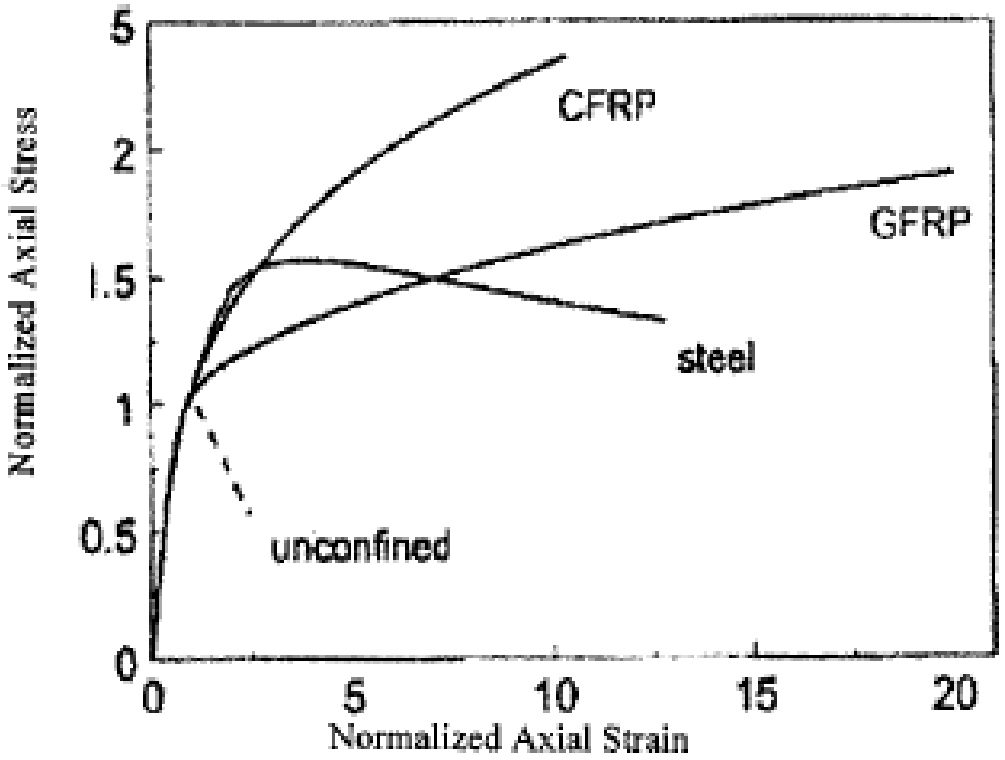

Figure 2.15: Axial stress-strain behaviour of confined concrete (Spoelstra and Monti 1999)

Samaan et al. (1998) attributed the difference in behaviour between steel-confined concrete and FRP-confined concrete to the distinctly different dilation behaviour of concrete as shown in Figure 2.16. The dilation response of FRP-confined concrete is initially similar to unconfined concrete. It reaches a peak value, after which it decreases and finally stabilizes. Steel jackets effectively confine the concrete and control dilation before yielding. After yielding of the confining steel, the lateral confining pressure from steel confinement becomes essentially constant, thus allowing for increasing lateral dilation of confined concrete with increasing axial strains.

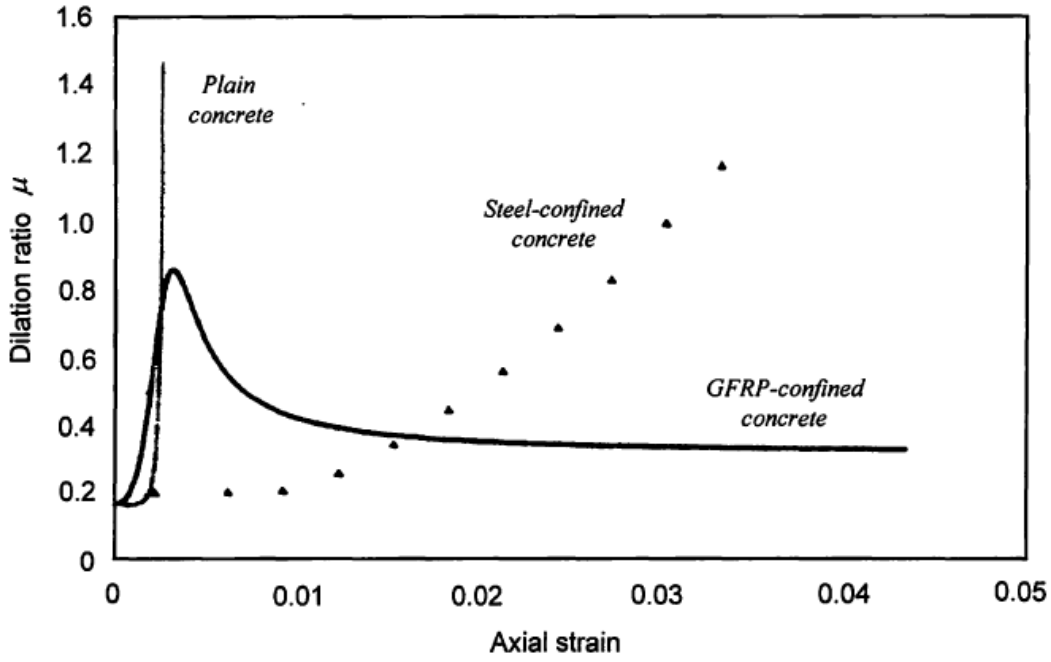

Figure 2.16: Dilation curves of GFRP-confined concrete versus steel-confined concrete (Samaan et al 1998)

Fam and Rizkalla (2001b) reported the following equation that summarizes the critical parameters affecting the confinement pressure σ_R in circular CFFT, which directly contributes to the enhanced axial strength of the concrete.

$$\sigma_R = \frac{\upsilon_c}{\frac{R}{E_f t} + \frac{1-\upsilon_c}{E_c}} \varepsilon_{cc} \tag{2.13}$$

At any axial strain level ε_{cc}, σ_R is increased as the stiffness of the tube in the hoop direction ($E_f t/R$) is increased, where E_f is the equivalent orthotropic elastic modulus of the tube in the hoop direction, t is the thickness of the tube, and R is the radius. The confinement pressure σ_R also increases as the dilation of concrete increases as reflected by its Poisson's ratio ν_c. E_c is the modulus of the concrete core. Equation (2.13) represents an FRP tube fully utilized in the circumferential direction (debonded from concrete and not loaded axially), as shown in Figure 2.23.

2.6 Critical Review on the Structure Behaviour of CFFT Members Subjected to Axial Forces or Combined Axial and Bending

The axial stress-strain behaviour of unconfined and confined concrete differs significantly as mentioned previously. Confining a concrete member is accomplished by orienting the fibers transverse to the longitudinal axis of the member. In this orientation, the transverse or hoop fibers are similar to conventional spirals or reinforcing steel ties. Any contribution of longitudinally aligned fibers to the axial compression strength of a concrete member should be neglected (ACI 440.2R-08 (2008)). FRP jackets provide passive confinement to the compression member, remaining unstressed until dilation and cracking of the wrapped compression member occur. This means that confining pressure is engaged by the transverse dilation of concrete resulting from principal axial strains—the Poisson effect (shown schematically in Figure 2.17). For this reason, intimate contact between the FRP jacket and the concrete member is critical.

Passive confinement may be constant or variable through an axial load history. Constant confining pressure is generated in cases where the confining material behaves in a plastic manner. This is typically assumed to be the case where confinement is provided by conventional transverse reinforcing steel. Variable confining pressure is generated when the confining material has an appreciable stiffness. FRP jackets and steel that is still elastic generate variable confining pressures. Variable passive confinement is dependent on the axial and transverse behaviour of the concrete, which in turn is dependent on the amount and stiffness of confinement provided.

As reported by (Harris and Kharel 2002) the confinement of the concrete with FRP depends on the stiffness of the FRP confining material. These behaviours and the transition between them are described in Figure 2.18 as follows:

(a) Lightly confined concrete: In the case of lightly confined one- and two-ply E-glass confined cylinders, the jackets did not fail at the peak axial load. A significant post-peak behaviour is observed. This is because the jacket is not stiff enough to provide sufficient

confining pressure at lower axial strains to increase the load-carrying capacity of the concrete. The FRP jacket is ruptured when rupture strain of the jacket is achieved. The confined concrete, at this point, is confined rubble. For lightly confined concrete, the limiting dilation ratio is not reached due to the limited strain capacity of the jacket.

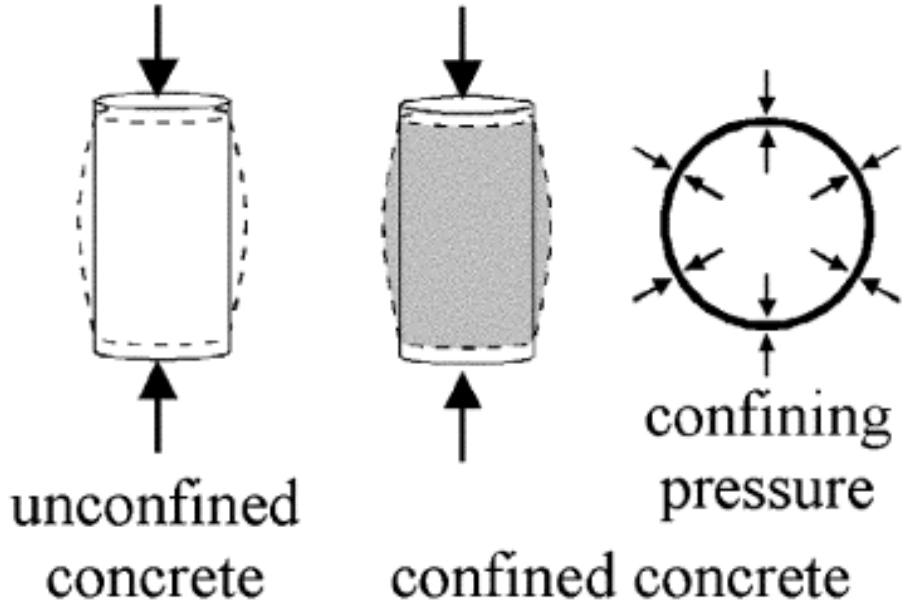

Figure 2.17: Confining pressure engaged by dilation of concrete (Harris and Kharel 2002)

(b) Heavily confined concrete: In the case of heavily confined 12- and 15-ply E-glass and three-ply carbon-confined cylinders, the jackets are stiff enough to provide enough confining pressure to increase the load capacity, resulting in larger dilation strains. When the confining material fails, the now-overloaded unconfined concrete experiences a very brittle failure. In this case, no Post-peak behaviour is observed. In the case of heavily confined concrete, an approximately bilinear stress-strain behaviour is seen. In these cases, the dilation ratio increases to some limiting value after which it remains essentially constant. The ultimate axial stress and strain achieved is, therefore, related to the strain rupture of the confining material by the dilation ratio.

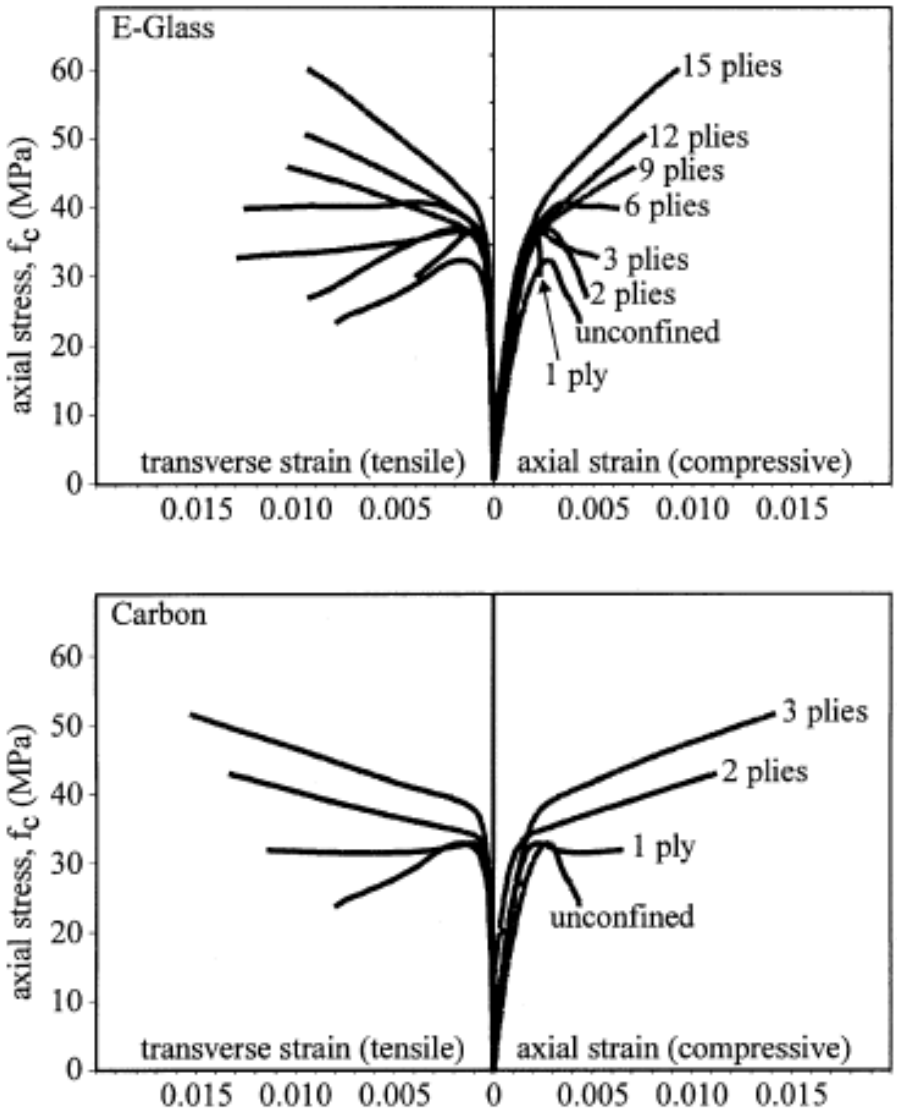

Figure 2.18: Representative axial stress versus axial and transverse strain responses (Harris and Kharel 2002)

(c) Moderately confined concrete: The behaviour of moderately confined concrete falls between the behaviours as described previously. A relatively smooth transition of response parameters between lightly and heavily confined concrete is observed. In these tests, this transition between responses appears around the six-ply E-glass- confined specimens.

When CFFT circular members are subjected to bending, experimental studies (Davol et al. 2001; Fam and Rizkalla 2002) have shown that the benefits of concrete confinement are less in bending than in purely axial loading case however, the ductility of the member is

improved. The studies also showed that the behaviour is controlled by the laminate architecture of the FRP tubes and that concrete-filled FRP tubes with thick walls typically fail in compression. Figure 2.19 shows the axial strain versus the lateral strain behaviour of the FRP tube in the compression zone of a beam, tested by Fam and Rizkalla (2002), versus that of a column of the same type. The figure shows that the behaviour is bilinear for columns, with significant increase in lateral strains due to confinement. For beams, however, the behaviour is linear, with a slope proportional to the longitudinal Poisson's ratio of the tube, which indicates lack of confinement. This is attributed to the strain gradient, where most of the cross section of the beam is in tension. In addition, their study showed that the flexural behaviour is highly dependent on the stiffness and diameter-to-thickness ratio of the FRP tube, and to a lesser extent on the concrete strength. Fam et al. (2005) tested three concrete-filled rectangular FRP tubes (CFRFT) beams. The beams included totally filled tubes and a tube partially filled with concrete, which had a central hole for reducing deadweight. The effect of reinforcement ratio was examined by using tubes of two different sizes. Flexural behaviour of CFRFT was compared to concrete-filled rectangular steel tubes (CFRSTs) of similar reinforcement ratios. They showed that CFRFT is a feasible system that could offer similar flexural strength to CFRST. The tube laminate structure and its progressive failure contribute to the slightly nonlinear behaviour of beams. The CFRFT beam with inner hole had an overall strength to- weight ratio, 77% higher than the totally filled beam, but failed in compression. Bulging of CFRFT columns has limited their confinement effectiveness.

Mirmiran and Shahawy (1999) performed a detailed study on concrete-filled FRP tubes under various combinations of axial and flexural loads. Two types of FRP tubes were used to simulate the conditions of over-reinforcement (where compression failure governs) and under-reinforcement (where tension failure governs). The over-reinforced specimens were prepared using 348 mm diameter tubes with a wall thickness of 14 mm, while the under-reinforced specimens used 369 mm tubes with a 6 mm wall thickness. The reinforcement ratios (ratio of area of FRP shell to area of concrete core) for the over and under-reinforced concrete-filled tubes were 18.27 and 7.56 percent, respectively. Since the strength of the FRP tubes were different for these specimens, the authors proposed the use of a reinforcement index, defined as the reinforcement ratio multiplied by the ratio of the axial tensile strength of the FRP tube to the concrete compressive strength. The reinforcement indices of the over and under–

reinforced sections were 3.39 and 0.19, respectively. The over-reinforced specimens were found to behave better as beam-columns. They deflected to a lesser extent (ultimate deflections of the over-reinforced specimens were about 25 to 50 percent lower than the under-reinforced specimens), and failed at much higher bending moments. Failure of the over-reinforced specimens while in compression was considered to be gradual or ductile. The under-reinforced failure mode was brittle and sudden. Based on this study, the authors concluded that concrete-filled FRP tubes could be used for beam-column applications, and recommended the use of over-reinforced specimens. Test observations also indicated that bond-failure or slippage in beam columns is not as significant as in beam specimens (pure flexure), as long as end connections are designed properly. For beam specimens shear transfer mechanisms such as internal ribs or treatments of the inner surface of the tubes were recommended to enhance the composite action between the FRP shell and the concrete core.

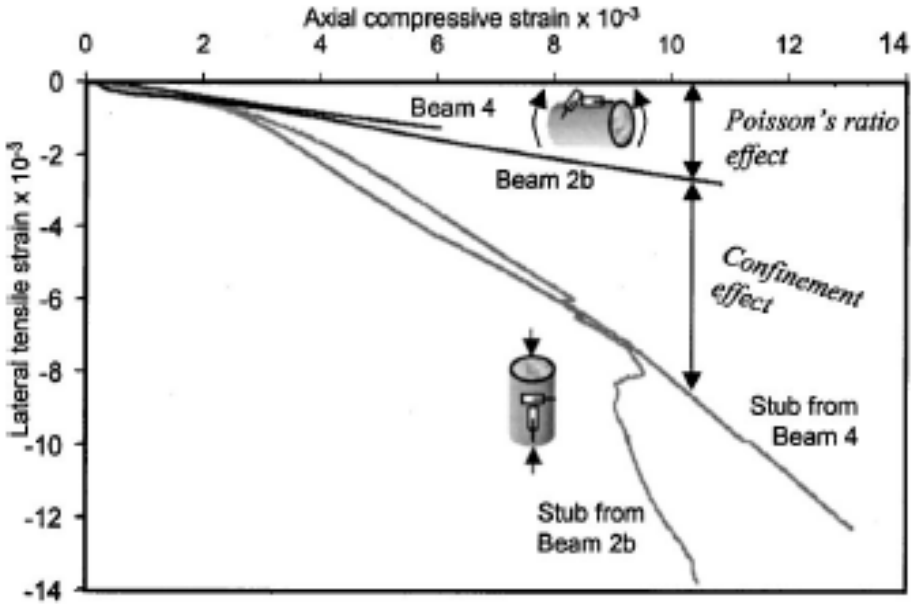

Figure 2.19: Comparison between axial-lateral behaviour in beams and columns (Fam and Rizkalla 2002)

Fam et al. (2003a) studied the axial load/bending moment interaction diagrams of concrete-filled FRP tubes, of two different types. The two types of tubes have almost the same diameter and wall thickness; however, the laminate structure of the Type I tube resulted in higher confinement efficiency compared with Type II due to the lower Poisson's ratio and higher hoop stiffness. They concluded that the laminate structure of FRP tubes significantly

affects the interaction diagram. Type I tubes had higher effective elastic modulus in the hoop direction and significantly lower Poisson's ratio than Type II tubes, which resulted in better confinement as evident from the larger size of interaction curve and load-axial strain behaviour of the columns of Type I. In addition, for both concrete-filled thin and thick tubes, increasing the ratio of fibers in the axial direction significantly increases the flexural strength while increasing the ratio of fibers in the hoop direction would increase the axial strength of concrete-filled thin tubes only. The axial strength of concrete-filled thick tubes tends to increase by increasing the amount of fibers in the axial direction rather than in the hoop direction. In thick tubes, the contribution from axial stiffness of the tube is more significant than the gain from confinement of concrete. For small-thickness tubes, changing the proportion of fibers in the axial and hoop directions results in a family of interaction curves, intersecting at certain points, which provide an optimum laminate structure for a particular eccentricity for a given wall thickness. For relatively thick tubes, the interaction curves do not intersect and the optimum laminate seems to be the one with maximum axial stiffness and minimum hoop stiffness, regardless of the eccentricity.

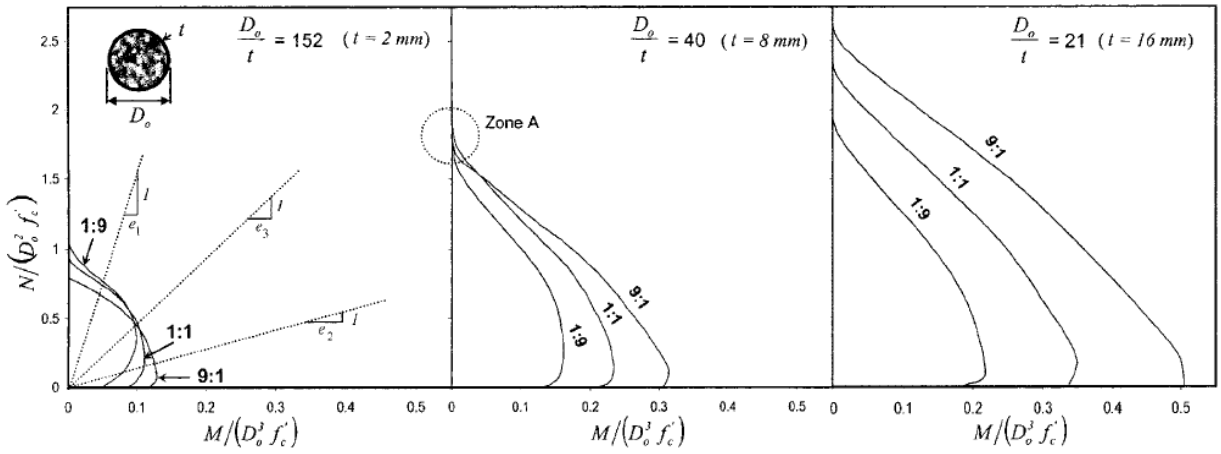

Figure 2.20: Normalized interaction diagram for concrete-filled FRP tubes of different thickness and laminate structures (Fam et al. 2003a)

Mohamed and Masmoudi (2008) investigated the performance of the CFFT columns under eccentric loads. The experimental program conducted on five unconfined concrete cylinders, two confined CFFT cylinders (152 x 305 mm), five CFFT columns, and two control steel spiral reinforcement concrete columns (152 x 912 mm). The internal diameter of the GFRP tubes which used in this investigation was 152 mm while the tube thickness was 2.70

mm and the fiber orientation mainly in the hoop direction (±60 degree). The composite FRP tubes were fabricated using the filament winding technique; E-glass fiber and Epoxy resin were utilized for manufacturing these tubes. The CFFT columns were loaded with different eccentricity 15, 30, 45 and 60 mm from the center of the columns. The results indicated that the behaviour of the concrete filled GFRP tubes is significantly affected by the eccentric load. The confinement provided by the GFRP tubes improves both the load-carrying capacity and the ductility of the concrete columns under concentric load. The stress-strain curve of the CFFT tube columns is bilinear and non-linear for the concentric and eccentric loading, respectively. Increasing the eccentricity values decrease the ultimate load capacity and increase the horizontal and axial deformation of the CFFT columns. The load-axial deflection curves and the load-horizontal deformation curves for the concentrically and eccentrically loaded CFFT columns are presented in Figure 2.21 and Figure 2.22, respectively.

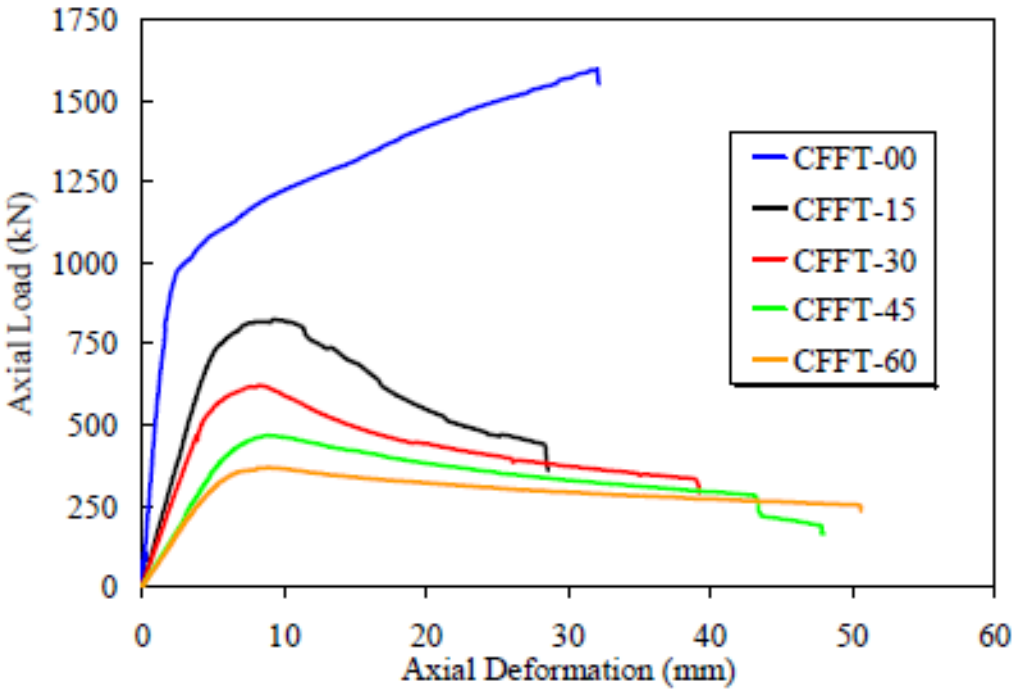

Figure 2.21: Load-axial deformation relationships (Mohamed and Masmoudi 2008)

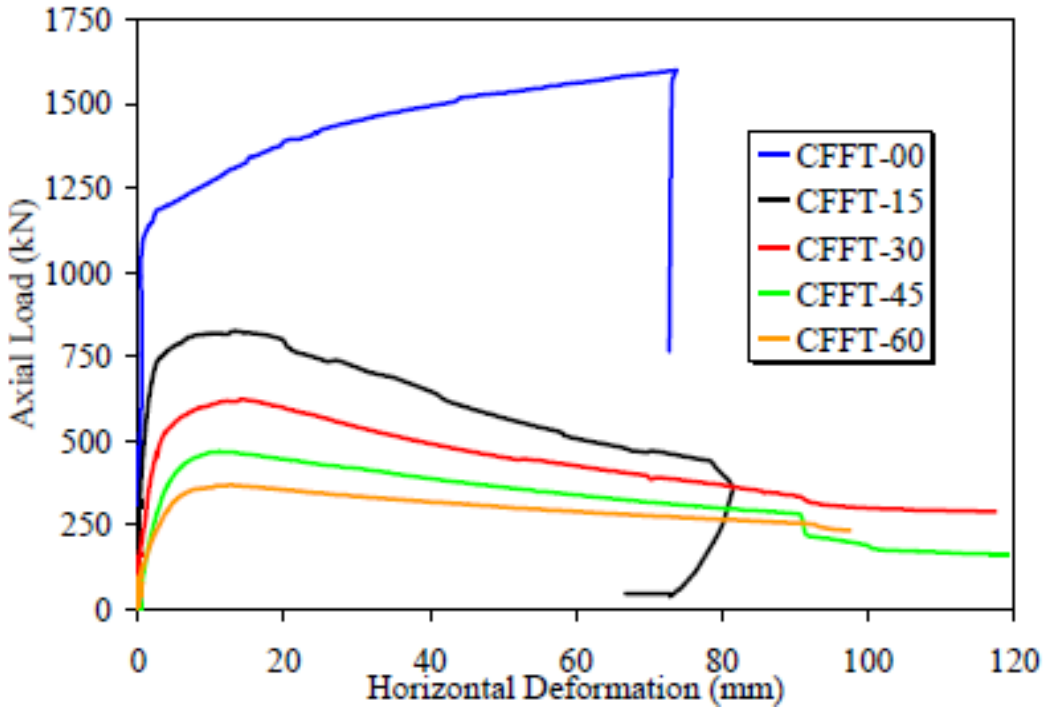

Figure 2.22: Load-horizontal deformation relationships (Mohamed and Masmoudi 2008)

2.6.1 Effect of loading tube axially

For an optimum use of the FRP tube in the hoop direction for confinement, some studies considered the case of applying the axial load to the concrete core only (Mirmiran and Shahawy 1997) (see Figure 2.23 a). In this case, slip could take place between the concrete and the outer tube, and consequently the member would not resist bending (Fam and Rizkalla 2001a). While axial loading of the tubes is often unavoidable due to friction, adhesion, and surface irregularities, which provide some axial load transfer to the shell, as shown in Figure 2.23 (b). Fam and Rizkalla (2001a&b) investigated the behaviour of concrete-filled (GFRP) tubes under axial compression loading conditions to simulate the practical applications to carry axial compression loads and possible bending moments. They concluded that ignoring the effect of axial loading of the tube in a concrete- filled GFRP tube under compression and assuming the development of the full hoop strength overestimates the confinement effectiveness. The tube is bi-axially loaded under the effect of axial compressive and hoop tensile stresses; therefore, the material strength is governed by the biaxial strength envelope (see Figure 2.23 c). In addition, loading the tube causes lateral expansion and results in less contact (confining) pressure with concrete.

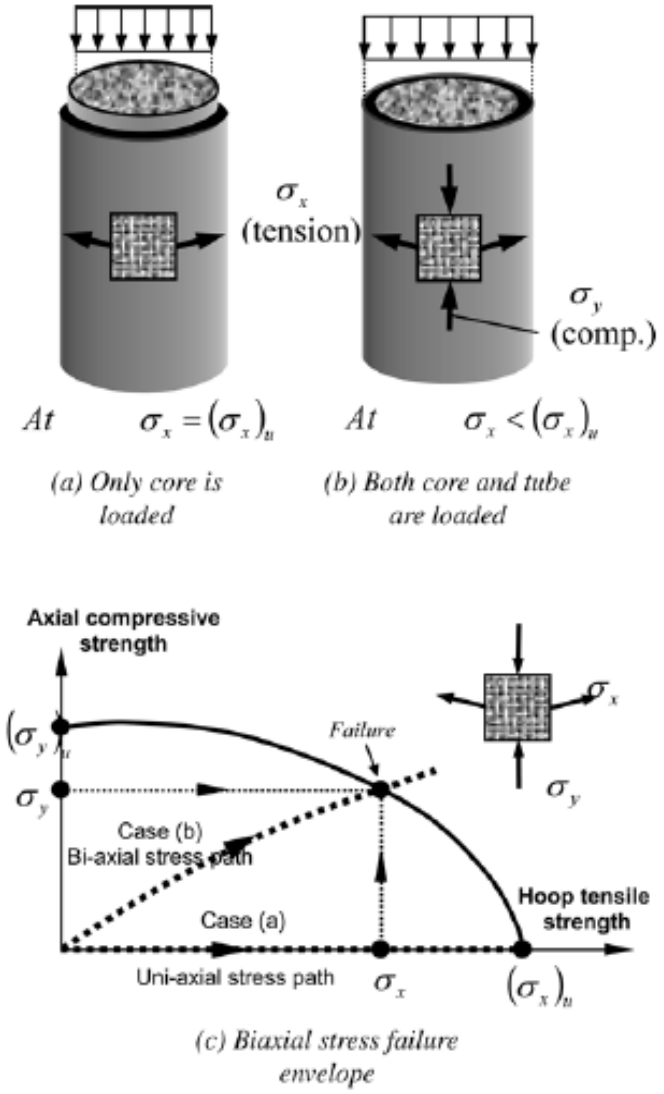

Figure 2.23: Effect of loading FRP tube axially (Fam and Rizkalla 2001 a&b)

2.6.2 Effect of central holes

Fam and Rizkalla (2001a) studied completely filled and partially filled GFRP tubes with a central hole as well as a tube-in-tube system with concrete filling between the two tubes. The GFRP tubes were designed to provide strength in both the axial and transverse directions and were axially loaded with the concrete core. The study showed that completely filled GFRP tubes provide the most effective confinement. Although an inner hole offers material saving and reduced self-weight, it reduces the confinement effect even though a high level of ductility is maintained; however, if the hole is maintained by an inner GFRP tube, the confinement effectiveness is improved and could approach that of a completely filled tube, depending on

the stiffness of the inner tube. The outer and inner tubes are subjected to hoop tensile and compressive stresses, respectively. In addition, stress-strain response of GFRP confined concrete is bilinear with the transition zone near the peak strength of the unconfined concrete. The slope of the second branch is governed by the stiffness of the tube as well as the inner hole size. Moreover, initiation of the confinement mechanism can be detected from the bilinear axial-lateral strain behaviour of the tube. The slope of the first part almost represents Poisson's ratio of the tube. A change of slope occurs when concrete expands, producing more lateral strains in the tube (see Figure 2.19). Figure 2.24 shows the effect of void size on confinement level of different column stubs.

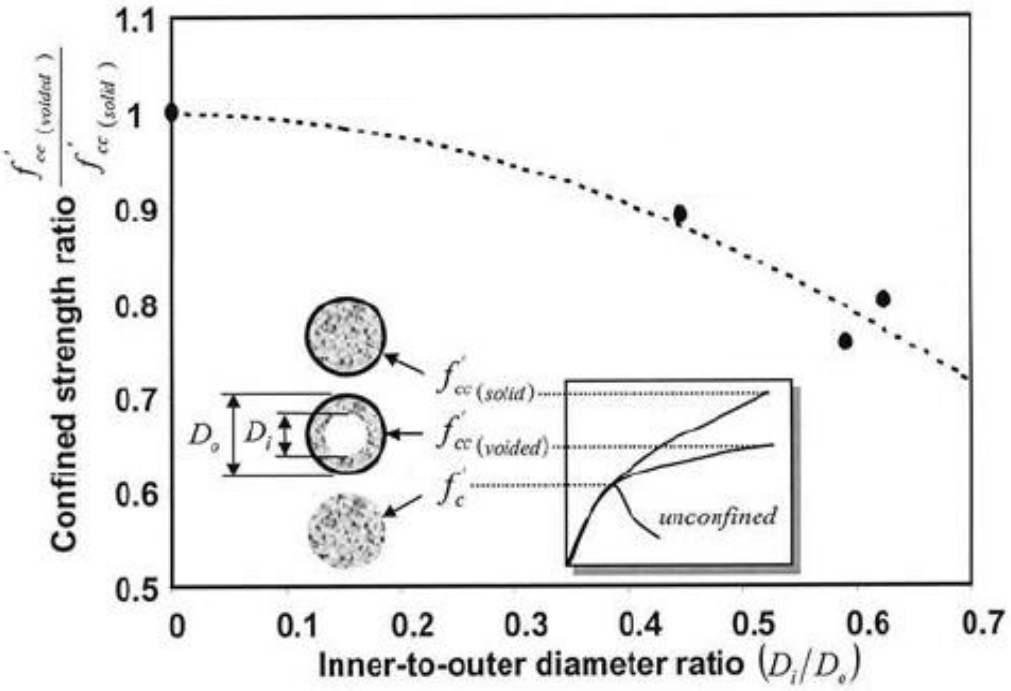

Figure 2.24: Effect of void size on confinement level (Fam and Rizkalla 2001a)

Lignola et al., (2007) conducted a study on hollow square columns wrapped with CFRP in the hoop direction and tested them under various eccentricities. The test results showed that horizontally oriented wraps could improve strength and ductility of hollow core square columns under eccentric loading. However, the strength enhancement was more pronounced for specimens loaded with a smaller eccentricity. Ductility increases with the increase of eccentricity. When eccentricity was larger, the increase in strength was reduced meanwhile the ductility increased.

Wong et al., (2008) tested a series of axial compression tests on short FRP-confined circular columns with an inner void to examine the behaviour of concrete in such FRP-confined annular sections. This study was motivated by the need to understand and model the behaviour of concrete in a new form of double-skin tubular columns (DSTCs) composed of a steel inner tube, an FRP outer tube, and a concrete infill between the two tubes. To this end, three types of specimens were tested: FRP-confined solid cylinders (FCSCs), FRP-confined hollow cylinders (FCHCs), and short DSTCs (cross-sectional shapes as shown in Figure 2.25). The main parameters examined include the section configuration, the void ratio, the diameter-to-thickness ratio of the inner steel tube, and the thickness of the FRP tube. Wong et al. concluded that the presence of an inner void reduces the effect of external FRP confinement, but this loss of confinement effectiveness can almost be completely compensated for through the provision of a suitable steel tube. In addition, the DSTCs were superior to FCHCs in both the general behaviour and the effectiveness of confinement of concrete. They declared that the inner steel tube plays an important role in preventing the concrete near the inner edge from inward spalling. Thus, the concrete in the new hybrid DSTCs is very effectively confined by the two tubes and local buckling of the inner steel tube is either delayed or suppressed by the surrounding concrete, leading to a very ductile response and increase in the strength of the concrete as a result of in the state of triaxial confinement. Moreover, they stated that the thickness of the outer FRP tube has a significant effect on the behaviour of concrete in FCSCs and DSTCs, but a smaller significant effect on the behaviour of concrete in FCHCs, especially when the void ratio is large.

Kusumawardaningsih and Hadi (2010) studied the effectiveness of FRP confinement on hollow high strength RC columns. Both circular and square columns with either circular or square hollow core were cast and tested under axial concentric loading. The FRP in the hoop direction was also used to wrap specimens in their experiment. It was found that FRP confinement increased the strength and ductility of hollow core high strength RC columns. Hollow core columns having circular holes showed better performance as compared to columns having square holes.

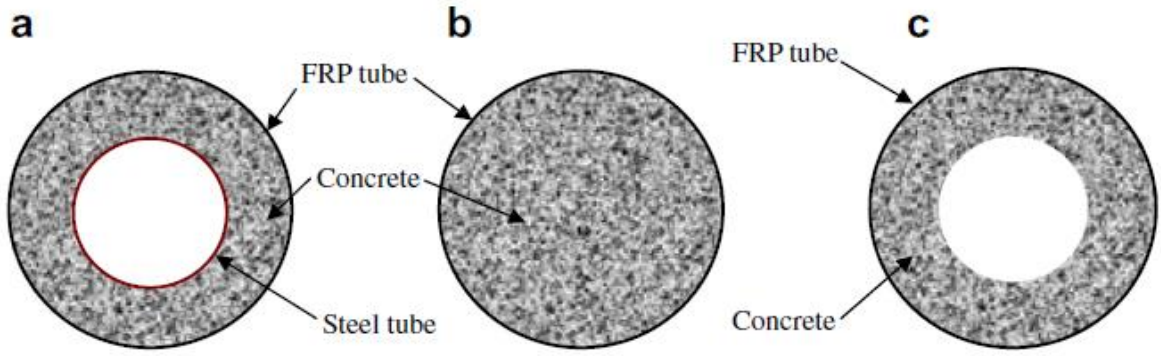

Figure 2.25: Cross-sections of (a) DSTCs, (b) FCSCs, and (c) FCHCs

2.6.3 Effect of tube stiffness on confinement

In 1997, Mirmiran and Shahawy tested concrete-filled GFRP tubes with different stiffnesses (Et/R) (Stubs 1, 2, 8, 11, and 12 as shown in Figure 2.26). The 152.5 x 305 mm stubs included GFRP tube with 1.3, 2.1, and 3.0 mm wall thicknesses, filled with 32 MPa concrete, and tested in compression by loading the concrete core only. The tubes consisted of a filament-wound angle ply of polyester resin with E-glass fibers at ±15 degrees with the hoop direction, resulting in elastic moduli of 37.2 to 40.7 GPa and strengths of 524 to 641 MPa in the hoop direction for the 1.3 to 3.0 mm thick tubes. The results of their study and other results reported in (Fam and Rizkalla 2001a) are presented in Figure 2.26. The figure shows the increase in the strength of confined concrete by increasing the stiffness of the tube. This could be achieved by using a higher thickness-diameter ratio or using GFRP tubes with higher elastic moduli in the lateral direction (Fam and Rizkalla 2001a). In addition, it is clearly shown that axially loaded GFRP tubes showed less confinement effectiveness under the same stiffness level. This is mainly attributed to the fact that the GFRP tubes expanded outward due to Poisson's ratio effect under their own share of axial load, which results in less contact pressure with concrete. Another factor is that the tubes were also bi-axially loaded under axial compression and lateral tension, which reduces their tensile strength in the hoop direction, whereas the GFRP tubes in (Mirmiran and Shahawy 1997) were fully utilized in the hoop direction under uniaxial tensile stresses, which allows the development of the full tensile strength as also described in Figure 2.23.

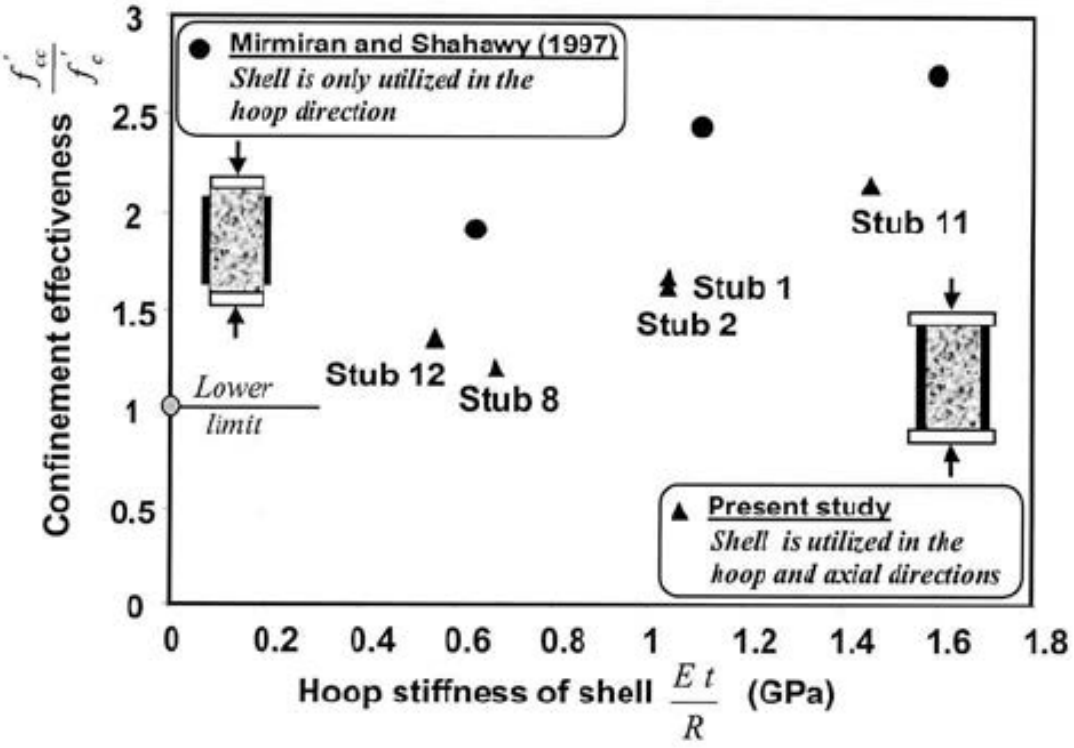

Figure 2.26: Effect of stiffness of tube on confinement effectiveness (Fam and Rizkalla 2001a)

2.6.4 Slenderness effect

Generally, the compression axially loaded CFT members can fail in two principal ways: in terms of slenderness and material properties. In the case of short columns, mechanical properties play an important role in their behaviour. The failure state is attained when the FRP tube reaches the maximum tensile strength of FRP and concrete crushing, which is known as a strength criterion. On the other hand, stability will essentially govern the ultimate load capacity of slender CFT columns, where the members are more likely to fail as a result of buckling and second-order effects becoming more critical (Sakino, 2006); therefore, the critical buckling load, P_{ct}, which represents the load at which slender column buckles is more crucial for the column. It can be seen that the stiffness fundamentally influences the column's strength more in slender columns, but that this is not the case for short columns where the strength is mainly depends on the material strength and cross-sectional area.

Mirmiran et al (1998) tested 24 circular CFFTs with three GFRP tube thicknesses of 1.45, 2.21, and 2.97 mm and four different lengths, *L,* including 305, 457, 610 and 762 mm to provide *(L/D)* ratios of 2:1 to 5:1 (within the range for short columns). The unconfmed

concrete strength was 44.8 MPa. Although some local buckling was observed, shear failure was noted as the primary mode of failure for the tubes. No overall buckling, as a result of slenderness, was noticeable since the length effects were insignificant within the range of *(L/D)* ratios studied, however, the ultimate strength was somewhat affected by the length. The strengths and strains at ultimate were normalized with respect to those of the 2:1 specimens and given in terms of *(L/D)* ratio in the following equations:

$$f_{cu}^{'} = f_{cu2:1}^{'}\left[0.028\left(\frac{L}{D}\right)^{2} - 0.263\left(\frac{L}{D}\right) + 1.418\right] \tag{2.14}$$

$$\varepsilon_{cu} = \varepsilon_{cu2:1}\left[0.0529\left(\frac{L}{D}\right)^{2} - 0.5214\left(\frac{L}{D}\right) + 1.8506\right] \tag{2.15}$$

Yuan and Mirmiran (2001) conducted a comprehensive parametric study which was carried out on the buckling of over 11 500 concrete-filled FRP tubes. Based on their study, they recommended that the current slenderness limit of 22 [as provided in CSA A23.3 (2014) and ACI 318 (2014)] for steel-reinforced concrete columns bent in single curvature be reduced to 11 for concrete-filled FRP tubes. A higher limit may be used for aramid tubes. Besides, they stated that the moment magnification method may be used for concrete-filled tubes, provided that the current stiffness reduction factor of 0.75 for steel-reinforced concrete sections be reduced based on the eccentricity ratio of the load and the modular ratio of the tube relative to concrete core.

Fitzwilliam and Bisby (2010) performed an experimental program to study the effects of slenderness on carbon FRP (CFRP) wrapped circular RC columns under eccentric axial loads. Eighteen circular RC columns with varying slenderness and CFRP strengthening schemes were tested to failure in monotonic eccentric axial compression. All columns were 152 mm in diameter and were reinforced internally with four D5 deformed steel bars (6.4-mm diameter) in the longitudinal direction and D5 closed circular steel ties spaced at 100 mm on center in the hoop direction. The cover was 25 mm to the longitudinal reinforcement. The internal reinforcement was chosen to simulate deficient columns with inadequate longitudinal reinforcement (a steel reinforcement ratio of only 0.7%) and with minimum hoop ties according to Canadian requirements (Canadian Standards Association (CAN/CSA 2005).

Figure 2.27 shows the effect of slenderness and CFRP warpped on peak load capacity. As shown in Figure 2.27 the slenderness effects were more significant for CFRP wrapped columns with higher levels of CFRP scheme on the confinement. The authors attributed that due to the flexure-dominated behaviour of the slender columns at high load levels, and to the fact that FRP hoop wraps do not increase the axial/flexural stiffness of the concrete at axial strains of less than about 0.2%. This highlights that engineers applying FRP strengthening in practice must take care to ensure that columns will not suffer instability under the envisioned increased service loads. On the basis of the tests presented herein, they concluded that CFRP hoop wraps increase the strength and deformation capacity of both short and slender circular RC columns, although the effects on strength are more significant for short columns and on deformability more significant for slender columns. The beneficial effects of CFRP confinement appear to be proportionally greater for RC columns subjected to mildly eccentric loads than for unreinforced columns subjected to concentric axial compressive loads. The specific reasons for this behaviour remain unknown; the writers have postulated that it may be influenced by an observed axial strain enhancement effect and by interactions between the CFRP wraps and the internal steel reinforcement (i.e., preventing buckling of the longitudinal reinforcing bars and spalling of the cover concrete). Longitudinal CFRP wraps can be used to improve the behaviour of slender CFRP wrapped circular concrete columns and allow them to achieve higher strengths, similar to equivalent short CFRP wrapped columns (although at larger lateral deflections). Longitudinal CFRP wraps appear to have no effect on the strength or deformation capacity of short columns.

Mohamed et al., (2010) conducted experimental and theoretical investigations on the buckling responses of axially loaded CFFT columns. The test results of this investigation contributed to understand the effect of the slenderness ratio on the critical buckling load of axially loaded CFFT columns. The effect of three parameters and the parameters' interaction on the buckling behaviour was investigated; namely, the FRP tube thickness, concrete compressive strength, and slenderness ratio. The experimental program consisted of testing 22 circular CFFT columns with a total height ranging from 305 to 1520 mm (12 to 60 in.) and an internal tube diameter of 152 mm (6 in.). The experimental results of this investigation showed that both the axial strength and stiffness of slender columns were increased as a result of the confining effect of the FRP tubes. The enhancement of the axial strength of the slender

columns was more pronounced for lower-strength concrete (30 MPa) than for higher-strength concrete (45 MPa). Furthermore, the uniaxial compressive strength of CFFT columns was reduced by 13 to 23% when the slenderness ratio increased from 4 to 20, depending on the concrete compressive strength and the thickness of FRP tubes. Besides, it was found that a slenderness ratio of 12 gave a safe value for design purposes. A more precise formula for the slenderness ratio, however, was proposed to control the buckling mode of failure.

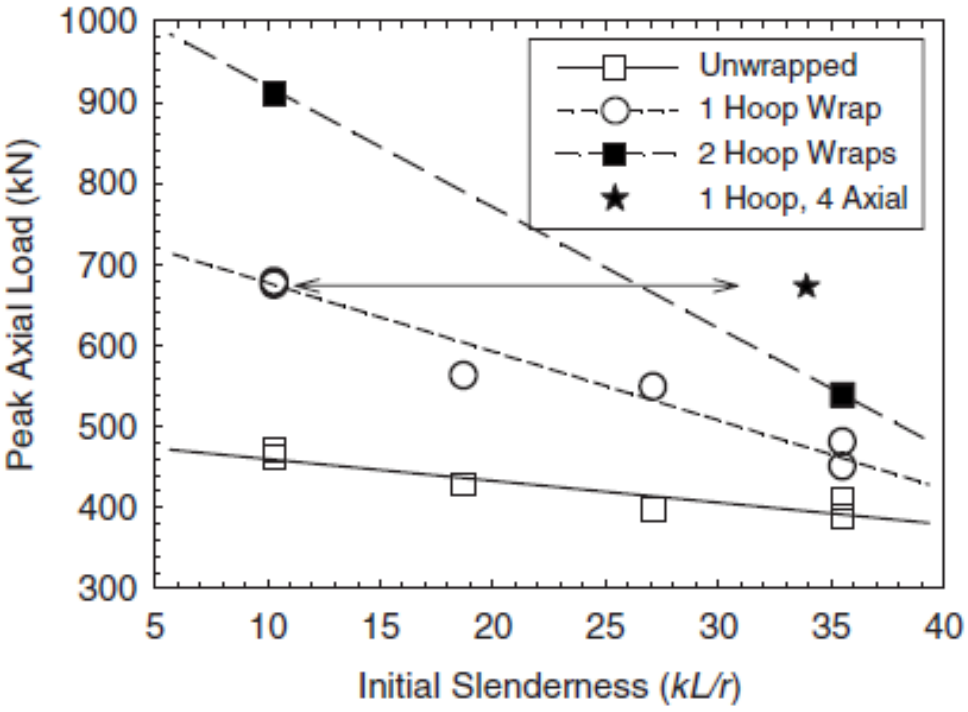

Figure 2.27: Effect of slenderness and CFRP warpping scheme on peak load capacity (Fitzwilliam and Bisby 2010)

Masmodui and Mohamed (2011) conducted an experimental investigation on the axial behaviour of CFFT columns internally reinforced with steel and/or CFRP bars with different slenderness ratios ranging from 4 to 20. The test results showed that the CFFT columns reinforced with CFRP bars behaved similar to that of CFFT columns reinforced with steel bars. The axial capacity of CFRP-reinforced CFFT resulted in 13%, 7%, 5% and 0% reduction as compared to steel-reinforced CFFT columns that had slenderness ratios 8, 12, 16 and 20, respectively.

Jiang and Teng (2013) conducted a systematic theoretical study to examine the behaviour of slender FRP-confined circular RC columns. The numerical investigation is exclusively studied for hinged columns with equal end eccentricities (i.e., standard hinged columns) and employs the assumption that the deflected shape of the column is a half-sine wave. Based on the numerical results, they concluded that the effectiveness of FRP confinement decreases as the column becomes more slender, which confirms existing experimental observations. While a high level of confinement can greatly enhance the compressive strength of concrete, it may lead to excessive lateral deflections that are not acceptable in practical design. The aforementioned results drew the conclusion that the increase of the slenderness ratio of CFFT columns reinforced internally with steel or FRP bars might be a critical factor that controls the mode of failure and might prevent such columns from attaining their ultimate load capacity.

2.6.5 Bond effects

Bond between the FRP jacket and the concrete core is more pronounced in flexural members than it is for axial members, and can be achieved by using adhesive or mechanical shear connectors. Mirmiran et al. (1998) tested square CFFTs, with shear connector ribs in the axial and transverse directions, under axial compression. The effect of bond was investigated, however, with the exception of three-square specimens, all circular specimens were fabricated by wrapping concrete cylinders, rather than filling prefabricated FRP tubes. Nevertheless, adhesive bonding had little effect on the confining pressure of the circular specimens, whereas mechanical bond (shear connectors) helped to distribute pressure more evenly around the square specimens and minimizing the stress concentrations at the corners, thus increasing its confining effect. Longitudinal ribs increased the buckling and compressive resistance. The horizontal ribs helped to maintain the cross-sectional shape of the skin and helped the shell in resisting hoop stresses. This study concluded that, whereas adhesive bond does not affect the load-carrying capacity of FRP-confined concrete, mechanical bond significantly improves the performance of the section. Fam and Rizkalla (2001b) have shown that, for circular CFFTs under axial compression, the confinement effect is higher if the tube is not loaded axially, which can be achieved by debonding and loading the core only while the interface condition effect had an insignificant effect on the behaviour, yet the maximum strength was not affected.

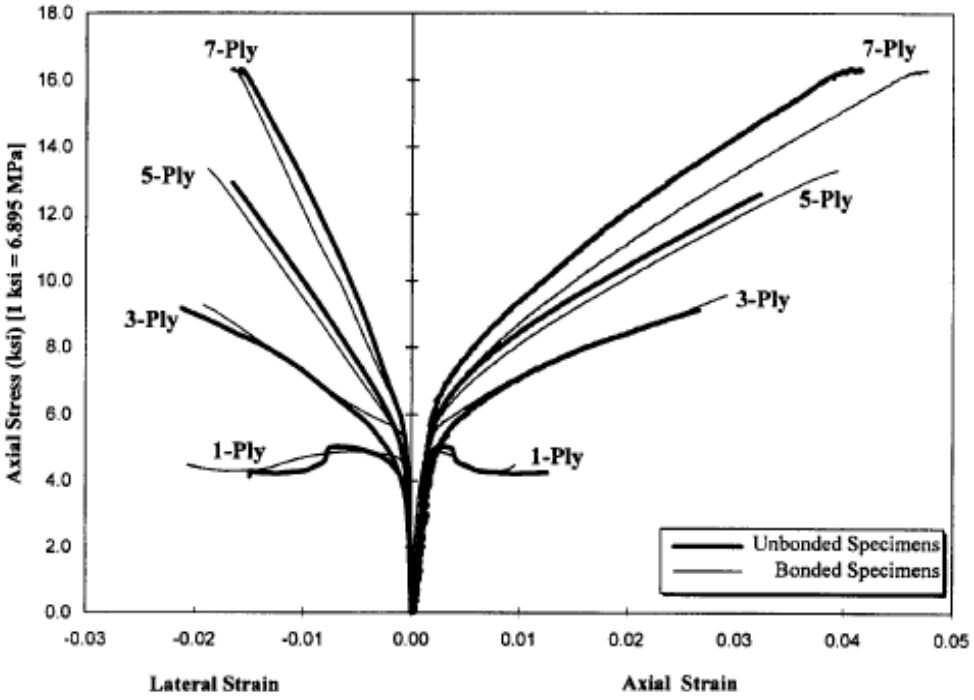

Figure 2.28: Biaxial stress-strain curves for bond effect specimens with multilayer shells (Mirmiran et al. 1998)

2.6.6 Effect of geometry and cross-section configuration

Mirmiran et al. (1998) reported twelve 152.5x152.5x305 mm concrete filled GFRP tubes with square cross section including round corners of 6.35 mm radius with three varying wall thicknesses using 6, 10, and 14 plies. The tubes were filament-wound E-glass with polyester resin wound at ±75 degrees with respect to the vertical axis. The unconfined concrete strength was 40 MPa and the axial compression load was applied on the concrete core only. Figure 2.29 shows the normalized stress-strain response of the square specimens, compared to the 152.5 mm diameter circular specimens with similar jackets, but using 30 MPa concrete. Unlike the circular sections, the ultimate strength of square sections is lower than their peak strength and stabilizes at about 70 percent of the peak strength, regardless of the tube thickness. The circular specimens failed by rupture of fibres near mid-height in the hoop direction whereas, in square tubes, significant load drop occurs after the peak strength is reached accompanied by noise. The specimens eventually failed due to stress concentration at the comers. Results showed that circular shaped tubes have a little more than twice the confining effectiveness of square cross-sections in terms of their ultimate compressive

strengths. This was explained by the uniform pressure exerted by circular tubes as opposed to the varying pressure from corner to edge, typically found in square sections (see Figure 2.29).

Rochette (1996) conducted a similar study using 33 specimens including circular, square, and rectangular cross sections, different fibres including carbon and aramid, different corner radius, different concrete strengths, 29 to 44 MPa, and different number of plies, 2 to 5 plies for carbon and 3 to 12 plies for aramid. Rochette concluded that the comer radius of the tube affects its confinement effectiveness. Using this data, Mirmiran et al (1998) introduced a modified confinement ratio MCR defined as follows:

$$MCR = \left(\frac{2R}{D - t_j} \right) \frac{f_r}{f_c'} \tag{2.16}$$

Where R is the comer radius, D is the average diameter of the tube and f_r is the confinement pressure given by:

$$f_r = \frac{2 f_j t_j}{D - t_j} \tag{2.17}$$

Where f_j is the hoop strength of the tube. f_r/f'_c is the confinement ratio for circular sections. The ratio of ultimate strength to peak strength of the confined concrete, f_{cu}/f'_{cc} was correlated to MCR for the specimens tested by Rochette (1996) as well as the square specimens tested by Mirmiran et al. (1998) as follows:

$$\frac{f'_{cu}}{f'_{cc}} = 0.169 \ln MCR + 1.32 \Rightarrow \text{ for MCR} < 0.15 \tag{2.18}$$

The MCR dictates whether or not a post peak descending part will be present in the response curve. The correlation indicated that for MCR less than 15 percent, the jacket is not very effective in confining the concrete core. There may be additional ductility due to crack opening containment, but no strength enhancement should be expected.

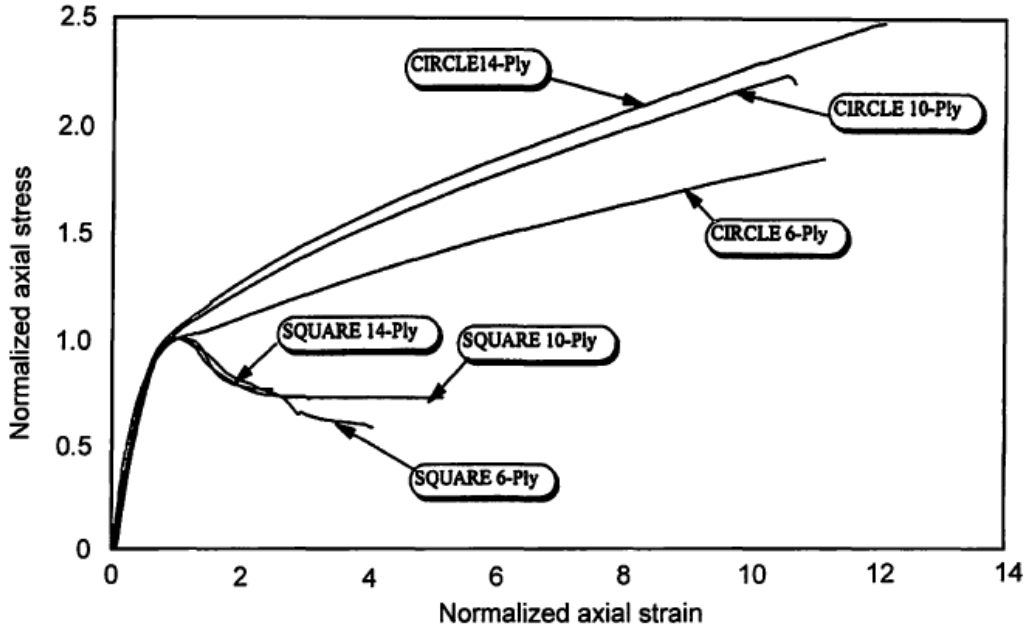

Figure 2.29: Normalized stress-strain curves of concrete-filled GFRP circular and square tubes (Mirmiran et al. 1998)

Fam et al. (2005) tested five concrete-filled rectangular FRP tubes (CFRFT) short columns under eccentric and concentric axial compression loads. The short columns were tested under eccentricity ratios (e/h) of 0, 0.09, 0.18, and 0.24, where h is the section depth. Based on this experimental investigation they concluded that CFRFT provides feasible and easy ways to construct structural members for beam and column applications. The FRP tube provides permanent formwork and is the sole reinforcement for concrete in the axial and transverse directions. Unlike steel tubes, strength and stiffness of FRP tubes can be controlled independently in the flanges and webs and also in both directions. Furthermore, the laminate stress–strain behaviour of FRP tubes could be quite nonlinear. Laminates with fibers oriented at ±45° show significant nonlinearity under tension and compression. Nonlinearity could also result from progressive failure of layers oriented at various directions. Short CFRFT columns loaded over the entire cross section could fail in a brittle manner by fracture of the FRP tube at the round corner, due to a high level of biaxial stresses while the round corners of CFRFT columns provide limited confinement. The flat sides of the FRP tube bend outwards and cause the column to bulge and the concrete core to lose restraint. Consequently, the confinement effect is further reduced.

Ozbakkaloglu and Oehlers (2008) conducted axial compression tests to investigate confinement effectiveness of rectangular FRP tubes with various arrangements. The tubes were designed as column confinement reinforcement and were manufactured using unidirectional carbon fiber sheets. The effects of the tube corner radius and the presence of internal FRP reinforcement were investigated experimentally. The results of the experimental investigation indicated that confinement of rectangular columns with FRP tubes lead to substantial improvement in the ductility of the columns. Confinement provided by the FRP tube may also improve the axial load-carrying capacity of the columns if the confinement effectiveness of the FRP tube is sufficiently high. The authors also studied the corner radius of the FRP tube they found that the corner radius has a significant influence on the confinement effectiveness of the rectangular FRP tubes while the effectiveness of confinement increases with the corner radius. Furthermore, the corner radius has a direct influence on the trend of the second branch of the stress–strain curve of confined concrete, and hence on the ultimate strength of confined concrete. On the other hand, the distribution of transverse strains along the perimeter of FRP-confined concrete columns is significantly affected by both the corner radius of the column and existence of internal FRP reinforcement. The uniformity of the distribution increases with corner radius and the use of internal transverse FRP reinforcement.

An experimental study on the behaviour of square and rectangular high-strength concrete (HSC)-filled (FRP) tubes (HSCFFT) under concentric compression were performed by Ozbakkaloglu (2013). The effects of the tube thickness, sectional aspect ratio, and corner radius on the axial compressive behaviour of (CFFTs) were investigated experimentally through the tests of 24 CFFTs that were manufactured using unidirectional carbon fiber sheets and high-strength concrete with 78 MPa average compressive strength. First and foremost, test results indicated that sufficiently confined square and rectangular HSCFFTs can exhibit highly ductile behaviour. The results also indicated that confinement effectiveness of FRP tubes increases with an increase in corner radius and decreases with an increase in sectional aspect ratio (long to short column sides). Both of these parameters significantly influence the overall trend of the second portion of the stress strain relationship of HSCFFTs. Increased corner radius improves the overall trend of this region, but may result in a reduced ultimate axial strain. An increase in sectional aspect ratio may also lead to a decrease in the ultimate strain. It is also observed that HSCFFTs having tubes of low confinement effectiveness may experience

a significant strength loss at the point of transition on their stress-strain curves. For rectangular HSCFFTs develop higher hoop strains along their short-spans than their long-spans at ultimate. The ratio of the short-to-long span strains increase with an increase in the aspect ratio. Furthermore, it is found that the behaviour of HSCFFTs at this region differs from that of normal-strength CFFTs and that it is more sensitive to the effectiveness of a confining tube.

2.6.7 Nature of loading (monotonic and cyclic)

An experimental study has been conducted by Ozbakkaloglu and Akin (2012) on the behaviour of FRP-confined normal- and high-strength concrete (NSC and HSC) under axial compression. A total of 24 aramid and carbon FRP-confined concrete cylinders with different concrete strengths and FRP jacket thicknesses were tested under monotonic and cyclic loading. The test results have also been compared with two cyclic axial stress-strain models for FRP-confined concrete. On the basis of the results, they concluded that the stress-strain curve envelope of cyclically loaded FRP confined concrete closely follows the stress-strain curve of the same concrete under monotonic loading. This is shown to be true for CFRP-confined HSC and AFRP-confined NSC and HSC. While the residual plastic strain of FRP-confined concrete is linearly related to the envelope unloading strain, and this relationship does not appear to be influenced significantly by (1) the amount of confinement; (2) the type of FRP; or (3) the unconfined concrete strength.

In general, they reported that the presence of unloading/reloading cycles leads to an increase in the ultimate strength and strain of FRP-confined concrete. For a given actual confinement ratio ($f_{lu,a}/f'_{co}$), both the strength-enhancement and strain-enhancement ratios decrease with the increase of unconfined concrete strength. Furthermore, the average hoop-rupture strain $\varepsilon_{h;rup}$ also decreases with increasing unconfined concrete strength. Therefore, direct application of the existing FRP-confined concrete stress-strain models to FRP-confined HSC can lead to significant overestimation of the ultimate condition of FRP-confined HSC. Concrete experiences a similar level of strength enhancement when confined with AFRP and CFRP jackets that provide the same actual confining pressure $f_{lu,a}$. On the other hand, the ultimate strain of the same concrete increases more significantly through AFRP confinement. In addition to the general conclusions of the experimental study reported in this paper, the

following observations can be made on the basis of the comparison of the test results of the present study with two cyclic axial stress-strain models for FRP-confined concrete:

a) The axial cyclic stress-strain model proposed by Lam and Teng (2009) is highly accurate in predicting both the unloading and reloading paths of FRP-confined NSC. The model closely predicts the shapes of the unloading and reloading curves and accurately estimates the plastic strains. When the model is applied to HSC specimens, on the other hand, the model predictions deviate significantly from the experimental results; this is caused largely by the inaccuracies in the calculation of the plastic strains of FRP-confined HSC.

b) Comparisons between the results of the present study and the predictions of the cyclic stress-strain model proposed by Shao et al. (2006) indicated that this model predicts the reloading paths reasonably accurately, but consistently overestimates the residual plastic strains and does not accurately capture the shape of the unloading paths.

2.6.8 Effect of unconfined concrete strength (f'_c)

Mandal et al. (2005) evaluated the effect of the unconfined concrete strength ($f'c$) ranging from 26 to 81 MPa on confinement effectiveness (f'_{cc}/f'_c) of FRP circular jackets in axial concrete members. On the basis of the experimental results they concluded that in general the confinement effectiveness reduces with an increase in the unconfined concrete strength for concrete-filled FRP tubes cylinders while the modulus, thickness, and tensile strength of the FRP jacket in the hoop direction significantly influence the confinement effectiveness for low- and medium-strength concrete. Moreover, the study showed that FRP tubes provide a substantial increase in strength and ductility for low- to medium-strength concrete, which shows a bilinear stress-strain response with strain hardening and the slope of the second linear part of the curve depends on the modulus and thickness of the FRP jackets. For high-strength concrete, however, enhancement in strength is very limited, with hardly any improvement in ductility. The response in this case shows a steep post-peak strain softening.

Ozbakkaloglu and Vincent (2013) presented an experimental study on the axial compressive behaviour of 83 monotonically loaded circular CFFTs. The effects of fiber type, concrete strength, specimen size, and manufacturing method on the compressive behaviour of CFFTs were investigated. The CFFTs were manufactured with (CFRP), high-modulus CFRP

(HMCFRP), or aramid FRP (AFRP) tubes, and their average unconfined concrete strengths ranged between 34–110 MPa. The diameters of the test specimens ranged from 75–300 mm with all specimens maintaining a 2:1 height-to-diameter ratio. The effect of the CFFT manufacturing method was investigated through AFRP specimens that were manufactured through either an automated filament winding or manual wet layup technique. The results clearly indicate that over a certain confinement threshold, high-strength CFFTs (HSCFFTs) exhibit a highly ductile behaviour. However, for the same nominal confinement ratio, compressive behaviour of CFFTs degrades as concrete strength increases while the behaviour of these CFFTs is highly sensitive to the level of confinement, and lightly confined HSCFFTs may not be able to maintain their load-carrying capacity after their initial peak strengths are attained. In addition, FRP tubes manufactured automatically by using a filament winding technique provide greater strength and strain enhancement ($f'_{cc}=f'_{co}$ and $\varepsilon_{cu}=\varepsilon_{co}$) for CFFTs compared with tubes manufactured manually using a wet layup process.

An experimental investigation has been conducted by Vincent and Ozbakkaloglu (2013a) on the effect of concrete compressive strength and confinement method on confined high and ultra-high-strength concrete (HSC and UHSC) specimens. A total of 55 (FRP) confined concrete specimens were tested under monotonic axial compression. All specimens were cylinders with 152 mm in diameter and 305 mm in height and confined by (CFRP). Three different concrete mixes were examined, with average compressive strengths of 35, 65, and 100 MPa. The effect of the confinement method was also examined with FRP wrapped specimens compared to FRP tube encased specimens. The results of this experimental study indicated that above a certain confinement threshold, FRP-confined HSC and UHSC exhibits highly ductile behaviour, however for the same normalized confinement pressures, axial performance of FRP-confined concrete reduces as concrete strength increases. While at the same actual confinement ratios ($f_{lu,a}/f'_{co}$), strength enhancement (f'_{cc}/f'_{co}) and strain enhancement ratios ($\varepsilon_{cu}/\varepsilon_{co}$) increase as the in-place concrete compressive strength (f'_c) decreases. The results also indicated that ultimate conditions of FRP-wrapped specimens were similar to those confined by FRP tubes; however, a performance difference is evident at the transition region. Furthermore, the authors reported that the performance of the existing stress–strain models of FRP confined concrete degrades significantly, in predicting both the ultimate strength and strain, when they are applied to HSC or UHSC. None of the assessed

models is able to provide sufficient accuracy in predicting the ultimate conditions of FRP-confined HSC and UHSC, with the majority of them significantly overestimating both the strength and strain enhancement ratios.

2.6.9 Fibre orientation and type

Hong and Kim (2004) performed both experimental and analytical investigations of axial behaviour of large-scale circular and square concrete columns confined by carbon composite tubes. The specimens were filament-wound carbon composite with 90° + 90°, 90° ± 60°, 90° ± 45°, and 90° ± 30° winding angles with respect to a longitudinal axis of a tube. The influence of transverse dilation, winding angle, thickness of a tube, as well as shape of the column section on stress–strain relationships of the confined columns is discussed. They reported that the strength of the confined concrete increases drastically as the winding angle is oriented toward circumferential direction of tubes like CFCT with 60° winding angle. The maximum confinement was obtained from the specimen with a winding angle of 90° ± 60°. Moreover, the stress–strain relationship of circular columns is characterized by bilinear response with mild softening of axial response. However, the stress–strain response of square columns is represented by bilinear stress–strain relationship with both sharp softening response and distinct transition.

Vincent and Ozbakkaloglu (2013b) conducted an experimental investigation on the effect of fiber angle and specimen end condition on axial compressive behaviour of (FRP)-confined concrete. A total of 24 (AFRP)-confined concrete specimens with circular cross-sections were tested. 18 of these specimens were manufactured as concrete-filled FRP tubes (CFFTs), whereas the remaining 6 specimens were FRP-wrapped concrete cylinders. The specimens were manufactured using two different concrete mixes with average compressive strengths of 50 (NSC) and 80 MPa (HSC). The influence of fiber orientation was examined through a group of CFFT specimens manufactured using an automated filament winding technique, with fibers aligned at 45, 60, or 75 degrees with respect to the longitudinal axis. Additional filament wound specimens with fibers aligned along the hoop direction were also prepared to allow a comparison between specimens with inclined fibers and hoop oriented fibers.

The authors presented the influence of fiber orientation on the axial stress–strain curves in Figure 2.30. As shown in the figure the specimens that displayed descending branches had their ultimate conditions defined when the axial stress dropped below a threshold of $0.8f'_{cc}$. This region is represented by dashed lines in Figure 2.30. It can be clearly seen in this comparison that an increase in fiber inclination results in an improved axial stress–strain behaviour. It can also be seen in Figure 2.30 that specimens with fibers partially aligned in the axial direction (i.e., 45, 60, and 75 degrees orientations) can exhibit regions of unstable strength loss and plateau due to the gradual rupture of the fibers that leads to a progressive failure of the specimen.

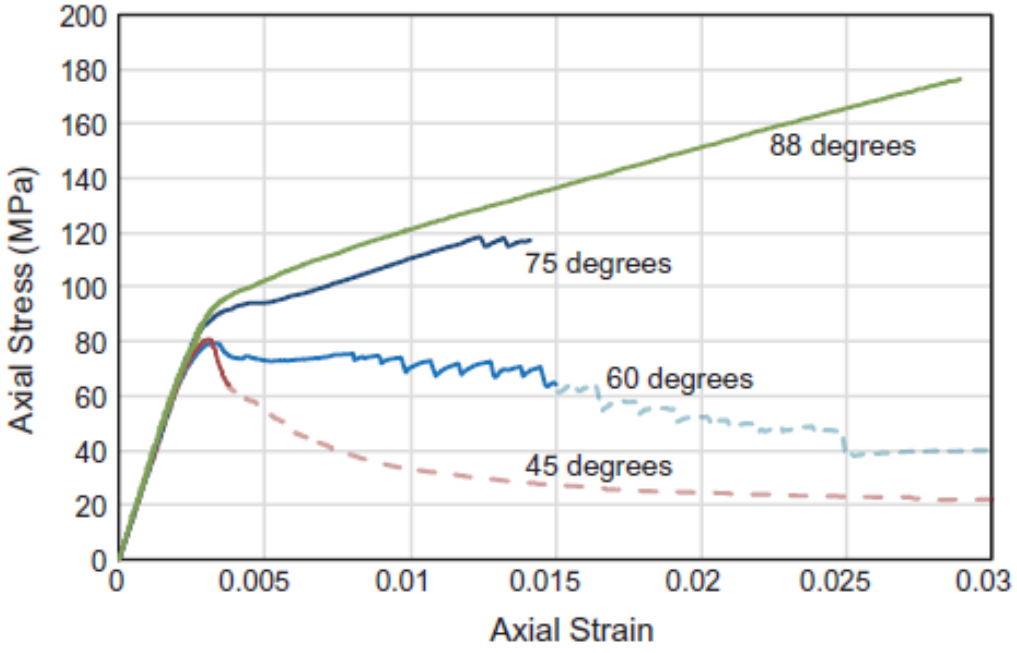

Figure 2.30: Influence of fiber orientation on axial stress-strain behaviour of CFFTs (Vincent and Ozbakkaloglu 2013b)

Figure 2.31 illustrates the influence of fiber angle on axial stress-orientation strain relationship for specimens with inclined fibers. It can be seen in the figure that substantial differences exist between the relationships of specimens with different fiber orientations, with only the specimens with hoop-oriented fibers developing orientation strains close to ultimate tensile strain of the fibers (ε_{fu}). This observation further indicates that fibers used for FRP-confinement of concrete are most effective when aligned in the hoop direction, with fiber efficiency reducing significantly with an increase in fiber alignment with respect to the hoop

direction. In addition, they concluded that adequately confined (HSC) can exhibit highly ductile behaviour. While confinement method has no significant influence on axial stress–strain behaviour of FRP-confined concrete, with FRP wrapped specimens performing similar to CFFTs. However, it was observed that FRP-wrapped specimens developed slightly higher ultimate strains (ε_{cu}) and slightly lower peak stresses (f'_{cc}) than companion CFFTs.

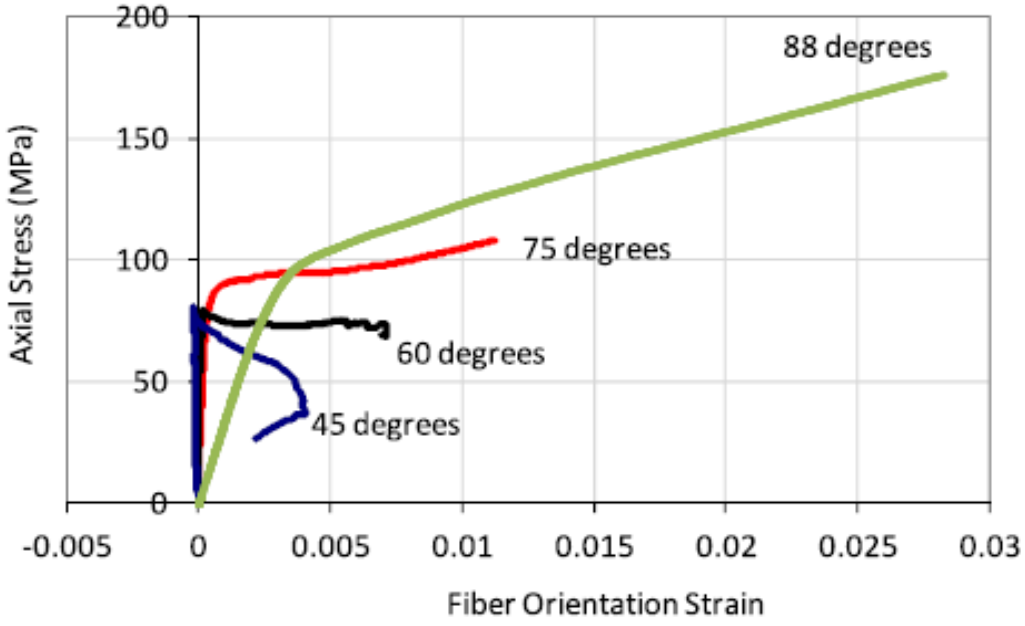

Figure 2.31: Variation of axial stress-fiber orientation strain relationships with fiber orientation (Vincent and Ozbakkaloglu 2013b)

Hadi and Le (2014) tested twelve hollow core square reinforced concrete columns wrapped with (CFRP). The effect of fibre orientation on the performance of specimens under concentric and eccentric loads was investigated. Twelve specimens (200 mm x 200 mm in cross-section, 800 mm in height and having an 80 mm square hole) were divided into four groups with three specimens each. The specimens in the first reference group were unwrapped, while the specimens in the remaining groups were wrapped with CFRP of different wrap combinations of three fibre orientations (0º, 45º, and 90º with respect to the circumferential direction). The specimens in each group were tested under three eccentricities: 0 (concentric), 25, and 50 mm up to failure. The test results showed that the fibre in the hoop direction can significantly increase the ductility of hollow core square reinforced concrete columns under concentric or eccentric loading. Compared to VHF (vertically wrapped with one CFRP layer along the specimen's axial axis) and AHF (wrapped with two CFRP layers oriented at ±45º

with respect to specimen's axial axis, and then horizontally wrapped with one layer of CFRP) columns, HF (laterally wrapped with three CFRP layers with respect to the specimen's axial axis) columns can sustain much larger deformation before failure. However, the increment of the compressive strength of FRP-confined hollow core columns is marginal. Furthermore, columns were tested under eccentric loading; the contribution of vertical and ±45° angle layers was evident in resisting the bending moment. This contribution was more noticeable as the eccentricity increased. In fact, specimens AHF-50 (eccentricity=50 mm) and VHF-50, which were wrapped with one and two hoop CFRP layers gained maximum axial load even greater than that of Specimen HF-50, which was wrapped with three CFRP layers in the hoop direction. Finally, all of the three wrapping combinations used in this study increased the performance of hollow core square columns. The enhancement in ductility was more evident than the enhancement in strength for all types of wrapping, in particular for columns wrapped with only hoop-oriented layers.

2.7 Codes and Guidelines

2.7.1 CSA approach [S806-12]

The factored axial load resistance P_r of the confined columns provided by CAN/CSA-S806-(2012) building code is equals:

$$p_r = 0.85\left[\alpha_1\varphi_c f'_{cc}\left(A_g - A_s\right) + \varphi_s f_y A_s\right] \tag{2.19}$$

where the material resistance factors are equal k_e=0.85, ϕ_c=0.60, ϕ_s=0.85 and ϕ_{FRP}=0.75. The CAN/CSA-S806 (2012) uses (Eq. 2.20) to evaluate the confined concrete compressive strength f'_{cc}

$$f'_{cc} = 0.85 f'_c + k_l k_c f_l \tag{2.20}$$

where k_l=6.7(f_l)$^{-0.17}$, and factor k_c accounts for the shape of the cross section, which is equal to 1.0 for circular section and 0.4 for square and rectangular section. The CAN/CSA-S806 (2012) limits the FRP hoop strain to 0.006 times its elastic modulus E_f.

$$f_l = \frac{2n_F t_F f_F}{D} \tag{2.21}$$

where f_F = the smaller of $0.006E_f$ or $\phi_f f_{fu}$

2.7.2 CSA approach [CSA-S6-06]

According to the Canadian Highway Bridge Design Code (CAN/ CSA-S6-06), the factored axial load resistance P_r of a confined column is given by the following equation:

$$p_r = k_e\left[\alpha_1\varphi_c f_{cc}^{/}\left(A_g - A_s\right) + \varphi_s f_y A_s\right] \tag{2.22}$$

where k_e=a strength reduction factor applied for unexpected eccentricities, which equal to 0.80, and ϕ_c=0.75, ϕ_s=0.9 where ϕ_c and ϕ_s =material resistance factors for concrete and steel, respectively. The value depends on the unconfined concrete compressive strength α_1=0.85–0.0015 $f_c^{/} \geq 0.39$.

The compressive strength of the confined concrete $f_{cc}^{/}$ shall be calculated as follows:

$$f_{cc}^{/} = f_c^{/} + 2f_{lFRP} \tag{2.23}$$

$$f_{lFRP} = \frac{2t_{FRP}\phi_{FRP}f_{FRPu}}{D} \tag{2.24}$$

where ϕ_{FRP}=0.65=material resistance factors for FRP. The CAN/CSA-S6-06 limits the confinement pressure f_{lFRP} at the ultimate limit state (ULS) that shall be designed to be between $0.1f_c^{/}$ and $0.33f_c^{/}$. Note that Eq. 2.22 to Eq. 2.24 is valid only for concrete strength less than 50 MPa.

2.7.3 ACI approach [ACI-440.2R-08]

Strengthening by FRP jackets of RC members subjected to axial force or combined axial and bending forces is presented in Chapter 12 of ACI-440.2R-08. Equations for the axial compressive strength of a non-slender, normal-weight concrete member confined with an FRP jacket using the confined concrete strength are presented as follows:

For members subjected to axial force:

- For non-prestressed members with existing steel spiral reinforcement

$$\varphi p_n = 0.85\varphi\left[0.85 f_{cc}^{/}\left(A_g - A_{st}\right) + f_y A_{st}\right] \tag{2.25a}$$

While for spiral columns ϕ=0.75. Where the axial force acting on an FRP-strengthened concrete member should be computed using the load factors required by ACI 318-11 (2011), and the axial compression strength should be calculated using the strength reduction factors ϕ for spiral and tied members required by ACI 318-11 (2011).

- For non-prestressed members with existing steel-tie reinforcement

$$\varphi p_n = 0.8\varphi\left[0.85 f_{cc}^{/}\left(A_g - A_{st}\right) + f_y A_{st}\right] \tag{2.25b}$$

for tied columns ϕ=0.65.

The stress-strain model by Lam and Teng (2003) for FRP-confined concrete has been adopted by the (ACI 440.2R-08) (see Figure 2.32) and computed using the following expressions:

$$f_c = \begin{cases} E_c\varepsilon_c - \dfrac{\left(E_c - E_2\right)^2}{4 f_c^{/}}\varepsilon_c^2 & 0 \le \varepsilon_c \le \varepsilon_t^{/} \\ f_c^{/} + E_2\varepsilon_c & \varepsilon_t^{/} \le \varepsilon_c \le \varepsilon_{ccu} \end{cases} \tag{2.26a}$$

$$E_2 = \frac{f_{cc}^{/} - f_c^{/}}{\varepsilon_{ccu}} \tag{2.26b}$$

$$\varepsilon_t^{/} = \frac{2 f_c^{/}}{E_c - E_2} \tag{2.26c}$$

The maximum confined concrete compressive strength f'_{cc} is based on a model proposed by Lam and Teng (2003) as follows:

$$f_{cc}^{/} = f_c^{/} + \Psi_f 3.3 k_a f_{lFRP} \tag{2.27}$$

Where $f_c^{/}$ is the unconfined cylinder compressive strength of concrete, Ψ_f (an additional reduction factor) = 0.95 and the efficiency factor (κ_a) accounts for the geometry of the section, circular, and noncircular. For circular columns (κ_a) = 1 while for noncircular columns the

shape factors (κ_a) depend on two parameters: the cross-sectional area of effectively confined concrete A_e, and the side-aspect ratio h/b,

$$k_a = \frac{A_e}{A_c}\left(\frac{b}{h}\right)^2 \tag{2.28}$$

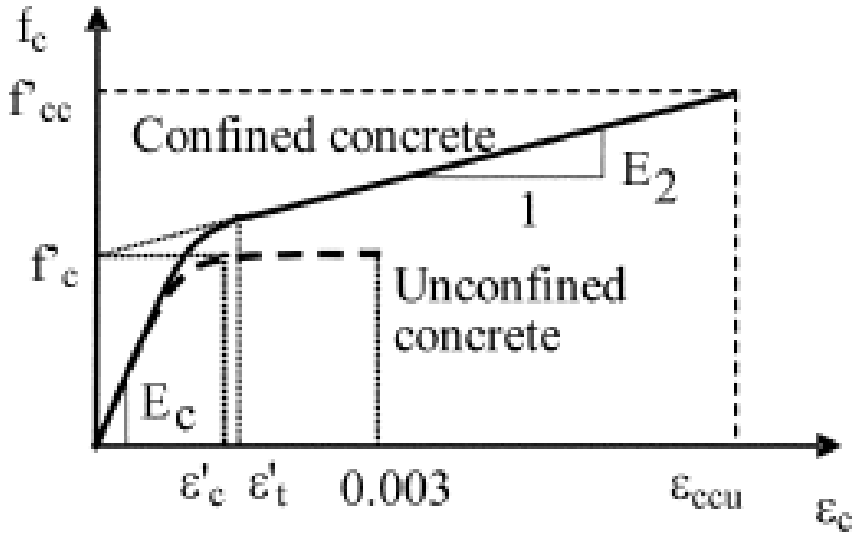

Figure 2.32: Lam and Teng's stress-strain model for FRP confined concrete (Lam and Teng 2003)

Where the generally accepted theoretical approach for the definition of A_e consists of four parabolas within which the concrete is fully confined, and outside of which negligible confinement occurs (Figure 2.33.). The shape of the parabolas and the resulting effective confinement area is a function of the dimensions of the column (b and h), the radius of the corners r_c, and the longitudinal steel reinforcement ratio ρ_g, and can be expressed as:

$$\frac{A_e}{A_c} = \frac{1 - \dfrac{\left[\left(\dfrac{b}{h}\right)(h-2r_c)^2 + \left(\dfrac{h}{b}\right)(b-2r_c)^2\right]}{3A_g}}{1-\rho_g} \tag{2.29}$$

The maximum confinement pressure f_{lFRP} are equal:

$$f_{lFRP} = \frac{2E_f n t_f \varepsilon_{fe}}{D} \tag{2.30}$$

For noncircular cross sections

$$D = \sqrt{b^2 + h^2} \tag{2.31}$$

Where the effective strain level in the FRP at failure ε_{fe} is given by

$$\varepsilon_{fe} = k_{\varepsilon}\varepsilon_{fu} \tag{2.32}$$

A strain efficiency factor κ_{ε}=0.55 is provided based on the experimental results, which were carried out by Pessiki et al. (2001). This factor accounts for the difference between in situ jacket rupture strains and FRP rupture strains determined from tensile coupon tests. In the same manner, the minimum level of lateral pressure f_{lFRP} is limited to be not less than $0.08 f_c^{/}$. This is the minimum level of confinement required to assure a non-descending second branch in the stress-strain behaviour Lam and Teng (2003). In addition, the maximum ultimate strain is limited to 0.01 to prevent excessive cracking and the resulting loss of concrete integrity.

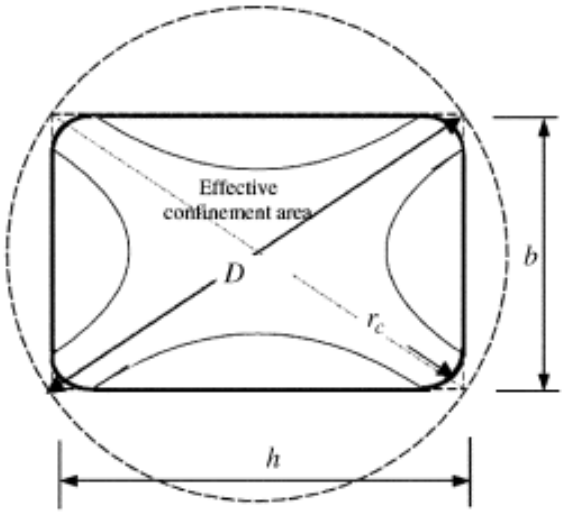

Figure 2.33: Equivalent circular cross section Lam and Teng (2003)

For members subjected to combined axial compression and bending:

Eq. (2.25) is applicable when the eccentricity present in the member is less than or equal to 0.1h. When the eccentricity is larger than 0.1h, the method and equations 2.25 to 2.32 can be used to determine the concrete material properties of the member cross section under compressive stress. Based on that, the P-M diagram for the FRP-confined member can be constructed using well-established procedures (Bank 2006).

The following limitations apply for members subjected to combined axial compression and bending:

1) The effective strain in the FRP jacket should be limited to the value given in (Eq. 2.32) to ensure the shear integrity of the confined concrete $\varepsilon_{fe} = 0.004 \le k_{\varepsilon}\varepsilon_{fu}$
2) The strength enhancement can only be considered when the applied ultimate axial force and bending moment, P_u and M_u, fall above the line connecting the origin and the balanced point in the P-M diagram for the unconfined member (Figure 2.34). This limitation stems from the fact that strength enhancement is only significance for members in which compression failure is the controlling mode (Bank 2006).

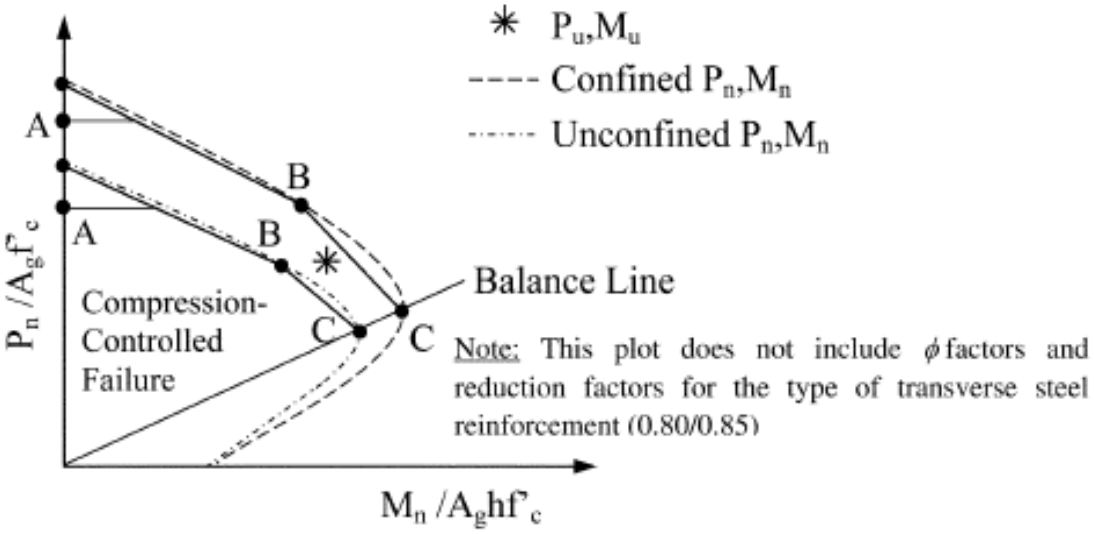

Figure 2.34: Representative interaction diagram (ACI 440.2R-2008)

2.8 Summary

First, this chapter provides brief information on the FRP materials and their characteristics compared to steel reinforcement, modeling FRP tubes and test methods to evaluate the mechanical properties of FRP tubes. Then, the confinement mechanism by later steel reinforcement, steel tubes, as well as FRP tubes was addressed. An overview of the background literature carried out to investigate the structural behaviour of CFFT members subjected to axial forces or combined axial and bending with different critical factors affecting confinement was reviewed. Finally, design guide (recently published in Canada and USA) of the concrete infill columns structures were also covered.

A number of such studies have been reported in the literature. However, the majority of these studies have been concerned with circular short, unreinforced, small-scale concrete cylinders and intermediate CFFTs columns, and only few studies have investigated the axial compressive behaviour of slender as well as eccentricity and cyclic axial behaviour of CFFT columns, particularly those reinforced internally with longitudinal reinforcement steel and/or FRP bars. Furthermore, all the FRP design provisions suffer from one important limitation: the effect of column slenderness (i.e., the second-order effect) is not included, that is, all these design provisions are limited to the design of FRP jackets for short columns for which the second-order effect is negligible. This limitation can be attributed to the limited amount of research on the behaviour of slender FRP confined reinforced concrete columns. Using FRP bars instead of conventional steel bars in the CFFT columns can provide a step forward to develop a promise totally corrosion-free new structural system. Nonetheless, the axial behaviour of FRP bars as longitudinal reinforcement in CFFT columns has been quite limited. Thus, this experimental study is designed to investigate the axial behaviour of CFFT long columns reinforced with longitudinal steel and FRP bars under monotonic and cyclic axial compression loading. The effect of GFRP tubes wall thicknesses, internal reinforcement type and amount, and nature of loading (monotonic and cyclic) on the strength and mode of failure of CFFT long columns are addressed.

CHAPTER 3
EXPERIMENTAL PROGRAM

3.1 General

The experimental program aimed at investigating the axial compression behaviour of circular CFFT long columns internally reinforced with steel, GFRP and CFRP bars tested under monotonic and cyclic axial loading. The experimental program presented herein included construction and testing of ten full-scale RC and CFFT long columns reinforced with different configurations. Through the experimental program, the effect of the following parameters are investigated:

- GFRP tube thickness (2.9mm and 6.4mm);
- Internal reinforcement type and amount (steel, GFRP and CFRP) bars;
- Lateral reinforcement type (steel stirrups and GFRP tube) ;
- Axial nature of loading pattern (monotonic and cyclic).

This chapter presents the details of test specimens, fabrication, instrumentation, test setup, and test procedure. In addition, this chapter gives the detailed properties of different materials used in the experimental program, and obtained by testing representative samples of each material. More details regarding the mechanical properties and standard tests of the different materials (steel and FRP bars and tubes) that are used in the presented thesis can be found elsewhere (Mohamed 2010).

3.2 Materials Properties

Four materials were used in fabricating the test specimens. These materials are concrete, FRP tubes, steel reinforcing (bars and stirrups), and FRP bars. The following sections provide a description of the different experimental tests conducted to evaluate the mechanical properties of the different materials used herein.

3.2.1 Concrete

The columns were constructed using a ready-mixed normal weight concrete with an entrained-air ratio of 5% to 8%. The targeted normal concrete compressive strength was 35 MPa after 28 days for all specimens. The slump of the fresh concrete was measured before casting and was between 80 mm to 100 mm. Twelve concrete cylinders 150 × 300 mm were cast and cured under the same conditions as the test columns. Six cylinders were tested in compression at the day of column testing and the stress–strain relationships were measured. The remaining three cylinders were tested in tension by performing the split cylinder test at the day of columns testing. Figure 3.1 and Figure 3.2 show the compression and splitting testing of concrete cylinders, respectively. Figure 3.3 shows typical axial stress-strain curves for the concrete cylinders. The average concrete compressive strength and tensile strength were 44.0 MPa and 4.2 MPa, respectively.

Figure 3.1: Compression test of the standard concrete cylinders

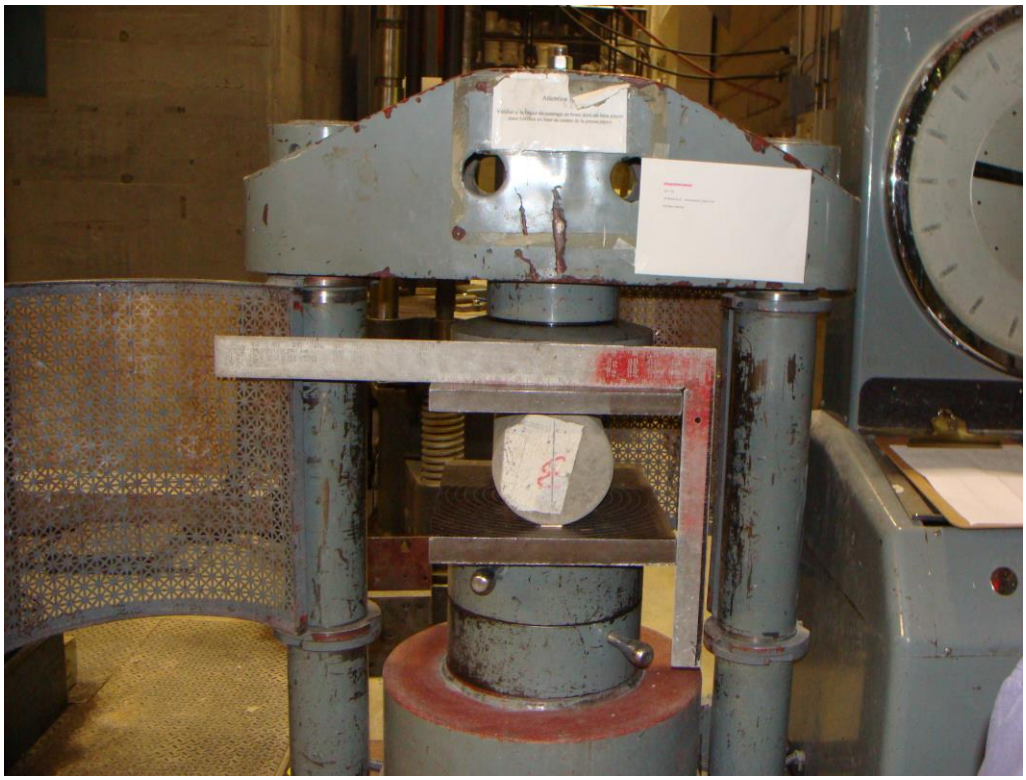

Figure 3.2: Splitting test of the standard concrete cylinders

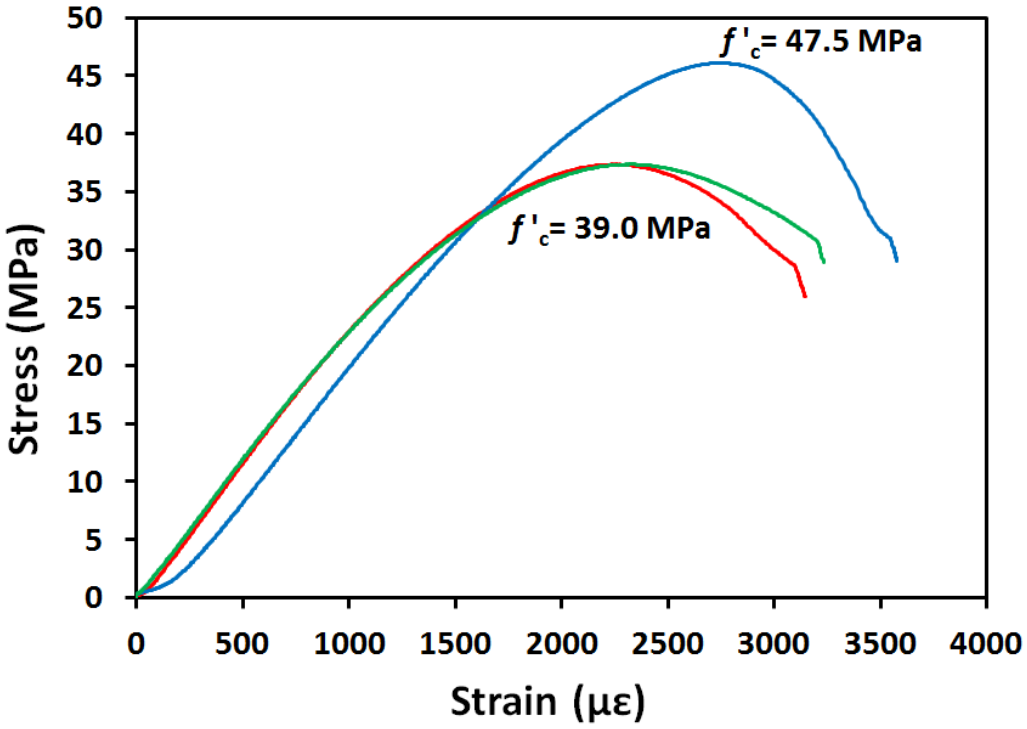

Figure 3.3: Typical axial stress-strain relationships for concrete cylinders

3.2.2 FRP tubes

Two types of GFRP tubes were used as structural stay in-place formwork for the tested specimens herein. The GFRP tubes were fabricated using filament-winding technique; E-glass fiber and Epoxy resin were used for manufacturing these tubes. The two types of GFRP tubes (types A&B) were used with different thicknesses and having the same internal diameters 213 mm. The tubes were manufactured using continuous filament winding process adopted by FRE Composites, St-Andre-d'Argenteuil, Quebec, Canada. The thickness of tube (A) equals 2.90 mm, while for tube B equals 6.40 mm. Different fibre angles with respect to the longitudinal axis of the tubes were used (±60°, ±65°, ±45°, and 90°). The fibre orientations of the tubes were mainly in the hoop direction, and no fibres in the longitudinal direction. The winding angles of tubes (A) were optimized for below underground pipe applications, while tubes (B) were designed for pipe telecommunication applications. Figure 3.4 shows the filament wound GFRP tubes used in this study. The glass fibre volume fraction as provided by the manufacture was 68% ± 3%. Typical test samples of the coupon tests and split-disk test in the hoop direction for GFRP tubes are shown in Figure 3.5 and Figure 3.6, respectively. The material properties for both the fibre and the resin, as given by the manufacture, are presented in Table 3.1 and Table 3.2. Table 3.3 shows the dimensions and mechanical properties of FRP tubes. More details regarding the mechanical properties and standard tests of these tubes can be also found elsewhere (Mohamed 2010).

Figure 3.4: Filament wound GFRP tubes

Table 3.1: Mechanical properties of glass fibres (Mohamed 2010)

Fiber type	Linear mass (g/km)	Nominal Yield (yards/Ib)	Tensile modulus (MPa)	Shear modulus (MPa)	Poisson's ratio
Glass	2000	250	80000	30000	0.25

Table 3.2: Mechanical properties of resin (Mohamed 2010)

Resin type	Density (kg/ m^3)	Tensile modulus (MPa)	Shear modulus (MPa)	Poisson's ratio
Epoxy	1200	3380	1600	0.4

Table 3.3: Dimension, details, and mechanical properties of FRP tubes (Mohamed 2010)

Tube type	D (mm)	t_{frp} (mm)	No. of layers	Stacking sequence	f_{FRPU} (MPa)	ε_{FRPU} (%)	E_{FRPU} (MPa)	f_X (MPa)	ε_X (%)	E_X (MPa)
A	213	2.90	6	[60 º, 90_4, 60]	548	1.70	32260	55.2	0.62	8865
B	213	6.40	12	[±60 º, 90_2, ±60, 90_6]	510	1.69	30200	59.2	0.75	7897

D and t_{frp} are the internal diameter and thickness of the FRP tubes, respectively. f_{FRPU}, ε_{FRPU}, and E_{FRPU} are, respectively, the ultimate strength, ultimate tensile strain, and Young's modulus in the hoop direction; while f_X, ε_X, and E_x are the ultimate strength, ultimate tensile strain, and Young's modulus in the axial direction, respectively;

Test setup

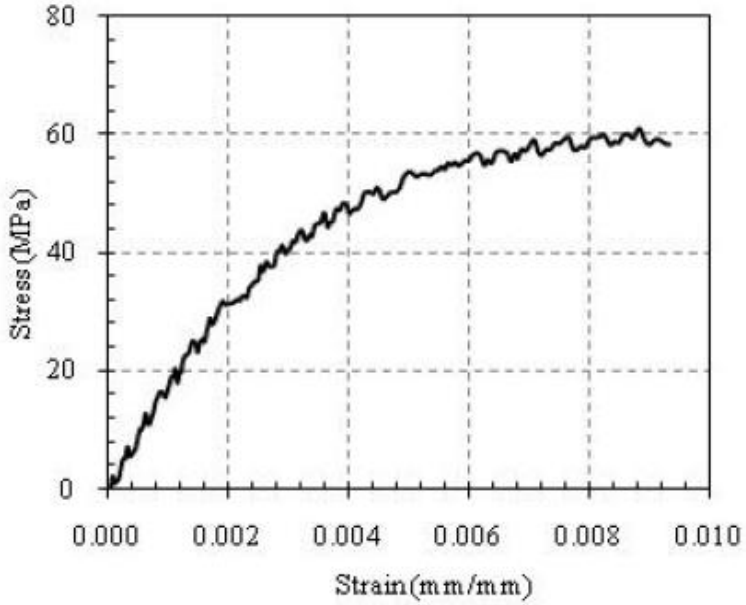

Figure 3.5: Test setup and load-strain curve for the FRP tubes for coupon tensile test (Masmoudi and Mohamed 2011)

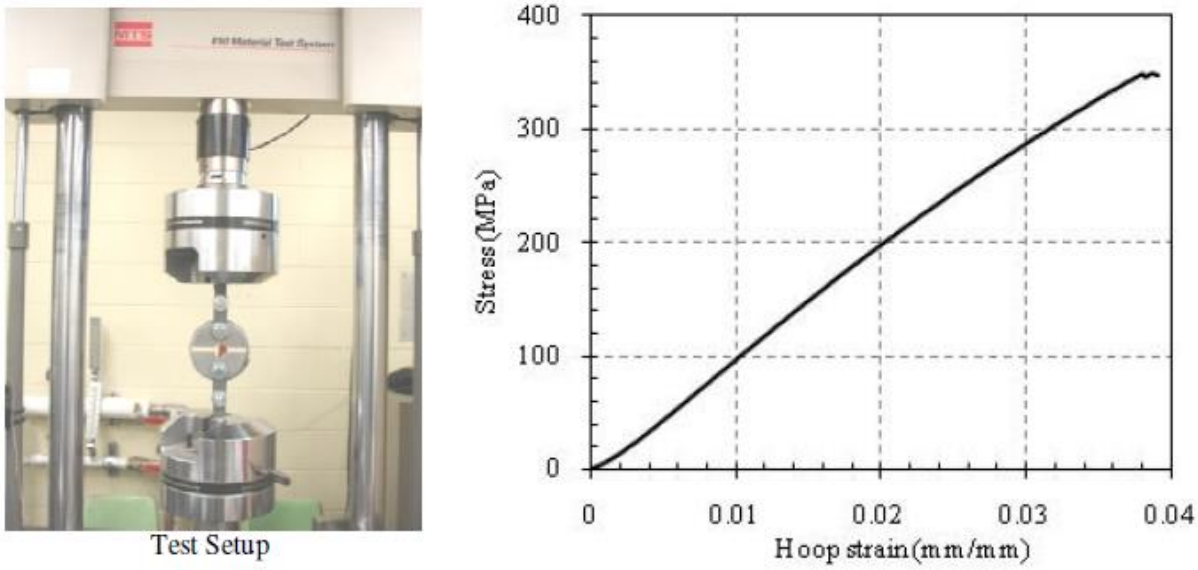

Figure 3.6: Test setup and stress-hoop strain behaviour of the FRP tubes for split-disk test (Masmoudi and Mohamed 2011)

3.2.3 Steel bars

In this study, two different steel bars were used to reinforce the control and CFFT specimens. Wire mild steel bars 3.4 mm in-diameter were served as transverse spiral reinforcement for the control specimens. Deformed steel bars M15 (16 mm in diameter; 200 mm^2 in cross-sectional area); were used as a longitudinal reinforcement for test specimens. The mechanical properties of the steel bars obtained from standard tests that were carried out according to ASTM A615/A615M-09 (2009), on five specimens for each type of the steel bars. The mechanical properties of the steel bars are presented in Table 3.4.

Table 3.4: Mechanical properties of steel reinforcing bars (Mohamed 2010)

Reinforcement type	Nominal diameter (mm)	Nominal area (mm^2)	Tensile modulus of elasticity (GPa)	Yield strength (MPa)	Ultimate strength (MPa)	Yield strain (%)
Wire (mild steel)	3.4	9	200	675	850	0.30
15M (deformed)	16	200	200	419	686	0.21

3.2.4 FRP bars

Three types of sand-coated FRP bars manufactured by a Canadian company [ADS Composites/Pultrall Inc., Thetford Mines, Quebec] were used as longitudinal reinforcement for the tested columns. Sand-coated surface was made to improve the bond between the bars and surrounding concrete. Two types of FRP bars were made from continuous glass fibres and one type was made from continuous carbon fibres with a fibre content of 73% and impregnated in a vinyl ester resin through the pultrusion process. GFRP bars No. 3 and No. 5 (9.5 mm and 15.9 mm in-diameter; 71 mm^2 and 199 mm^2 in cross-sectional area, respectively) and CFRP bars No. 3 (9.5 mm-in diameter; 71 mm^2 in cross-sectional area) were used. Table 3.5 shows the mechanical properties of the FRP bars as provided by the manufacture.

Table 3.5: Properties of reinforcing FRP bars (Pultrall 2007)

Reinforcement type	Nominal diameter (mm)	Nominal area (mm^2)	Tensile modulus of elasticity (GPa)	Yield strength (MPa)	Ultimate strength (MPa)	Ultimate strain (%)
GFRP	9.5	71	45.4	-	856	1.89
	15.9	199	48.2	-	751	1.60
CFRP	9.5	71	128	-	1431	1.20

3.3 Test Specimens' Details

A total of 10 RC and CFFT circular columns, comprising 3 RC control columns and 7 steel or FRP-reinforced CFFT columns, were fabricated and tested under concentric axial monotonic or cyclic compression loading. The test specimens were divided into two series denoted as Series I and II. Table 3.6 provides complete details of all specimens and Figure 3.7 shows typical details of the reinforcement layout. The specimens in Table 3.6 were labeled as follows: the first letters S, A, or B are defining "the type of lateral reinforcement: steel spiral stirrups, GFRP tube type (A), or tube type (B), respectively". This was followed by a letter S, G, or C. These letters were used to indicate "the longitudinal reinforcement type: steel, GFRP, or CFRP bars, respectively", followed by a subscript indicating "the longitudinal reinforcement ratio". The final letter refers to the nature of loading type "M for monotonic or C for complete unloading/reloading cyclic loading". For instance, the specimen (A-$S_{(3.4)}$-C)

was laterally confined with GFRP tube type (A), reinforced internally with steel bars with a reinforcement ratio of 3.4%, and tested under cyclic axial compression loading.

Table 3.6: Specimen's details

Series number	ID	Tube type or spiral stirrups	*H* (mm)	*D* (mm)	Longitudinal bars	
					Type	*Amount*
I	S-$S_{(3.4)}$-C	ϕ3.4@50.6	1900	213	Steel	6 M 15
	S-$G_{(3.4)}$-C	ϕ3.4@50.6			GFRP	6 No. 5
	S-$G_{(3.4)}$-C*	ϕ3.4@50.6			GFRP	6 No. 5
II	A-$S_{(3.4)}$-C	A			Steel	6 M 15
	A-$G_{(3.4)}$-C	A			GFRP	6 No. 5
	B-$G_{(3.4)}$-C	B			GFRP	6 No. 5
	B-$G_{(1.2)}$-C	B			GFRP	6 No. 3
	B-$G_{(1.2)}$-M	B			GFRP	6 No. 3
	A-$C_{(1.2)}$-C	A			CFRP	6 No. 3
	A-$C_{(1.2)}$-C*	A			CFRP	6 No. 3

* X-$Y_{(aa)}$-Z*: X= lateral reinforcement type, where S=Steel spiral stirrups; A=GFRP tube type; and B= GFRP tube type B; Y=longtiudianl reinforcment type, where S=steel bars; G= GFRP bars; and C=CFRP bars; aa=longitudianl reinforcment ratio; Z=loading type, where C=cyclic axial loading; and M=monotonic axail loading; * inditical speciemens (if any).

Both series had the same height (h=1900 mm) to diameter (D=213 mm) ratio of 9.0. The investigated test parameters were: (i) GFRP tubes thicknesses (2.9 and 6.4 mm); (ii) internal reinforcement type (steel; GFRP; or CFRP bars) and amount; and (iii) nature of loading (i.e. monotonic and cyclic). Series I includes three control RC specimens reinforced longitudinally with reinforcement ratio (ρ_L) equal to (3.4%), one specimen reinforced with longitudinal steel bars and two identical specimens reinforced with GFRP bars. Steel spiral stirrups (pitch = 50.6 mm) were used as transverse reinforcement to have approximately similar hoop stiffness of the GFRP tube (Type A). Series II consists of seven reinforced CFFT columns laterally confined with GFRP tubes (Type A or B). One specimen was internally reinforced with deformed steel bars (6 M15; ρ_L = 3.4%) and laterally confined with tube type (A). Four specimens were reinforced with 6 GFRP bars No. 3 or No. 5 (ρ_L = 1.2 and 3.4%, respectively) and laterally confined with tubes type (A and B). Besides, two identical specimens were reinforced with longitudinal CFRP bars (6 No. 3; ρ_L = 1.2 %) and laterally confined with tube type (A) and were designed to have similar axial stiffness as in specimen (A-$G_{(3.4)}$-C). In addition, all specimens were tested under single complete unloading/reloading cyclic axial compression

loading, except for specimen B-$G_{(1.2)}$-M which was tested under monotonic axial compression loading.

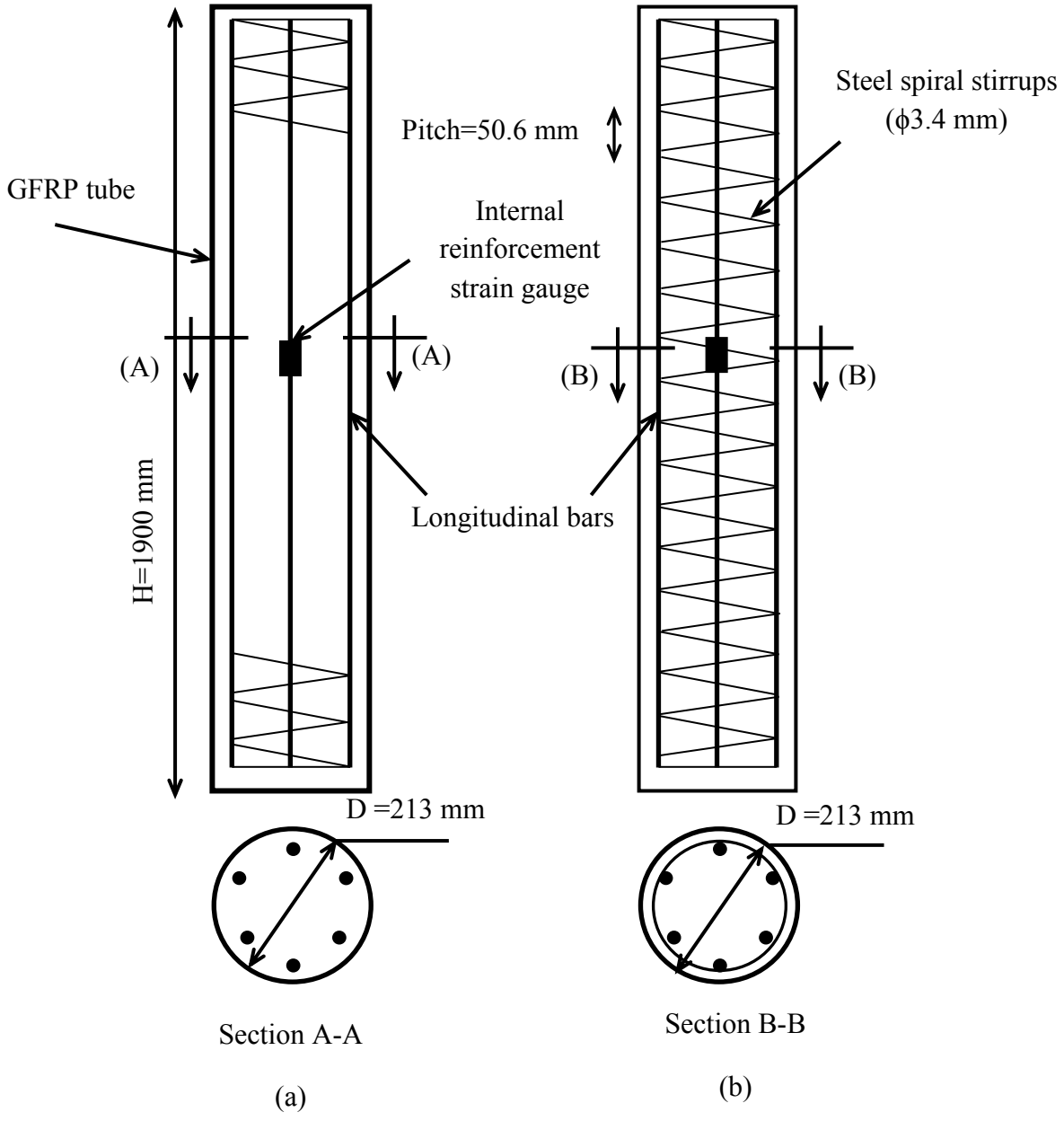

Figure 3.7: Typical details for the tested specimens and reinforcement layout: (a) CFFT columns; (b) control specimens

3.4 Fabrication of the test specimens

All specimens were casted with concrete in a vertical position. For the CFFT column, the GFRP tubes were used as permanent formwork while for control specimens' stiff cardboard

tubes were used as formwork and it were removed after casting (see Figure 3.8 a & b). The FRP tubes were cut to the proper length of 1.90 m-long, using a saw and then were cleaned and dried carefully. The cardboard tubes were attached with four vertical stiffeners using wood plate of 50 x 30 mm, cross section distributed at the perimeter of the tube. Reinforcement cages with different configuration were constructed from GFRP, CFRP, and steel bars. The rebar cage was designed to have an outside diameter of 193 mm, allowing for 10 mm clear spacing on all perimeters of the FRP tubes. All longitudinal bars were uniformly distributed inside the cross section (see Figure 3.7). For the CFFT columns, two steel stirrups were used at the top and the bottom of each specimen to fix the bars in their positions during casting.

(a) (b)

Figure 3.8: (a) FRP tubes; (b) and cardboard for columns (Mohamed 2010)

3.5 Instrumentations and Testing Procedures

Several strain gauges were mounted onto the internal reinforcement prior casting the concrete and onto the concrete or tube surface before testing. Two strain gauges were bonded on two longitudinal bars at 180^{o} degree apart at the mid-height of the column. Eight strain gauges were located at the column mid-height in both axial and lateral directions to measure the axial and lateral strains, respectively, as shown in Figure 3.9 and Figure 3.10. Two displacement transducers (DTs) were used to measure the axial deformation of the column

over the full height. Additionally, two in-plane linear variable displacement transducers (LVDTs) were located at the mid-height to record the lateral displacements of each column (see Figure 3.11 and Figure 3.12). A thin layer of the high strength sulphur was capped on both ends of all specimens to ensure the uniform load distribution during testing (see Figure 3.13). Before testing, both ends of the columns were further confined with bolted steel collars made from 10 mm thick steel plates in order to prevent premature failure at the ends, as shown in Figure 3.14. The specimens were loaded under axial compression load using a 6000-kN capacity-testing machine. Loading and unloading in compression tests were achieved with load control at a rate approximately equal to 2.3 kN/s. During the test, load, axial and lateral displacements, and strain gauges were recorded automatically using a data acquisition system connected to the computer. Figure 3.15 shows the schematic of the test setup and Figure 3.16 depicts photograph of the test setup. Figure 3.17 shows the testing machine and a data acquisition system.

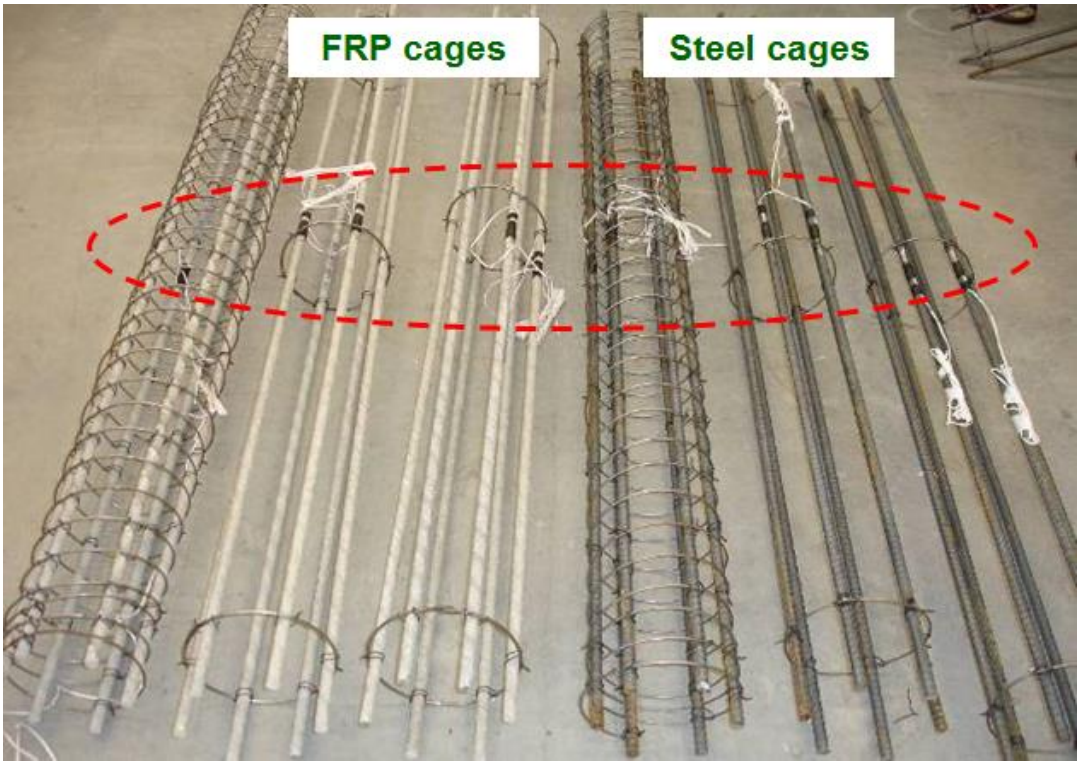

Figure 3.9: Reinforcement strain gauges instrumentations (Mohamed 2010)

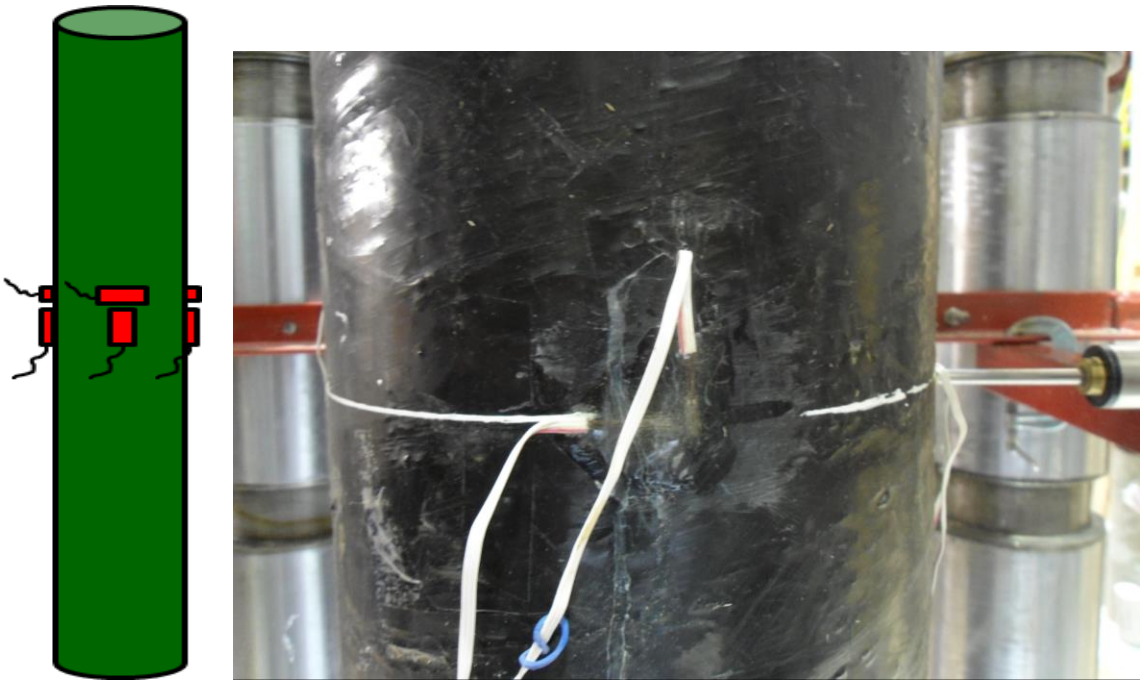

Figure 3.10: Vertical and horizontal strain gauges

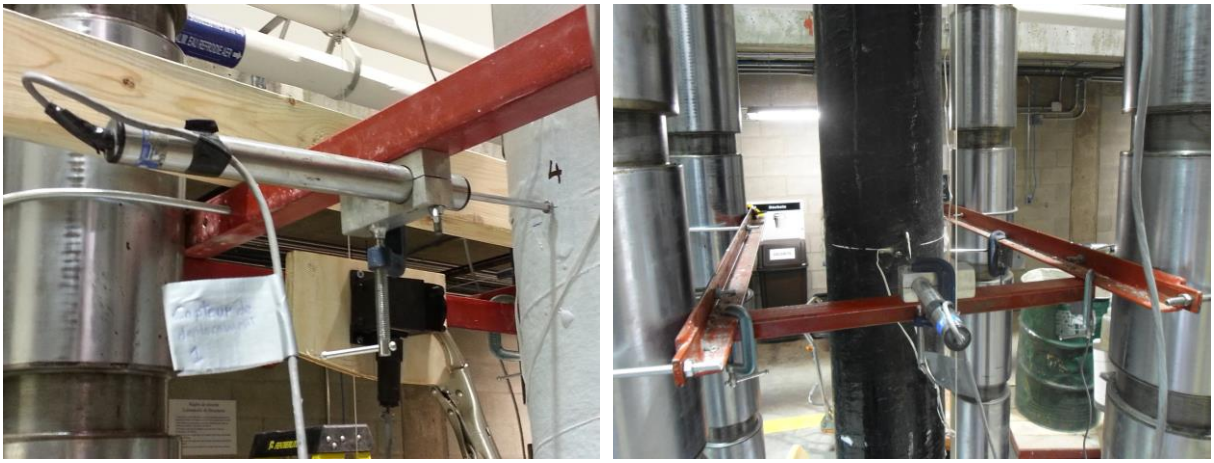

Figure 3.11: Horizontal LVDTs for measuring the lateral displacements

Figure 3.12: Vertical DTs for measuring the axial displacements

Figure 3.13: Column capping preparation

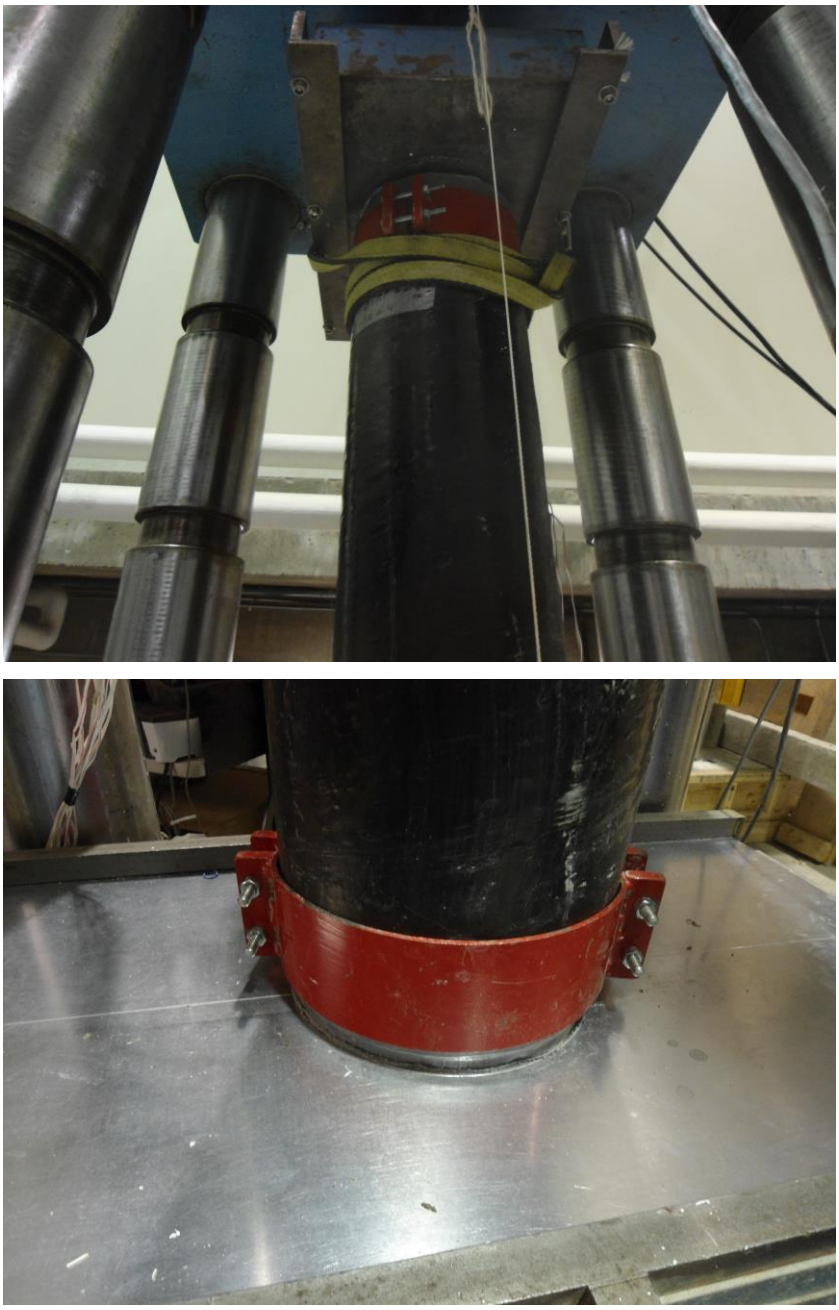

Figure 3.14: Top and bottom confined steel bolted plates

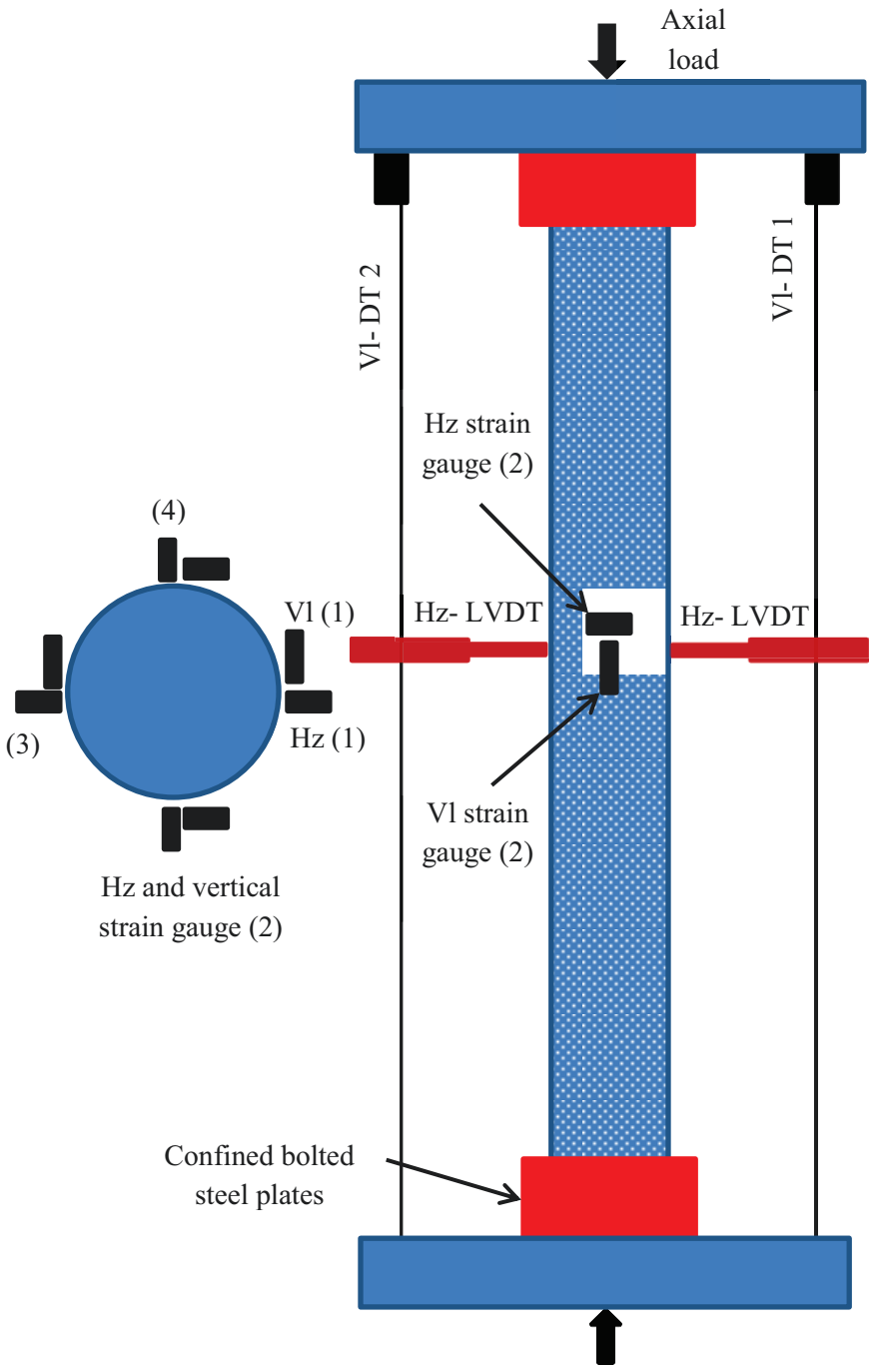

Figure 3.15: Schematic of the test setup and placing of specimen instrumentations

a) CFFT column b) Control column

Figure 3.16: Test setup

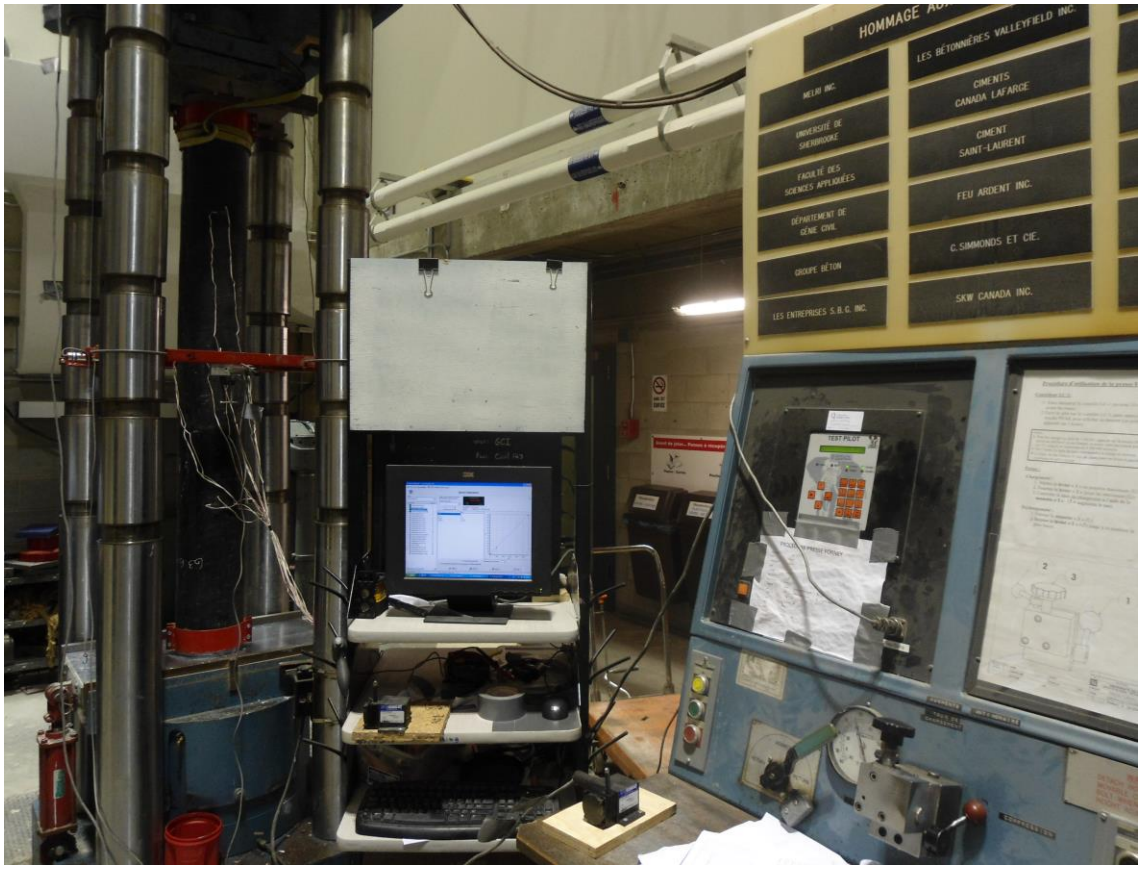

Figure 3.17: Testing machine and a data acquisition system

CHAPTER 4
TEST RESULTS AND DISCUSSION

4.1 General

This chapter presents the test results of an experimental study that have been submitted to the *Elsevier Journal of Engineering Structures*. The behaviour of RC and CFFT columns internally reinforced with longitudinal steel and FRP bars under axial compression loading is investigated. A total of ten RC and CFFT columns measuring 1900-mm in height and 213-mm in diameter were constructed and tested until failure. The behaviour of the tested columns is discussed in terms of failure mode, axial and lateral stress-strain responses, plastic strains and stress deterioration, and stress-strain responses of longitudinal reinforcement. Furthermore, the effect of the GFRP tubes thicknesses on confinement and loading pattern are also emphasized. Examination of the test results has led to a number of significant conclusions in regards to both the trend and ultimate axial strength and strain capacities.

4.2 General Behaviour and Mode of Failure

Different failure modes were observed for the tested control and CFFT reinforced columns as shown in Figure 4.1 to Figure 4.9. Test results indicated that the control specimens that were confined with steel spiral stirrups and reinforced with steel or GFRP bars showed similar initial elastic behaviour. Failure typically initiated with vertical cracks started to appear at approximately 85% of their peak loads and followed by concrete dilation and lateral deformation of transverse and longitudinal reinforcement leading to concrete cover spalling. Thereafter, the concrete core crushed and spiral stirrups fractured after buckling of the longitudinal bars. Moreover, inclined diagonal shear surface was observed, leading to a separation of the concrete core into two column parts, causing a sudden drop after reaching the peak load (see Figure 4.1 and Figure 4.2). It should be noted that the GFRP control columns failed in a more brittle manner than the steel-reinforced columns.

On the other hand, reinforced CFFT columns showed substantially different failure mode compared to that occurred for the control columns as shown in Figure 4.3 to Figure 4.9. The GFRP tube provided significant confinement attributing to shift the failure mode from axially dominated material failure to flexural-dominated instability failure (overall buckling associated with considerable bending of the specimens). The instability was evident in a significant single curvature mode shape of the bent column. This observation is in agreement with the previous research work conducted on slender FRP-confined columns (Mohamed et al 2010 and Fitzwilliam et al 2010). Despite, the specimens experienced much lateral deflections beyond the ultimate load, the deflected columns were still stable and carried more axial load. Loading the specimens continued until localized failure occurred near the mid height of the column. Finally, the failure happened suddenly and in a brittle manner. Furthermore, the FRP rupture, concrete crushing, and local buckling of steel bars or crushing of the FRP bars on the compression side of the column were observed in the specimens after removing the FRP tube.

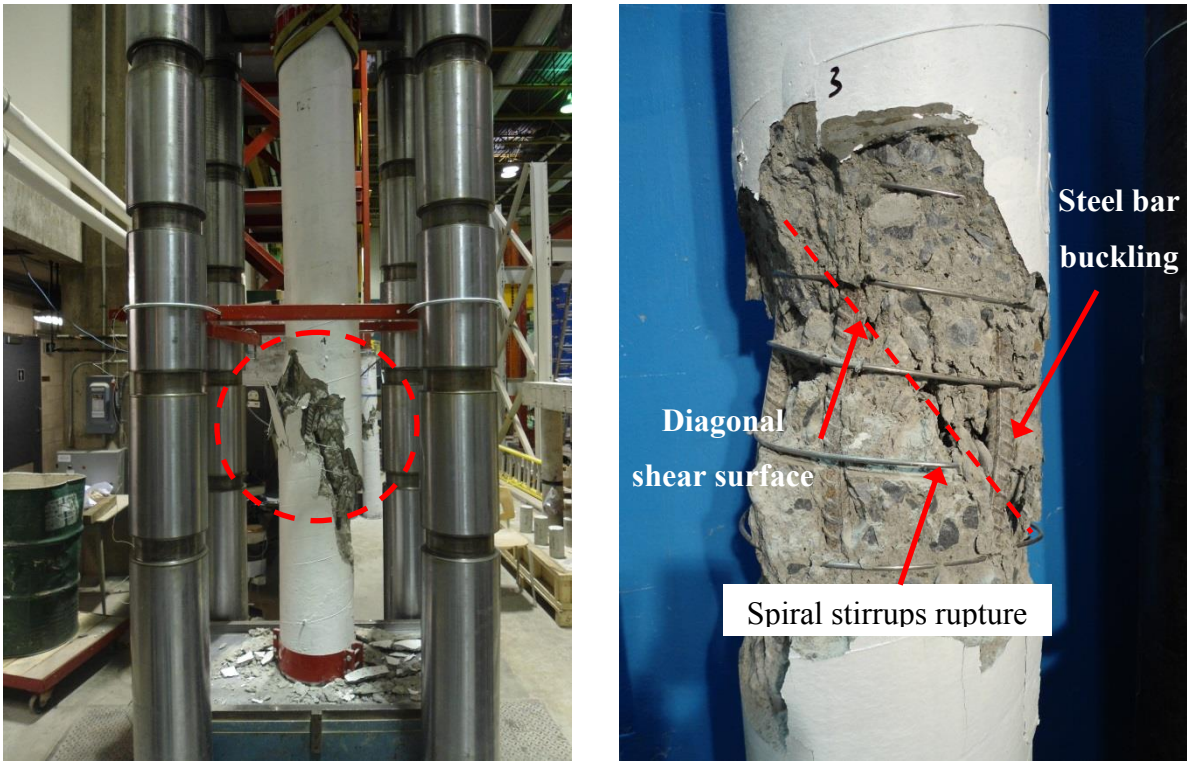

Figure 4.1: Failure mode of specimen S-$S_{(3.4)}$-C

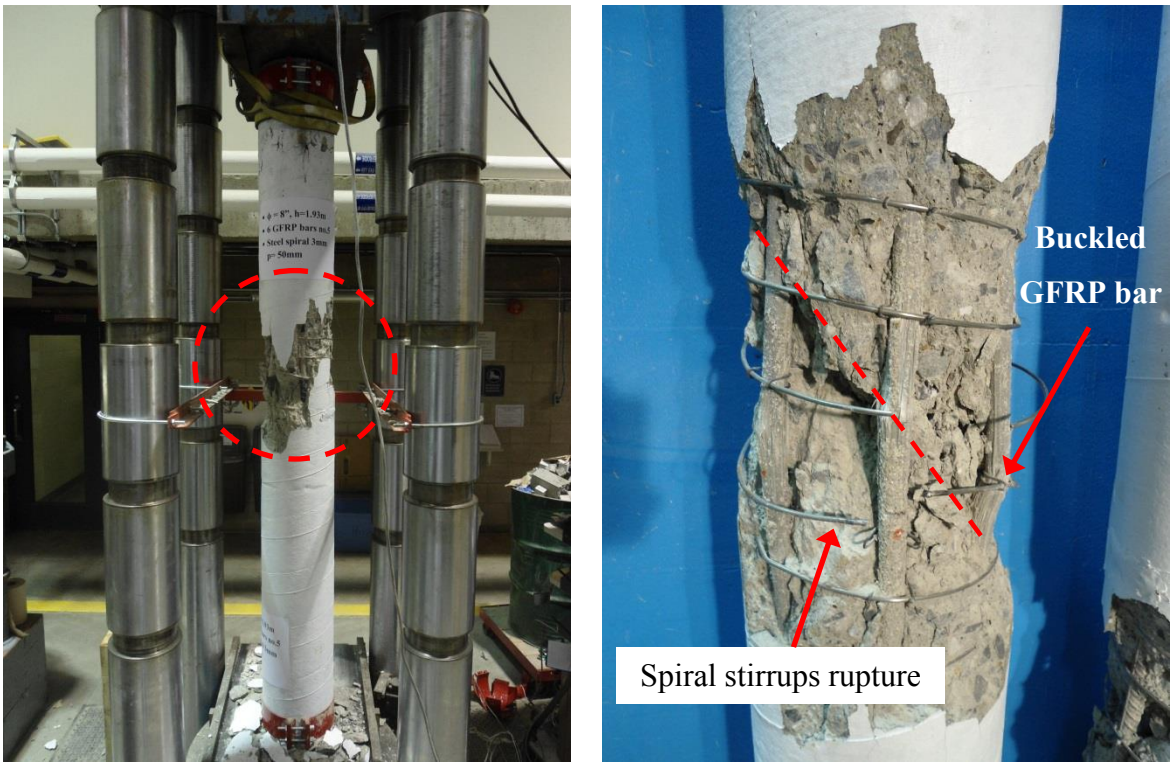

Figure 4.2: Failure mode of specimen S-$G_{(3.4)}$-C

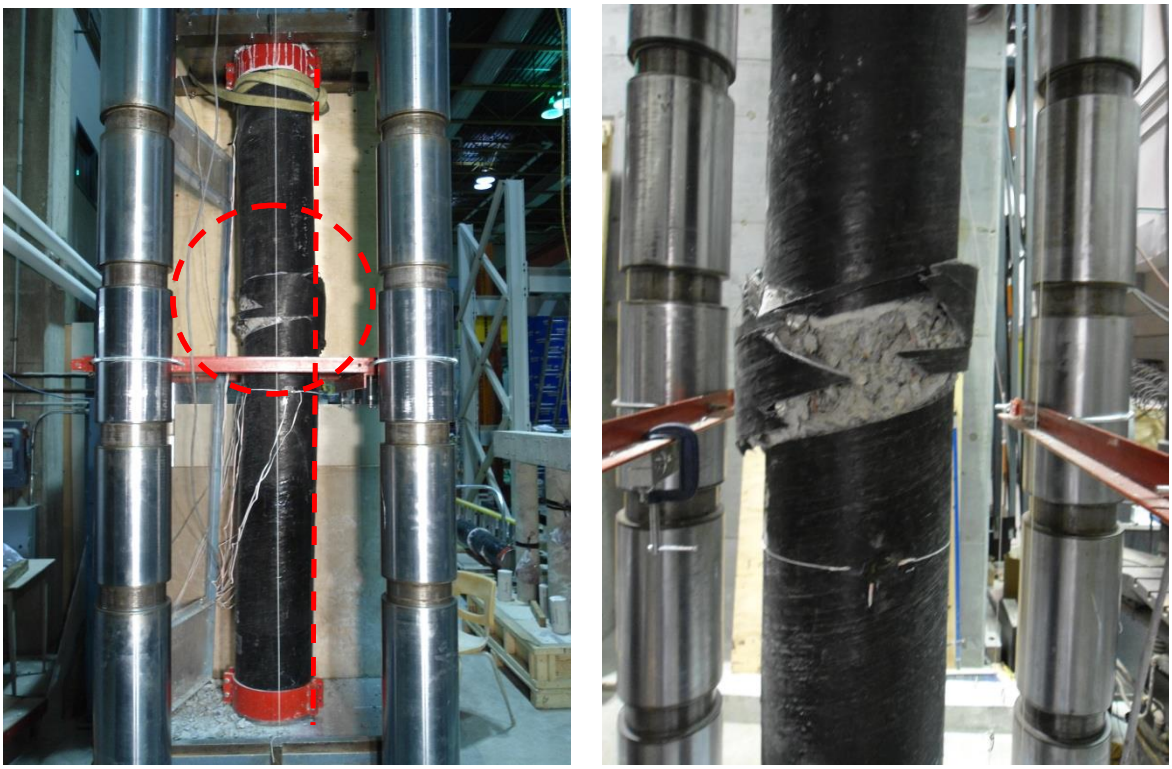

Figure 4.3: Failure mode of specimen A-$S_{(3.4)}$-C

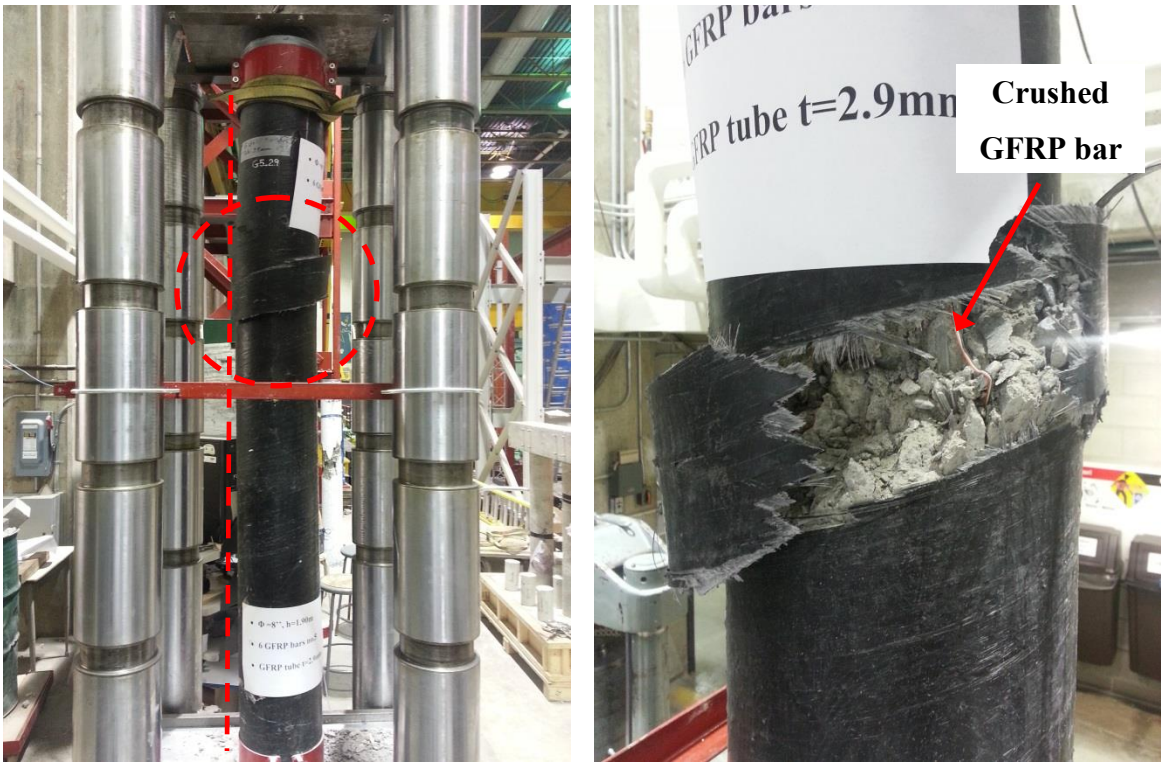

Figure 4.4: Failure mode of specimen A-$G_{(3.4)}$-C

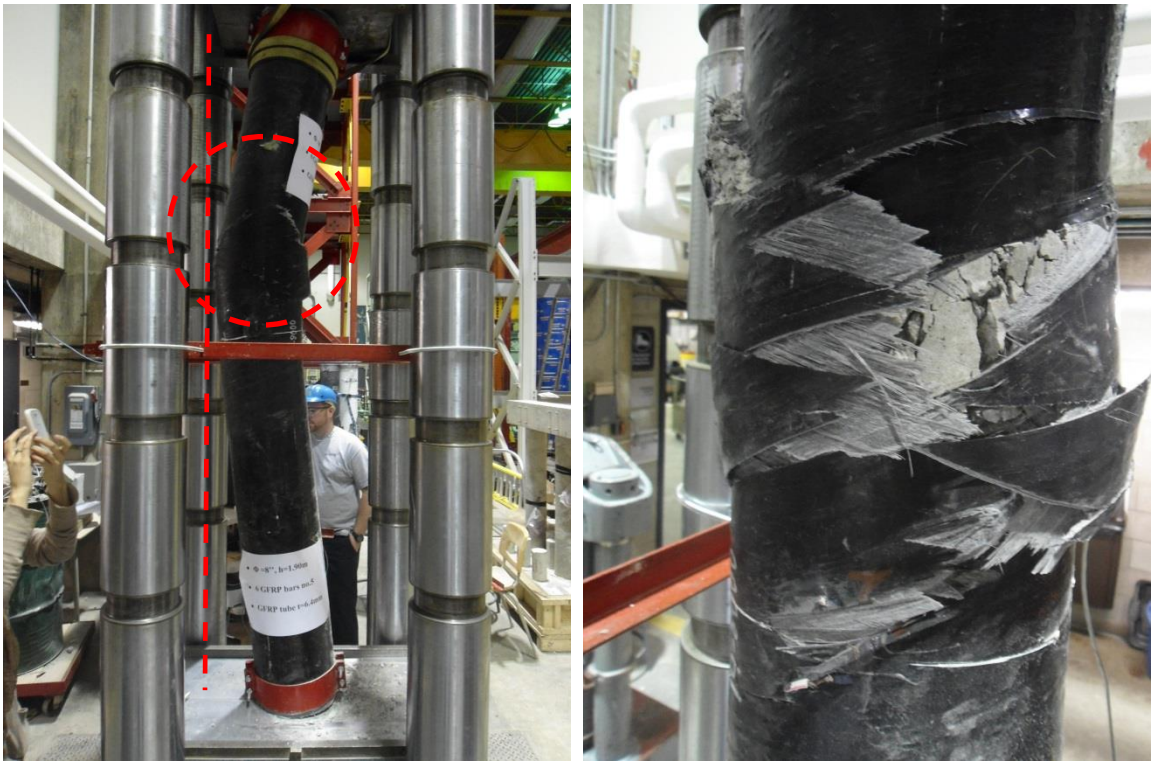

Figure 4.5: Failure mode of specimen B-$G_{(3.4)}$-C

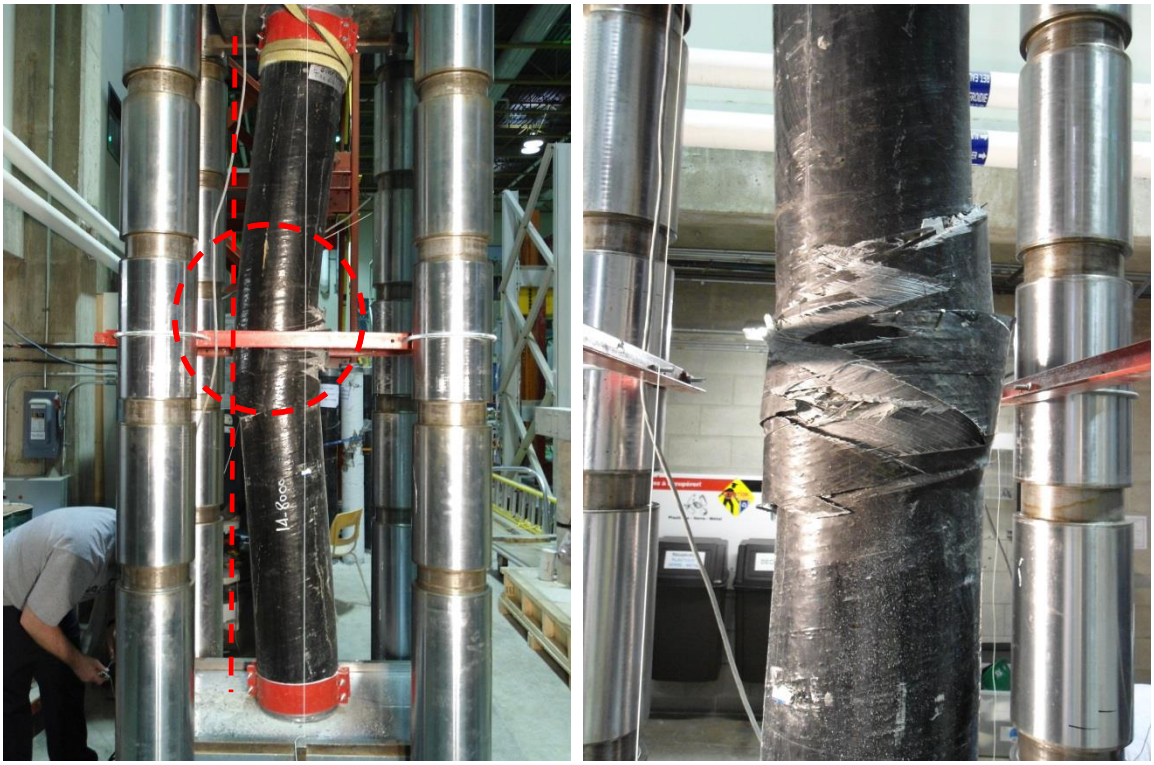

Figure 4.6: Failure mode of specimen B-$G_{(1.2)}$-C

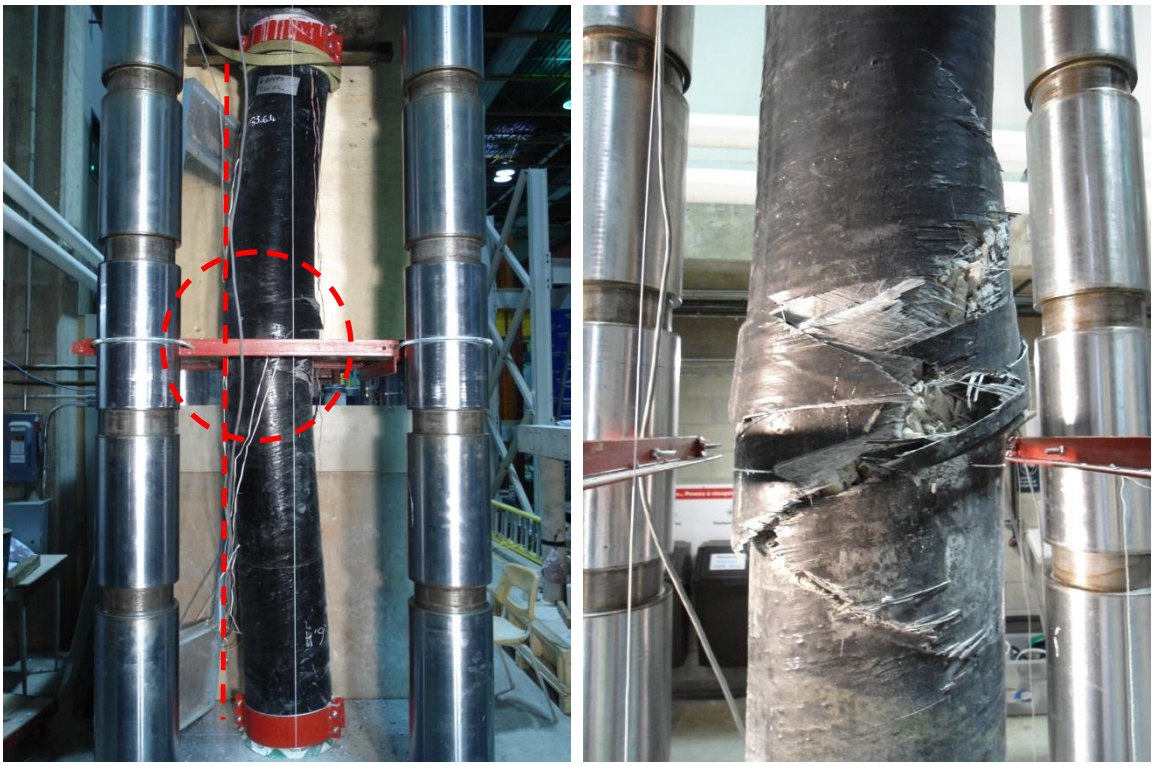

Figure 4.7: Failure mode of specimen B-$G_{(1.2)}$-M

Figure 4.8: Failure mode of specimen B-$G_{(1.2)}$-C^*

Figure 4.9: Overall failure modes of tested specimens

4.3 Axial and Lateral Stress-Strain Responses

Figure 4.10 to Figure 4.12 depict the cyclic and monotonic stress-strain relationships for reinforced control and CFFT columns. In Figure 4.10 to Figure 4.12, the axial stress and strain are presented as positive and the lateral strain as negative. Axial stress was obtained from dividing the axial load by the column cross-sectional area. The axial and lateral stress-strain curves were plotted from the ultimate strain gauges bonded in the vertical and hoop directions at the mid-height of the column. The key experimental results of the tested columns are shown in Table 4.1. In this Table 4.1, the experimental ultimate load (P_u), the confined concrete compressive strength ($f_{cc}^{'}$)-that is the maximum compressive strength at the ultimate load, the corresponding axial strain ($\varepsilon_{cc}^{'}$), the unconfined concrete compressive strength ($f_c^{'}$) from cylinders and the corresponding axial strain of unconfined concrete ($\varepsilon_{co}^{'}$) are reported. As shown in Figure 4.10 to Figure 4.12, the stress-strain diagrams for all columns exhibited almost similar initial stiffness with a relatively linear slope in the elastic range of the stress-strain curves, indicating that the elastic axial stiffness is not affected by confinement, regardless the investigated tested parameters. Lam and Teng 2003 and Karimi et al 2012 also noted that in the elastic range with axial strain values smaller than 0.002, the confinement of FRP-confined concrete is negligible. In addition, the maximum compressive strain at failure exceeds the elastic axial strain limit (taken as 0.002) indicating the inelastic buckling of the reinforced CFFT columns (Karimi et al 2012).

The stress-strain responses of the GFRP-reinforced control columns behaved similar to that of the steel-reinforced control column up to their peak load. However, the peak axial stress for steel-reinforced column was slightly higher than that of their counterpart reinforced with GFRP by 11% on average. In spite of the fact that the steel spiral stirrups for the control specimens were designed to have similar lateral stiffness as in Tube A, the ultimate capacity was significantly lower than that of CFFT specimens. This can be attributed to the continuity of the FRP tubes rather than the discontinuity of the steel stirrups, which reflects the superior confining behaviour of the FRP tubes compared to the steel stirrups to increase not only the strength but also the ductility of the CFFT columns (Mohamed et al 2010).

The envelop curves of the reinforced CFFT- columns, representing the upper boundary of the cyclic axial stress-strain responses, showed bilinear responses with a transition zone in the vicinity of the unconfined concrete (f_c') followed by nearly stabilization of the load carrying capacity at the end due to excessive lateral buckling until failure (i.e B-$G_{(3.4)}$-C and B-$G_{(1.2)}$-C). The initial slope was almost identical for all the specimens while the second slope is highly governed by GFRP tubes stiffness rather than the internal reinforcement type and amount, particularly in thicker tube thickness (see Figure 4.11 and Figure 4.12). The axial stress-strain curves for GFRP and steel reinforced CFFT columns showed similar shapes of the hysteresis loops for the unloading/reloading paths (Figure 4.11). However, the steel-reinforced CFFT column hysteresis loop starts to open after the yielding of steel bars. The unloading paths for the CFFT columns reinforced with steel or FRP bars exhibited non-linear behaviour. The degree of the non-linearity increases as the unloading axial strain increases. Moreover, the reloading paths could be represented as straight lines.

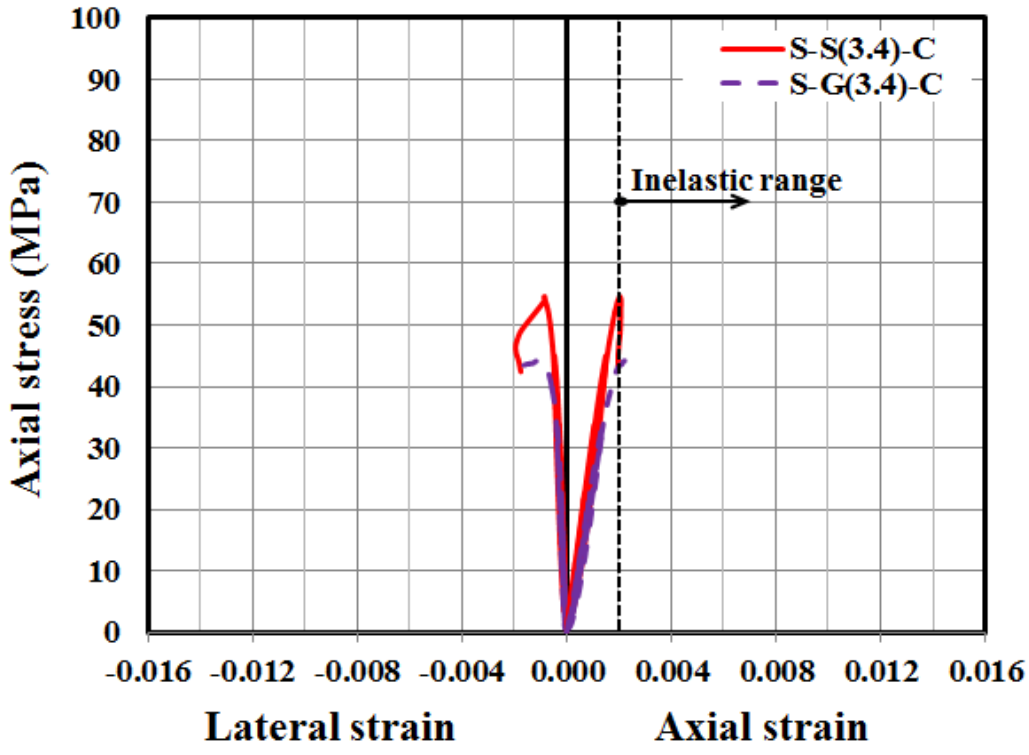

Figure 4.10: Axial cyclic stress-strain curves for control columns

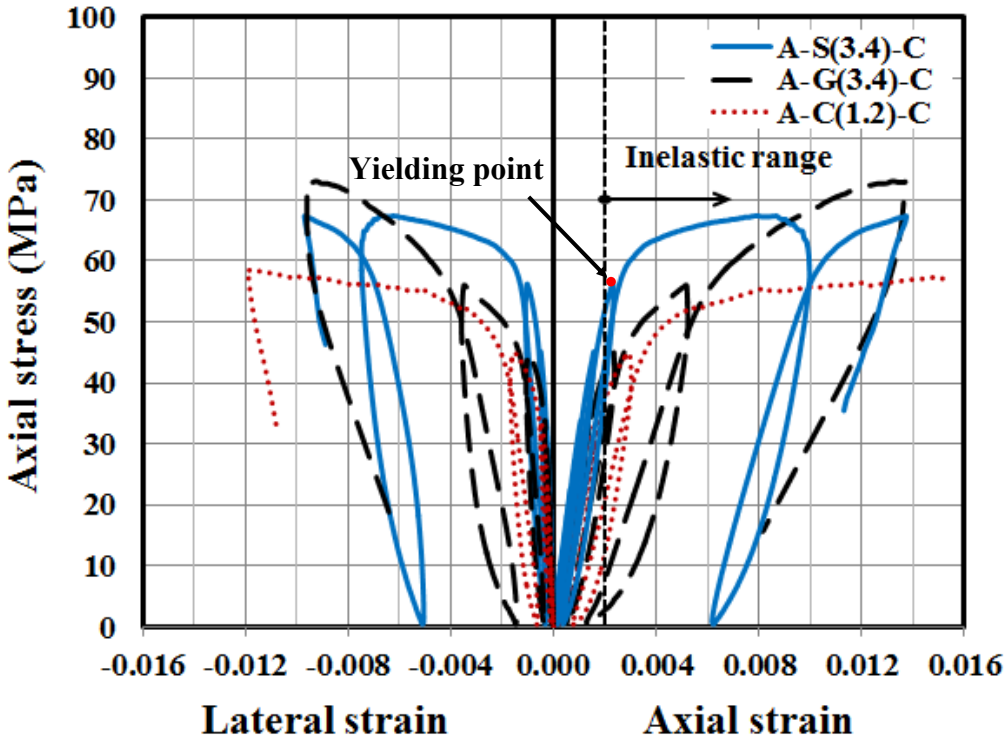

Figure 4.11: Axial cyclic stress-strain curves for the reinforced-CFFT columns confined with tube type A

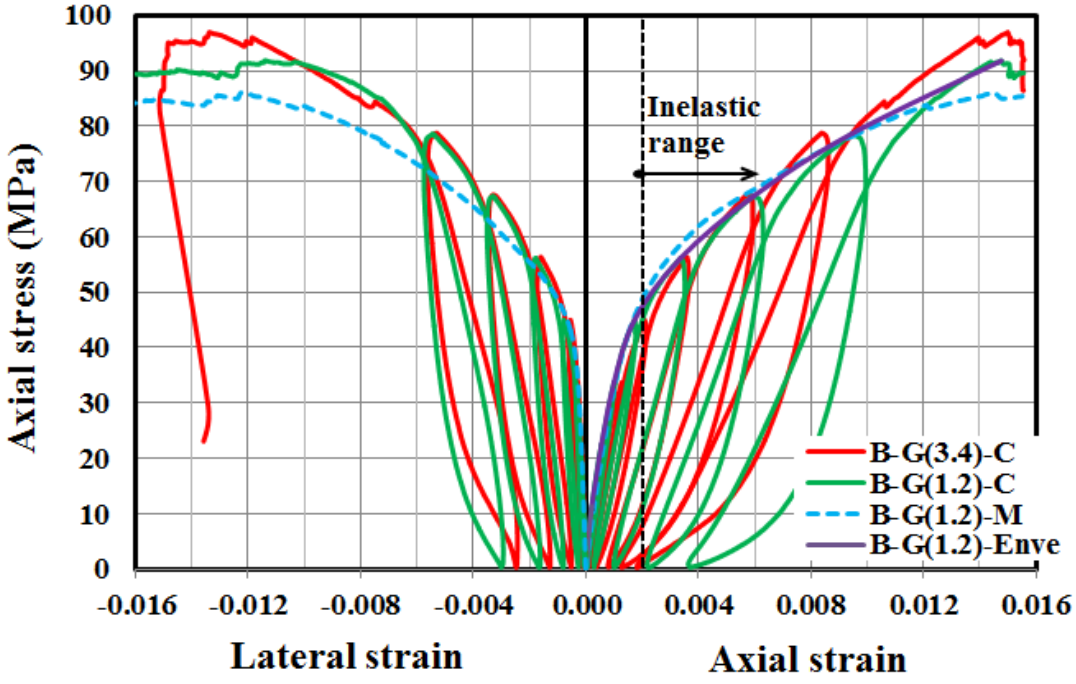

Figure 4.12: Axial cyclic stress-strain curves for the reinforced-CFFT columns confined with tube type B

Table 4.1: Test specimens' results

Series number	ID	P_u (kN)	f_c' (MPa)	f_{cc}' [a] (MPa)	f_{cc}'/f_c'	ε_{cc} (με)	$\varepsilon_{cc}/\varepsilon_{co}$	$\varepsilon_{h,min.}$ (με)	$\varepsilon_{h,aver.}$ (με)	$\varepsilon_{h,max.}$ (με)
I	S-$S_{(3.4)}$-C	1948	44.1	54.60	1.23	-2510	1.04	377	599	836
	S-$G_{(3.4)}$-C	1575		47.20	1.08	-2711	1.12	653	935	1144
	S-$G_{(3.4)}$-C*	1606		48.64	1.10	-2379	0.99	270	457	605
II	A-$S_{(3.4)}$-C	2402		67.38	1.53	-13749	3.83	2442	4697	9707
	A-$G_{(3.4)}$-C	2603		73.06	1.66	-13718	4.63	5172	8087	9610
	B-$G_{(3.4)}$-C	3455		96.97	2.20	-15578	5.49	4435	9745	15135
	B-$G_{(1.2)}$-C	3272		91.82	2.08	-15563	5.96	11456	13787	16113
	B-$G_{(1.2)}$-M	3068		86.09	1.95	-15514	5.15	3156	11356	16090
	A-$C_{(1.2)}$-C	2086		58.55	1.33	-15486	4.65	4190	8240	11913
	A-$C_{(1.2)}$-C*	2039		57.23	1.30	-15475	5.10	2738	8024	12947

* X-$Y_{(aa)}$-Z*: X= lateral reinforcement type, where S=Steel spiral stirrups; A=GFRP tube type; and B= GFRP tube type B; Y=longtiudianl reinforcment type, where S=steel bars; G= GFRP bars; and C=CFRP bars; aa=longitudianl reinforcment ratio; Z=loading type, where C= axial cyclic loading; and M=monotonic axial loading; * inditical speciemens (if any).

[a] $f_{cc}'=P_u/A_c$

4.4 Plastic Strains

The relationship between the plastic strain and envelop unloading strain ($\varepsilon_{un,env.}$) is an important aspect for modelling the unloading/reloading axial cycles. The plastic strain (ε_{pl}) in this thesis is defined as the residual axial strain when the axial stress is unloaded to zero stress of each unloading path (Wang et al 2012 and Lam and Teng 2009) (see Figure 4.13). Previous studies for unconfined, steel-confined, and FRP-confined concrete cylinders and square prisms (e.g. Saki and Kawashima 2006; Lam and Teng 2009; Abbasina et al 2012; 2013; Wang et al 2012; Ozabakkalogu and Akin 2012) have shown that the plastic strain is linearly proportional to envelop unloading strain. Yet, the proposed model of Lam and Teng (2009) is highly accurate in predicating both the unloading and reloading paths and estimate plastic strains for FRP-confined normal strength concrete cylinders (Ozabakkalogu and Akin 2012). Lam and Teng (2009) proposed the following equations to predicate the plastic strains: (1) $\varepsilon_{pl1} = 0$ when $\varepsilon_{un,env} \leq 0.001$; (2) a linear increase in ε_{pl} when $0.001 \leq \varepsilon_{un,env} \leq 0.0035$ (Eqn. 4.1); and (3) an additional linear increase relationship when $\varepsilon_{un,env} > 0.0035$ (Eqn. 4.2).

$$\varepsilon_{pl2} = [1.4\left(0.87 - 0.004 f_c'\right) - 0.64]\ \left(\varepsilon_{un,env} - 0.001\right) \tag{4.1}$$

$$\varepsilon_{pl3} = \left(0.87 - 0.004 f_c^{'}\right)\ \varepsilon_{un,env} - 0.0016 \tag{4.2}$$

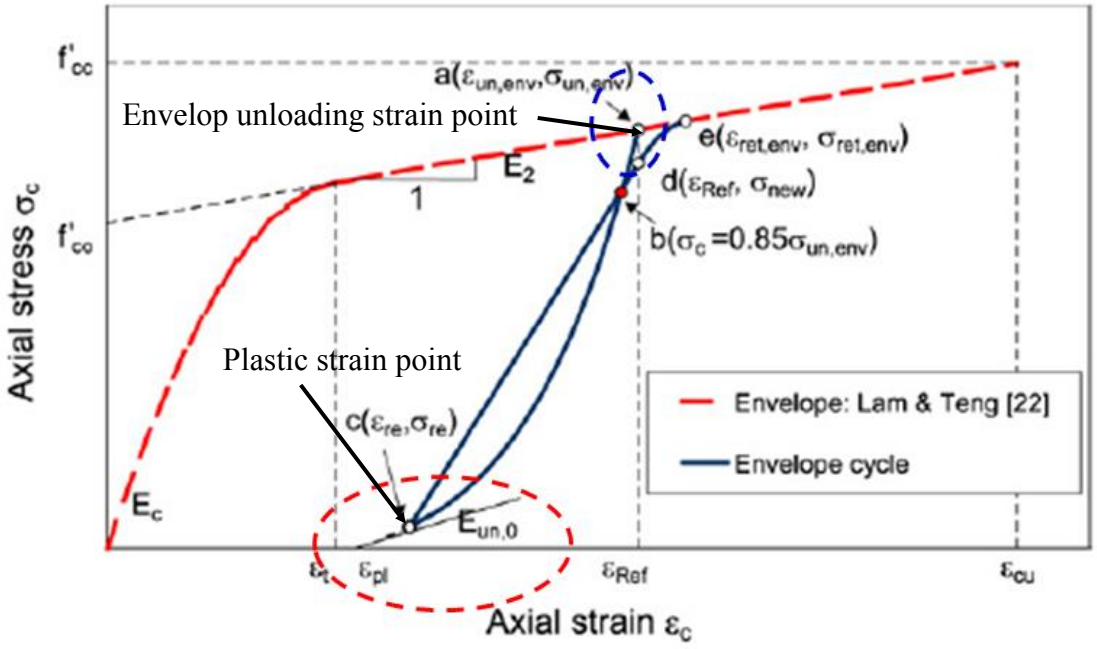

Figure 4.13: Typical axial cyclic stress-strain curves (Lam and Teng 2009)

A regression analysis of the CFFT tested columns was conducted by correlating the experimental plastic strain and the corresponding unloading envelop strain in each cycle as shown in Figure 4.14. In Figure 4.14, it can be observed that the plastic strains of the reinforced CFFT columns is linearly proportional with the envelop unloading strains. The strain region when ($0.001 \leq \varepsilon_{un,env} \leq 0.0035$) indicates that the residual plastic strains does not appear influenced significantly by the amount of confinement or the longitudinal reinforcement type and ratio. This observation is in a good agreement with the pervious tests conducted on FRP-confined unreinforced concrete cylinders (Lam and Teng 2009; Ozabakkalogu and Akin 2012) and reinforced concrete square prism (Wang et al 2012). However, in the strain region when $\varepsilon_{un,env} > 0.0035$, it was found that it depends little on the level of confinement as in the previous strain region but strongly on the internal longitudinal reinforcement type and ratio. The statistical characteristics of the trend lines for reinforced CFFT columns showed different trends. The slope of the trend lines of the specimens reinforced with GFRP bars decreases linearly with increasing the FRP longitudinal reinforcement ratio. Besides, the steel-reinforced CFFT column (after steel yielding) exhibited

larger plastic strains than the GFRP-reinforced CFFT columns at the same axial envelop unloading strain level.

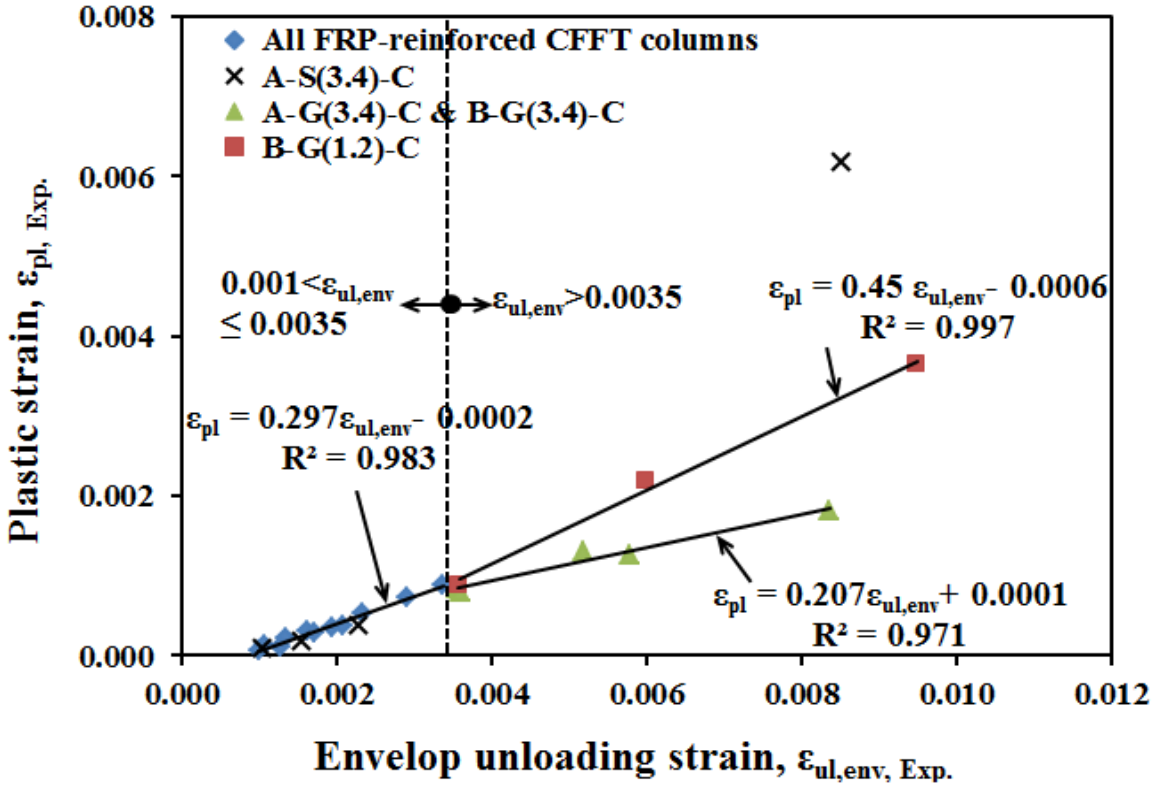

Figure 4.14: Plastic strain versus envelop unloading strain relationships of test specimens

4.5 Stress Deterioration

Previous investigations on the cyclic axial behaviour of confined concrete cylinders and square prisms unreinforced and reinforced internally with steel bars have shown that under unloading/reloading cycles that are subjected to stress deterioration (Lam and Teng 2009; Abbasina et al 2012; 2013; Wang et al 2012). In order to evaluate the degree of stress deterioration for the unloading/reloading paths of each cycle for the reinforced CFFT tested columns, a stress deterioration ratio is defined as follows:

$$\beta_1 = \frac{f_{new,1}}{f_{ul,env}} \tag{4.3}$$

where $f_{ul,env}$ is the envelop unloading stress, and $f_{new,1}$ is the stress where the first reloading path reaches to the point corresponding to $\varepsilon_{ul,max}$ (the maximum axial strain in the envelop

unloading path) (Abbasina et al 2012; 2013). Figure 4.15 shows the relationship between β1 and $\varepsilon_{ul,env}$. As shown in Figure 4.15, the stress deterioration for the CFFT columns reinforced with FRP bars is almost negligible when the envelop unloading strain is small and decreases gradually as the envelop unloading strain increases and remains approximately a constant value about 0.90, with a standard deviation equal to 0.009 at $\varepsilon_{un,env} > 0.002$. This is in agreement with Shao et al 2006 and Abbasina et al 2012; 2013 for FRP- confined concrete cylinders and square prisms, respectively. Besides, Figure 4.15 indicates that for FRP reinforced CFFT columns with different characteristics the stress deterioration ratio has the same trend. Thus, it can be concluded that the stress deterioration is independent of the FRP internal reinforcement and tubes thicknesses.

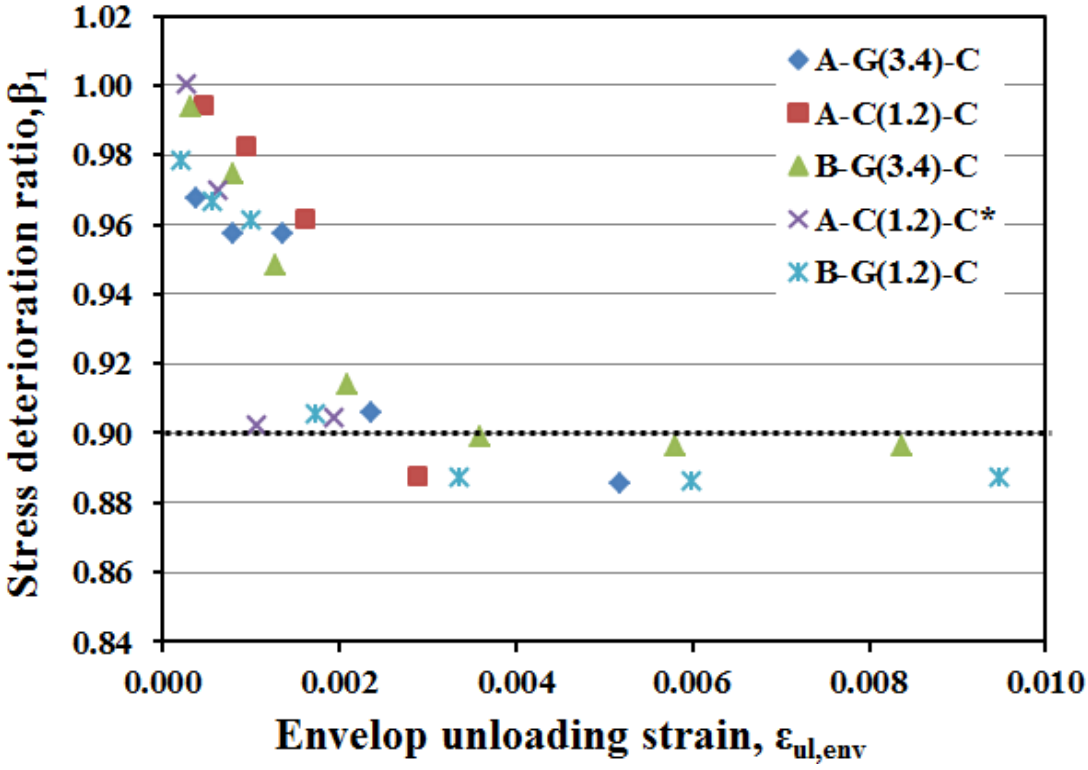

Figure 4.15: Stress deterioration ratio (β1) versus envelop unloading strain

4.6 Stress-Strain Responses of Longitudinal Reinforcement

Figure 4.16 to Figure 4.18 shows the axial stress-strain relationships for the longitudinal reinforcement of the tested specimens. As shown in Figure 4.16 that the axial stress-strain curves for steel and GFRP bars for control specimens exhibited a linear ascending branch

approximately at a strain level of 2100 με followed by a softening stress-strain response until failure. At the peak load level, the average axial strains for the GFRP and steel bars reached to 2495 and 2100 με, respectively. While the load carried by the reinforcement (computed by multiplying the area of the longitudinal reinforcement by the average axial strain and modulus of elasticity of the material) indicated that the GFRP and steel bars contributed to the ultimate load capacity of the columns by 10 and 15%, respectively. This confirms the integration of the GFRP bars used as the steel bars in compression for the tested columns (Mohamed et al 2014).

For steel-reinforced CFFT column, the stress-strain curve for steel bars showed a linear response until yielding stress at a stain approximately equal to 2100 με (Figure 4.17). After yielding, the axial stress- steel strain increased progressively in the horizontal direction until failure. It was observed that the yield load occurred at load level 83% of the ultimate capacity. This indicated that, for steel CFFT column, specimen (A-$S_{(3.4)}$- C) did not show much enhancement in the ultimate capacity after yielding. On the other hand, the GFRP-reinforced CFFT column initiated almost similarly response as steel-reinforced ones before steel yielding. However, the axial stress-strain response for steel-reinforced CFFT column at a strain level of 2000 με (close to yielding strain of steel) was slightly higher. This may attribute to axial rigidity of steel bars is higher than GFRP bars. While after strain level of 2000 με, the axial cyclic stress-strain curve for the GFRP-reinforced CFFT column started to deviate and continued to increase slightly until failure. This can be attributed to the linear behaviour of the FRP material. It should be noted that both specimens (A-$S_{(3.4)}$-C and A-$G_{(3.4)}$-C) at the same longitudinal ratio (ρ=3.4%) achieved similar axial strength. This indicated that the contribution of the GFRP bars in the axial capacity of the CFFT column is comparable to that of the steel bars (Masmoudi and Mohamed 2011).

The influence of the amount of longitudinal reinforcement was more pronounced for the specimens confined with thinner tube (Type A) than that with thicker tube (Type B). The specimens A-$C_{(1.2)}$-C and A-$G_{(3.4)}$-C (designed with similar axial stiffness) and confined with tube (A) did not maintain similar axial strength, the specimen A-$G_{(3.4)}$-C with higher reinforcement ratio exhibited higher axial capacity by 26%. On the other hand, increasing the longitudinal reinforcement ratio from 1.2 to 3.4% in the tested specimens (B-$G_{(3.4)}$-C and B-$G_{(1.2)}$-C) resulted in a increase in the axial load carrying capacity by only 5%.

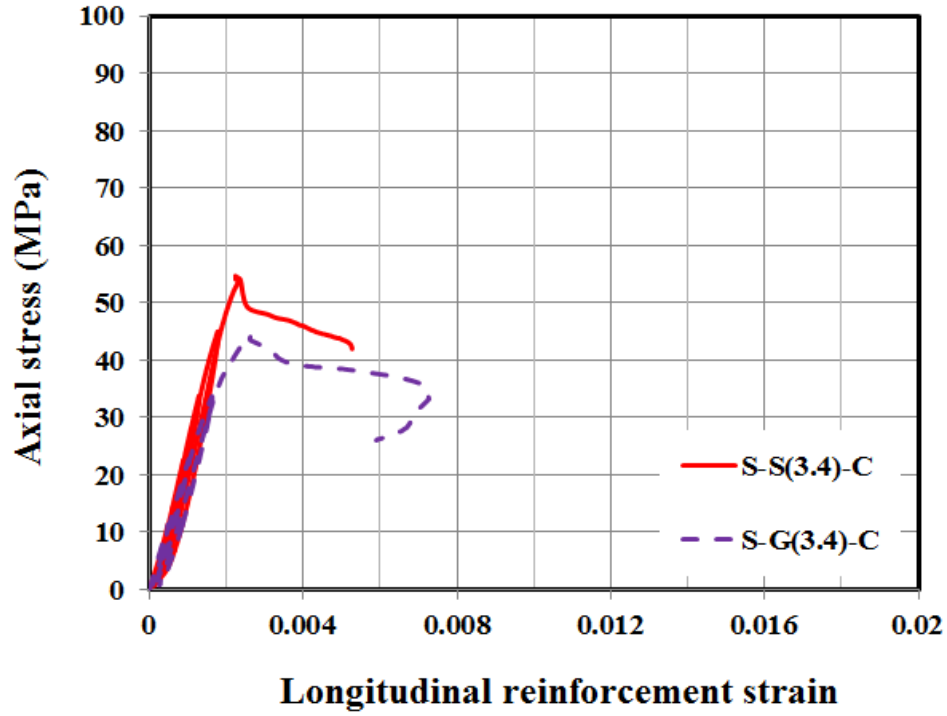

Figure 4.16: Axial stress-strain relationships for longitudinal bars for the control columns

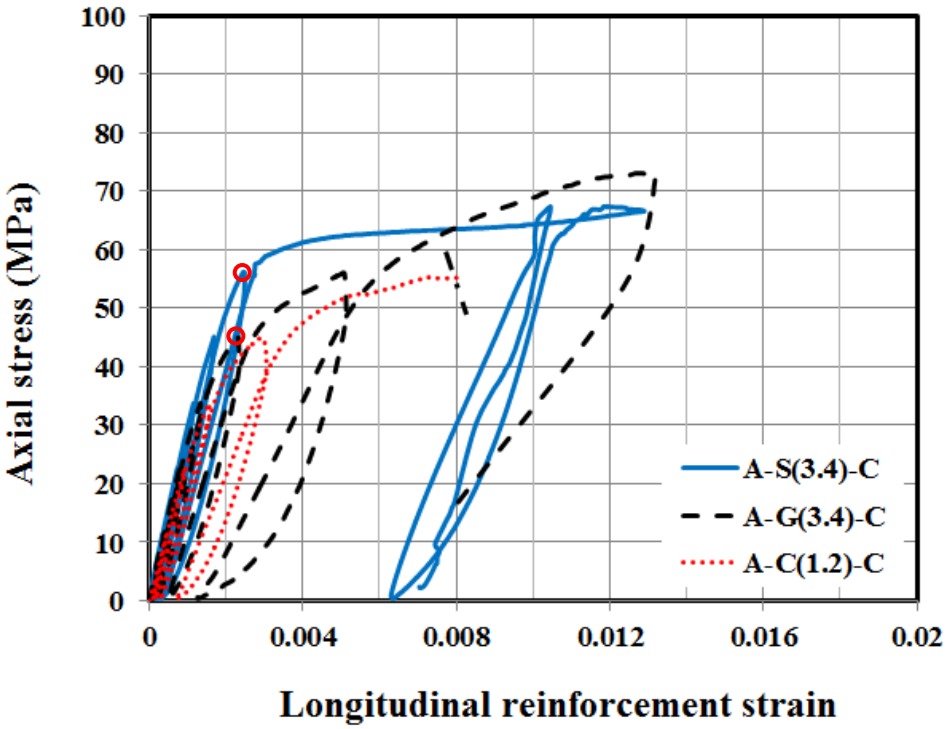

Figure 4.17: Axial stress-strain relationships for longitudinal bars for the reinforced-CFFT columns confined with tube type A

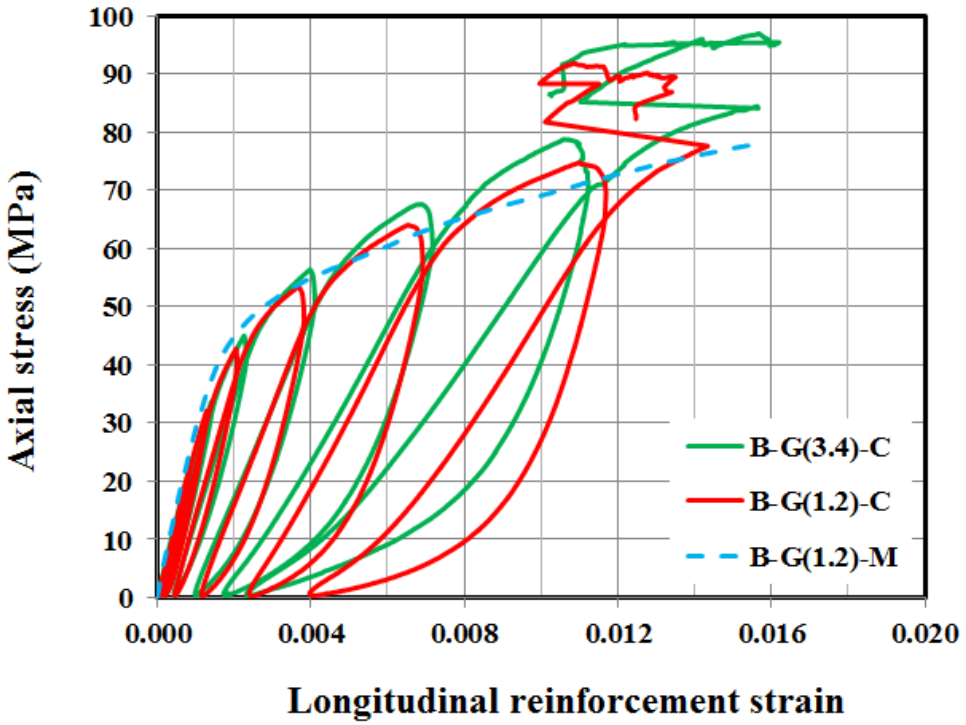

Figure 4.18: Axial stress-strain relationships for longitudinal bars for the reinforced-CFFT columns confined with tube type B

4.7 GFRP Tube Thickness Effect on Confinement

Table 4.1 shows the strength and strain enhancement ratios (f'_{cc}/f'_c and $\varepsilon_{cc}/\varepsilon_{co}$).Table 4.1 indicates that the strength and strain enhancement ratios of the CFFT columns (A-$S_{(3.4)}$-C and A-$G_{(3.4)}$-C) were increased ranging from 1.3 to 1.5 and 3.7 to 4.4 times their counterpart control specimens (S-$S_{(3.4)}$-C and S-$G_{(3.4)}$-C), respectively. Increasing the GFRP tube thickness from 2.9 to 6.4 mm enhanced both the strength and strain ratios by 25% and 12%, respectively. This can be attributed to the enhancement of lateral confinement, as a result of increasing the stiffness of the tube, which increased the ultimate axial stress capacities and strain of the tested CFFT columns. Typical distributions of axial and lateral strains at various loads of selected reinforced CFFT columns over the perimeter of the GFRP tube at the column mid-height are presented in Figure 4.19 to Figure 4.22. As shown in these figures, the uniform distribution of the lateral strains in the FRP tubes near loading level of 2000 kN indicates efficient confinement of the tubes. As a result of the instability failure of the reinforced CFFT columns due to buckling produced highly variable lateral confinement and induced significant

bending in the column before failure. The maximum, minimum, and average lateral strains in the hoop direction ($\varepsilon_{h,max,\ min,\ aver.}$) of the FRP tube at the ultimate load are reported in Table 4.1.

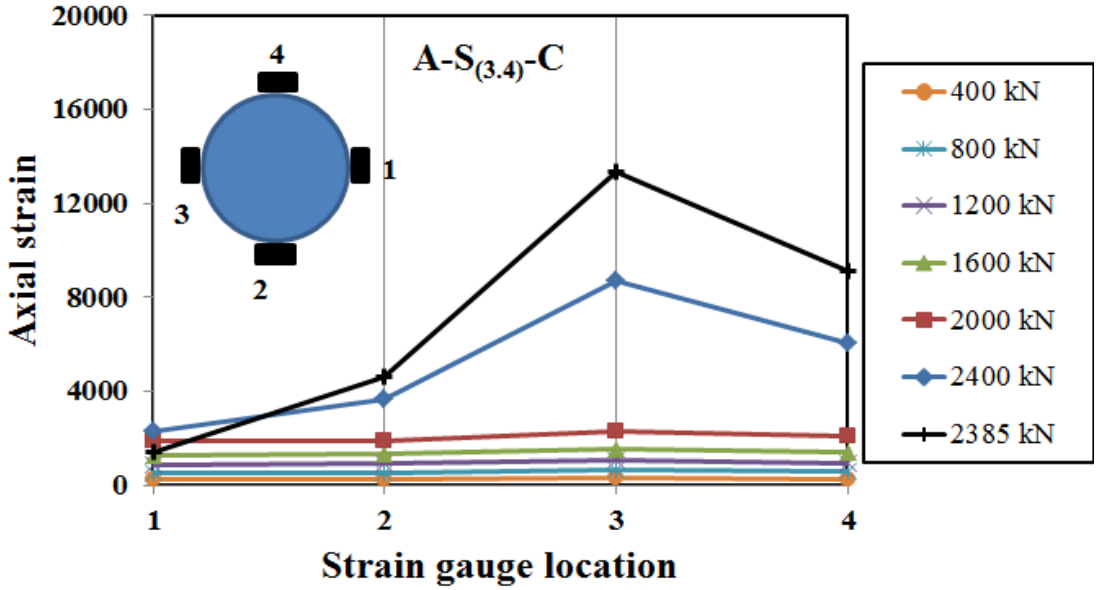

a) Axial strain distribution

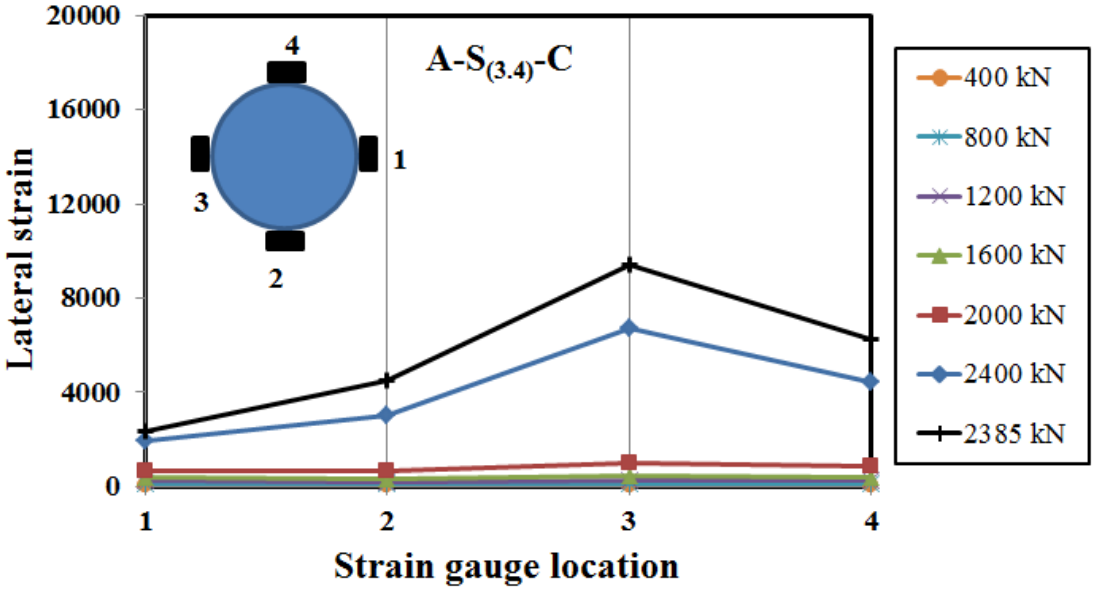

b) Lateral strain distribution

Figure 4.19: Strain distribution versus different strain gauges locations surrounding the column perimeter at the mid-height for specimen A-$S_{(3.4)}$-C

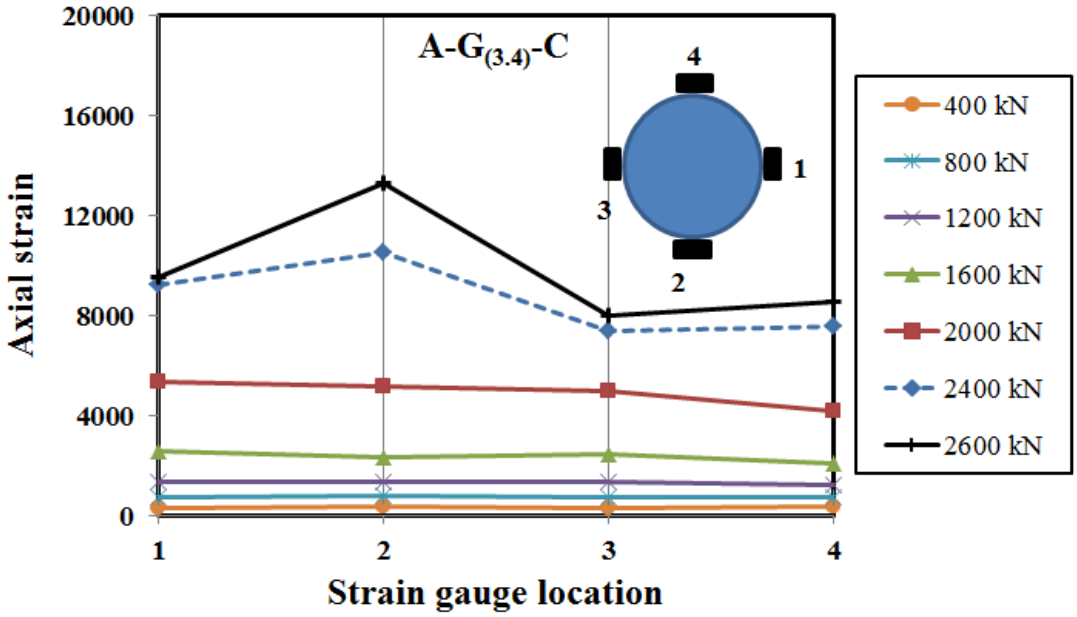

a) Axial strain distribution

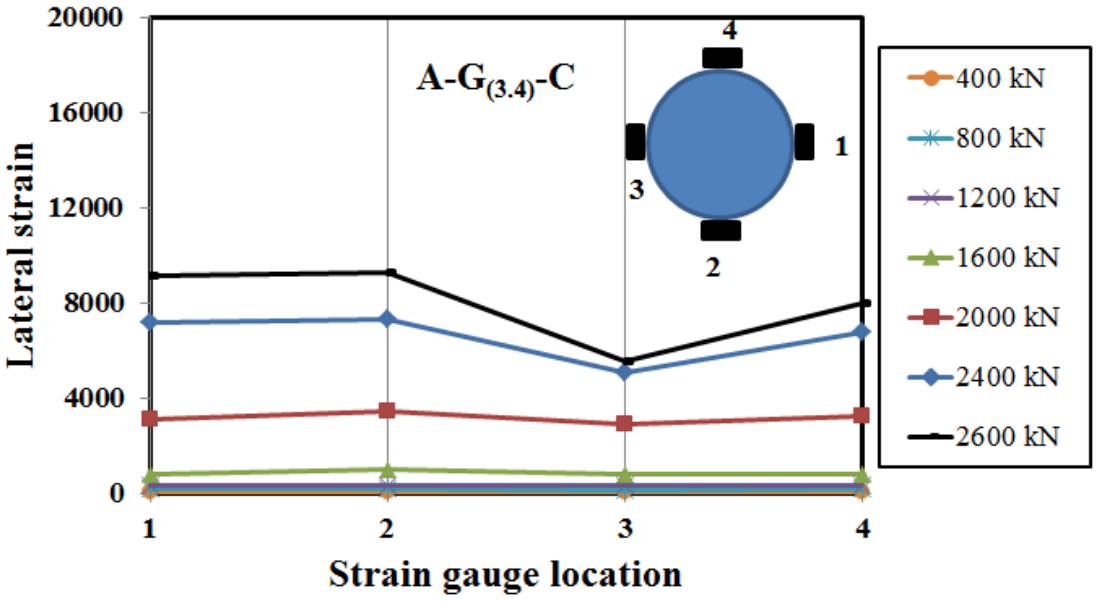

b) Lateral strain distribution

Figure 4.20: Strain distribution versus different strain gauges locations surrounding the column perimeter at the mid-height for specimen A-$G_{(3.4)}$-C

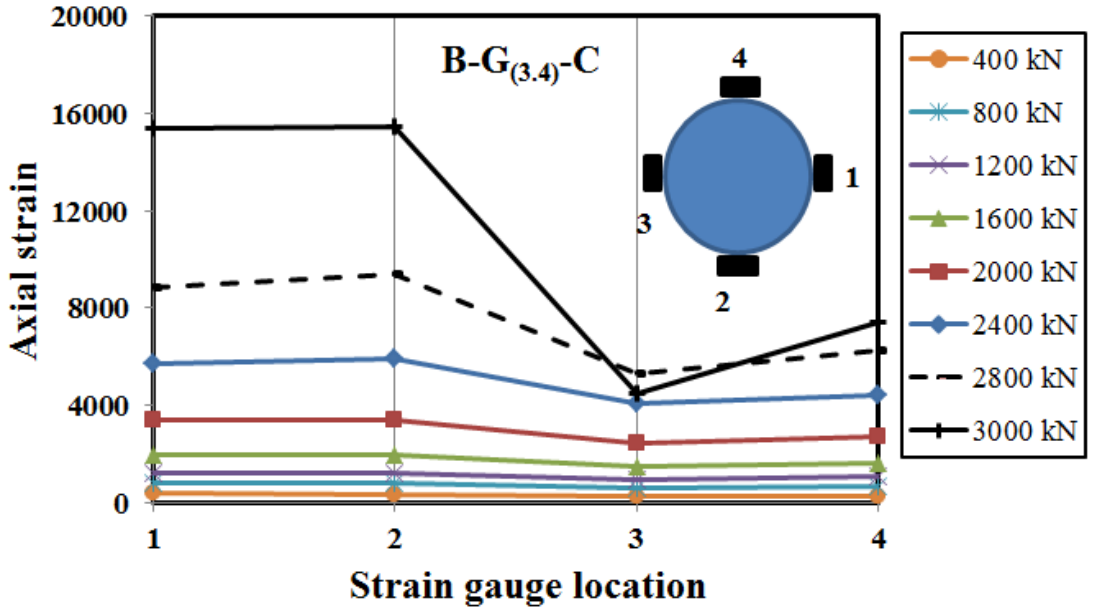

a) Axial strain distribution

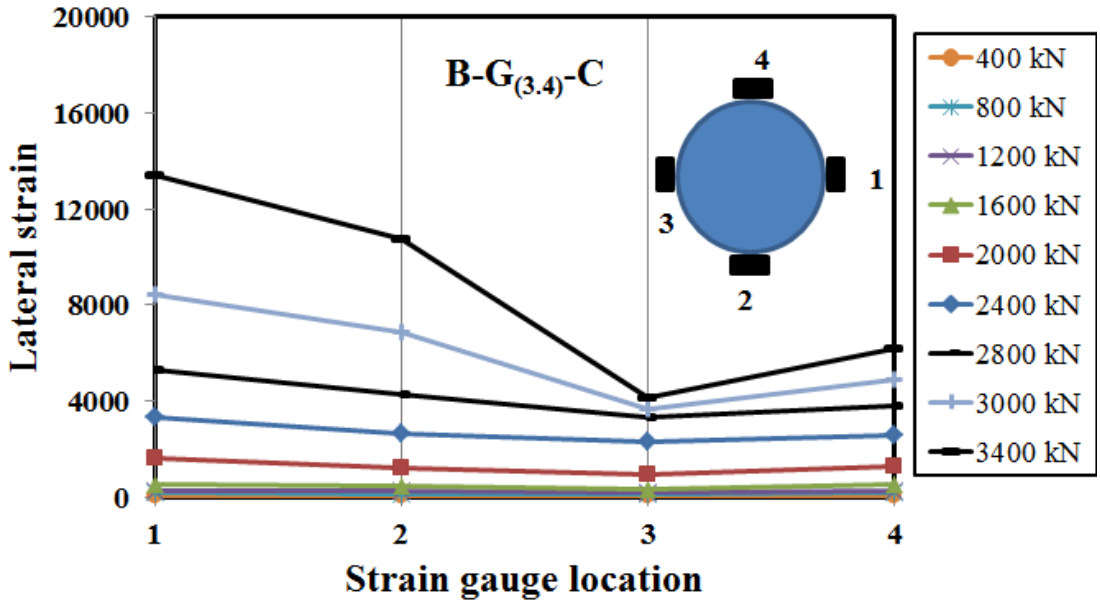

b) Lateral strain distribution

Figure 4.21: Strain distribution versus different strain gauges locations surrounding the column perimeter at the mid-height for specimen B-G$_{(3.4)}$-C

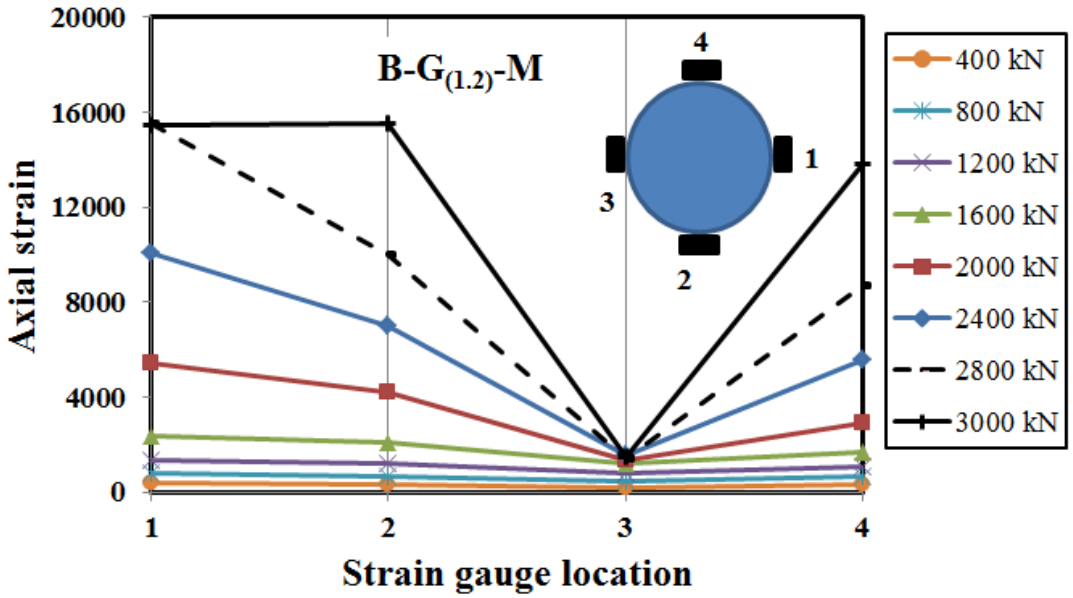

a) Axial strain distribution

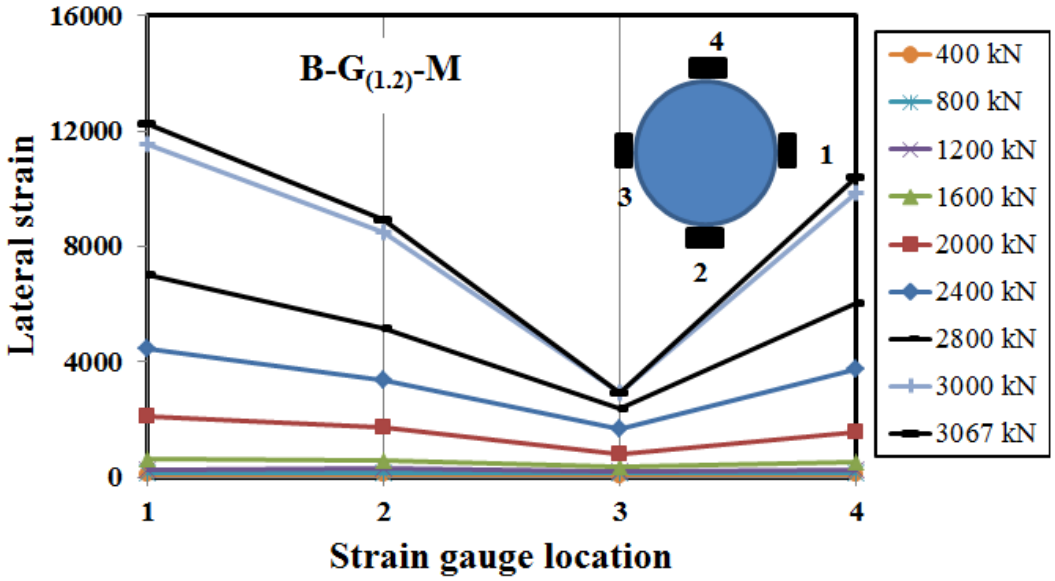

b) Lateral strain distribution

Figure 4.22: Strain distribution versus different strain gauges locations surrounding the column perimeter at the mid-height for specimen B-$G_{(1.2)}$-M

4.8 Effect of Loading Pattern

The responses in Figure 4.12 imply that the envelop curve of the long GFRP-reinforced CFFT column (B-$G_{(1.2)}$-C) subjected to cyclic loading was almost identical to the axial stress-

strain response of the monotonically loaded specimen (B-$G_{(1.2)}$-M). Generally, the ultimate axial strain of the cyclic loading specimen was slightly larger than that of the specimen subjected to monotonic loading. This observation is consistent with the tests on FRP-confined concrete cylinders (Lam and Teng 2009; Sho et al. 2006; Ozbakkaloglu and Akin 2012). Furthermore, the average ultimate lateral strains of specimen (B-$G_{(1.2)}$-C) were 18% (on average) higher than the specimen (B-$G_{(1.2)}$-M). This indicates that the unloading/reloading cycles can postpone the failure of the column. Lam and Teng 2009; Theodoros 2001 also reported the higher FRP ultimate lateral strains for cyclically loaded cylinders.

4.9 Code Predictions of the Axial Load Carrying Capacity

This section presents the predications of the axial load carrying capacity computed by the available North American design codes for steel and FRP bars with and without FRP confinement. The North American codes use the following equation to represent the theoretical nominal axial load capacity or yield point of short loaded steel-reinforced concrete (RC) columns under pure axial load (P_o):

$$p_o = k_c f_c^{/}\left(A_g - A_{st}\right) + f_y A_{st} \tag{4.4}$$

Where Ag is the gross sectional area of concrete, f '$_c$ is the ultimate concrete strength, f_y and A_{st} are the yielding strength and area of steel reinforcement bars, receptively. The parameter k_c is defined as the ratio between the in-place strength of concrete to concrete cylinder strength, $\left(f_{co}^{/} / f_c^{/}\right)$. The difference is attributed to the size effect, shape, and concrete casting practice between columns and concrete cylinders, a value of 0.85 is being suggested for k_c (Lyse and Kreidler 1932). The two Canadian codes CSA-S6-06 (2010) and CSA-A23.3 (2014) provide similar equations as in the ACI 318 (2014), except for introducing a material resistance factor for steel and concrete instead of the strength reduction factor specified in the ACI 318 (2014). In addition, the Canadian codes use the factor α_1 instead of k_c, which depends on the value of the unconfined concrete compressive strength. The ACI 440.R1 (2015), CSA S806 (2012), and S6-06 (2010) were used to calculate the maximum loading carrying capacity for the FRP-reinforced control specimens. However, the contribution of FRP bars in the ultimate capacity of the columns is neglected as specified by the design codes.

For the specimens confined with FRP tubes, the ACI 440.2R (2008) and the two Canadian codes (CSA S806 (2012), S6-06 (2010)) use the same equations of the conventional steel (RC) columns to predict the compressive strength but using $\left(f_{cc}^{/}\right)$ instead of$\left(f_{c}^{/}\right)$. The confinement models and the design equations for short FRP-confined-RC columns under axial load, as reported by the ACI 440.2R (2008) design guidelines and the two Canadian codes CSA-S6-06 (2010) and CSA S806 (2012) are summarized in Table 4.2 as more details have been given in Chapter 2.

Table 4.2: Axial load carrying capacity design equations for CFFT columns

Code	**Equation**	
CAN/CSA S806 (2012)	$p_r = 0.85\left[\alpha_1\varphi_c f_{cc}^{/}\left(A_g - A_s\right) + \varphi_s f_y A_s\right]$	(4.5)
	where: k_e=0.85, ϕ_c=0.60, ϕ_s=0.85 and ϕ_{FRP}=0.75	
	$f_{cc}^{/} = 0.85 f_c^{/} + k_l k_c f_l$	(4.6)
	where: k_l=6.7(f_l)$^{-0.17}$ k_c=1	
	$f_l = \frac{2 n_F t_F f_F}{D}$	(4.7)
	where: f_F = the smaller of $0.006E_f$ or $\phi_f f_{fu}$	
CAN/CSA S6-06 (2010)	$p_r = k_e\left[\alpha_1\varphi_c f_{cc}^{/}\left(A_g - A_s\right) + \varphi_s f_y A_s\right]$	(4.11)
	where: k_e=0.8, ϕ_c=0.75, ϕ_s=0.9 and ϕ_{FRP}=0.65	(4.12)
	α_1=0.85–0.0015 $f_c^{/} \geq 0.39$	
	$f_{cc}^{/} = f_c^{/} + 2 f_{lFRP}$	(4.13)
	$f_{lFRP} = \frac{2 t_{FRP}\phi_{FRP} f_{FRPu}}{D}$	(4.14)
	where: $0.1 f_c^{/} \leq f_{lFRP} \leq 0.33 f_c^{/}$	
ACI-440.2R-08	$\varphi p_n = 0.85\varphi\left[0.85 f_{cc}^{/}\left(A_g - A_{st}\right) + f_y A_{st}\right]$	(4.8)
	where: ϕ=0.75	
	$f_{cc}^{/} = f_c^{/} + \Psi_f 3.3 k_a f_{lFRP}$	(4.9)
	Where: Ψ_f=0.95, $(k_a) = 1$	
	$f_{lFRP} = \frac{2 E_f n t_f \varepsilon_{fe}}{D}$	(4.10)
	$\varepsilon_{fe} = k_\varepsilon \varepsilon_{fu}$, k_ε=0.55	
	where: $0.08 f_c^{/} \leq f_{lFRP}$, $\varepsilon_{ccu} \leq 0.01$	

4.9.1 Comparisons of predications versus experimental results

This section evaluates the applicability of the confinement models of the Canadian codes and the ACI design codes and guidelines to the tested columns and identifies the most and least conservative model's predictions. Table 4.3 and Table 4.4 present the predicated axial load carrying capacity versus the experimental test results for the control and CFFT-reinforced specimens as specified by the North American codes for steel and FRP bars, respectively. Figure 4.23 shows comparisons between the experimental results to the predicated axial carrying capacities of the tested specimens from different codes and guidelines. The safety and environmental reductions factors included in all the design equations were set to 1.0. Several limitations were also considered to control the $\left(f_{cc}^{/}\right)$ predications as recommended by the design codes and guidelines for instant the CAN/CSA-S806 (2012) limits the FRP hoop strain to 0.006 times its elastic modulus E_f while the CAN/CSA-S6-06 (2010) limits the confinement pressure f_{lFRP} at the ultimate limit state (ULS) to be between $0.1f_c^{/}$ and $0.33f_c^{/}$. Furthermore, the ACI 440.2R (2008) limits the maximum ultimate strain to 0.01 to prevent excessive cracking and the resulting loss of concrete integrity. When this limit is applicable, the corresponding maximum value of $\left(f_{cc}^{/}\right)$ should be recalculated from the stress-strain curve. The confining pressure f_{lFRP} was calculated based on the ultimate hoop tensile strength f_{FRPu}, which equals to the value obtained from the split disk test.

For the GFRP-reinforced control specimens, the ACI 440.R1 (2015), CSA S806 (2012), and CSA S6-06 (2010) predication values were an average (P_{test}/P_{pred}) of 1.45±0.02, 1.57±0.02, and 1.67±0.02 and COVs of 1.38%, respectively. The ACI 440.R1 (2015) was the closest predication values to the experimental results. However, all codes showed slightly higher conservative predication values for the GFRP-reinforced control specimens than for the steel-reinforced column. This might be due to neglecting the contribution of the compressive resistance of the GFRP bars to the axial carrying capacity. Tobbi et al. (2012) and Afifi el al (2014) reported that the compressive strength of the GFRP bars could be taken as a function of its tensile strength. Therefore, a new factor was introduced equal to 0.35 to account for the reduction in the compressive strength of the GFRP bars.

Table 4.3: Code predications comparisons versus test results for control (RC) columns

ID	P_{test}	ACI 440.R1 (2015)		CSA S806 (2012)		CSA S6-06 (2010)	
		$P_{Predict}$	P_{test} / $P_{Predict}$	$P_{Predict}$	P_{test} / $P_{Predict}$	$P_{Predict}$	P_{test} / $P_{Predict}$
S-$S_{(3.4)}$-C	1948	1524*	1.28*	1439*	1.35*	1354*	1.44*
S-$G_{(3.4)}$-C	1575	1097	**1.44**	1012	**1.56**	952	**1.65**
S-$G_{(3.4)}$-C*	1606	1097	**1.46**	1012	**1.59**	952	**1.69**
		Aver.	**1.45†**	Aver.	**1.57†**	Aver.	**1.67†**
		SD	**0.02†**	SD	**0.02†**	SD	**0.02†**
		COV%	**1.38†**	COV%	**1.38†**	COV%	**1.38†**

Note:
(*) Values calculated according to the ACI and CSA codes for steel.
(†) Average, SD and COV calculated for GFRP-reinforced control specimens only.

For FRP-reinforced CFFT columns, the ACI 440.2R (2008), CSA S806 (2012), and CSA S6-06 (2010) predication values were 1.68±0.31, 1.57±0.18, and 1.72±0.35 and a COV of 18.4%, 11.3%, and 20.5%, respectively. As shown in Table 4.4 the CSA S806 (2012) predications were better based on the average than the ones of the CSA S6-06 (2010) and ACI 440.2R (2008), particularly for specimens cast with tube Type B. However, all design codes and guidelines overestimated the values for the FRP-reinforced CFFT columns, particularly those specimens with tube Type B. It should be mentioned that the $\left(f_{cc}^{/}\right)$ provided by CSA S806 (2012) is governed by limiting the hoop tensile strain to be not more than 0.006. In addition, limiting the confinement pressure $f_{lFRP} \leq \left(0.33 f_{c}^{/}\right)$ according to the CSAS6-06 (2010) and the maximum ultimate strain to 0.01 according to the ACI 440.2R (2008) for the specimens cast with tube Type B leads also to be more conservative predictions. However, with no consideration for the confinement codes limits, the CSA S806 (2012) predication values was underestimation while the CSA S6-06 (2010) and ACI 440.2R (2008) yielded good yet conservative predication values (See Table 4.5 and Figure 4.24). It should be noted also that the final mode of failure of all CFFT specimens was instability failure. Moreover, omitting the contribution of the FRP bars in compression might also led to inaccurate predications values for the design codes. Therefore, further experimental investigations are needed to better understand and model the behaviour of CFFT columns internally reinforced with FRP and steel bars subjected to cyclic axial compression loading.

Table 4.4: Code predications comparisons versus test results for CFFT-reinforced columns (with allowable confinement codes limits)

ID	P_{test}	ACI 440.2R(2008)		CSA S806 (2012)		CSA S6-06 (2010)	
		$P_{Predict}$	P_{test} / $P_{Predict}$	$P_{Predict}$	P_{test} / $P_{Predict}$	$P_{Predict}$	P_{test} / $P_{Predict}$
A-$S_{(3.4)}$-C	2402	1998*	1.20*	1898	1.27*	1986*	1.21*
A-$G_{(3.4)}$-C	2603	1571	**1.66**	1471	**1.77**	1584	**1.64**
B-$G_{(3.4)}$-C	3455	1650	**2.09**	1976	**1.75**	1581	**2.19**
B-$G_{(1.2)}$-C	3272	1687	**1.94**	2020	**1.62**	1616	**2.02**
B-$G_{(1.2)}$-M	3068	1687	**1.82**	2020	**1.52**	1616	**1.90**
A-$C_{(1.2)}$-C	2086	1606	**1.30**	1504	**1.39**	1619	**1.29**
A-$C_{(1.2)}$-C*	2039	1606	**1.27**	1504	**1.36**	1619	**1.26**
		Aver.	**1.68†**	Aver.	**1.57†**	Aver.	**1.72†**
		SD	**0.31†**	SD	**0.18†**	SD	**0.35†**
		COV%	**18.4†**	COV%	**11.3†**	COV%	**20.5†**

Note:
(*) Values calculated according to the ACI and CSA codes for steel.
(†) Average, SD and COV calculated for FRP-reinforced CFFT specimens only (in bold).

Table 4.5: Code predications comparisons versus test results for CFFT-reinforced columns (with no consideration for allowable confinement codes limits)

ID	P_{test}	ACI 440.2R(2008)		CSA S806 (2012)		CSA S6-06 (2010)	
		$P_{Predict}$	P_{test} / $P_{Predict}$	$P_{Predict}$	P_{test} / $P_{Predict}$	$P_{Predict}$	P_{test} / $P_{Predict}$
A-$S_{(3.4)}$-C	2402	2185	1.10*	2712	0.89*	1986	1.21*
A-$G_{(3.4)}$-C	2603	1758	**1.48**	2285	**1.14**	1584	**1.64**
B-$G_{(3.4)}$-C	3455	2449	**1.41**	3442	**1.00**	2245	**1.54**
B-$G_{(1.2)}$-C	3272	2503	**1.31**	3519	**0.93**	2295	**1.43**
B-$G_{(1.2)}$-M	3068	2503	**1.23**	3519	**0.87**	2295	**1.34**
A-$C_{(1.2)}$-C	2086	1797	**1.16**	2336	**0.89**	1619	**1.29**
A-$C_{(1.2)}$-C*	2039	1797	**1.13**	2336	**0.87**	1619	**1.26**
		Aver.	**1.29†**	Aver.	**0.95**	Aver.	**1.42**
		SD	**0.13†**	SD	**0.10**	SD	**0.14**
		COV%	**9.8†**	COV%	**11.0**	COV%	**9.7**

Note:
(*) Values calculated according to the ACI and CSA codes for steel.
(†) Average, SD and COV calculated for FRP-reinforced CFFT specimens only (in bold).

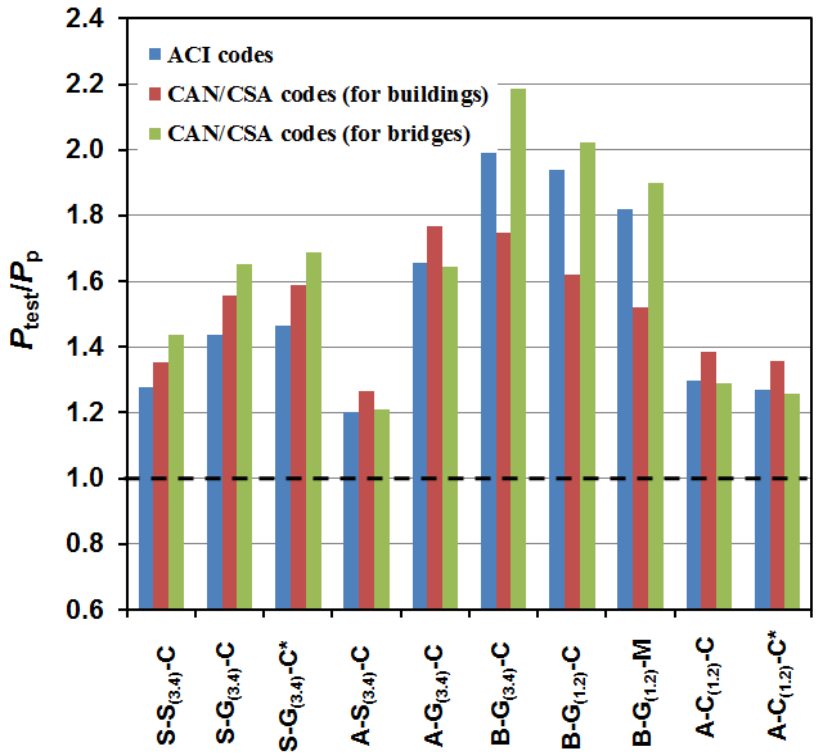

Figure 4.23: Experimental loads versus predicted values for the tested specimens (considering confinement codes limits)

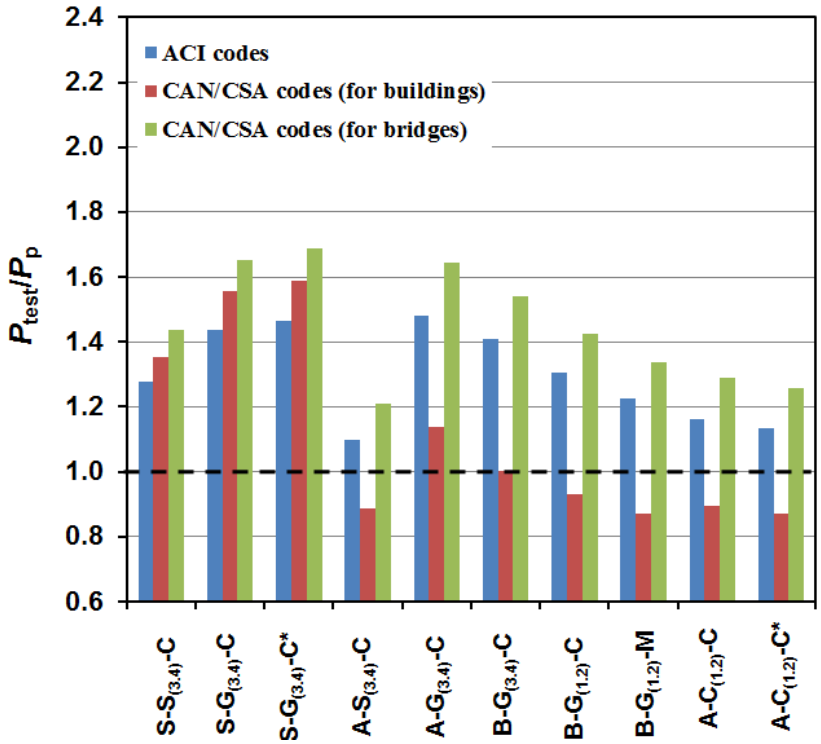

Figure 4.24: Experimental loads versus predicted values for the tested specimens (with no considering confinement codes limits)

CHAPTER 5
SUMMARY AND CONCLUSIONS

5.1 Summary

This research work presents the test results of an experimental study aimed at investigating the behaviour of concrete-filled fiber-reinforced-polymer (FRP) tubes (CFFT) long columns internally reinforced with longitudinal steel and FRP bars under axial compression loading. A total of ten reinforced concrete (RC) and CFFT columns measuring 1900-mm in height and 213-mm in diameter were constructed and tested until failure. The test specimens were divided into two series denoted as Series I and II. Series I included three control RC specimens reinforced with longitudinal reinforcement ratio (ρ_L) equal to (3.4%), one specimen reinforced with steel bars and two identical specimens reinforced with GFRP bars. Steel spiral stirrups were used as transverse reinforcement. Series II consisted of seven reinforced CFFT columns laterally confined with GFRP tubes (Type A or B). One specimen reinforced steel bars and laterally confined with tube type (A). Four specimens reinforced with GFRP bars (ρ_L = 1.2 and 3.4%) and laterally confined with tubes type (A and B). Besides, two identical specimens reinforced with CFRP bars (ρ_L = 1.2 %) and laterally confined with tube type (A). All specimens were tested under single complete unloading/reloading cyclic axial compression loading, except for one specimen, which was tested under monotonic axial compression loading. The investigated test parameters were: (i) GFRP tubes thicknesses (2.9 and 6.4 mm); (ii) internal reinforcement type (steel; GFRP; or CFRP bars) and amount; and (iii) natural of loading (i.e. monotonic and cyclic. The completion of this research program led to the following conclusions and recommendations.

5.2 Conclusions

The following general conclusions can be drawn based on the experimental test results and discussions of research work presented in this dissertation:

1. The CFFT columns reinforced with GFRP bars exhibited similar responses compare to their counterparts reinforced with steel bars at the same longitudinal reinforcement amount. No significant difference was observed in terms of ultimate axial strength and strain capacities.
2. The reinforced CFFT tested columns showed substantially different mode of failure compared to that occurred for the control columns. The FRP tube provided significant confinement attributing to shift the mode of failure from axially dominated material failure to flexural-dominated instability failure.
3. In general, the envelop curves for the CFFT tested specimens showed bilinear responses with a transition zone near of the peak strength of the unconfined concrete ($f_c^{'}$). The slope of the second branch is highly governed by GFRP tube stiffness rather than the longitudinal reinforcement amount and type.
4. The envelop curve of the CFFT reinforced column under cyclic loading is almost identical to the axial stress-strain curve of the same specimen under monotonic loading. However, the ultimate axial and hoop rupture strain was slightly larger for the specimen subjected to cyclic loading.
5. The unloading paths for the CFFT tested columns with steel or FRP bars exhibited non-linear behaviour. The degree of the non-linearity increases as the unloading axial strain increases. Moreover, the reloading paths could be resembled as straight lines.
6. Increasing the thickness of the GFRP tubes significantly increased the ultimate axial and strain capacities of the CFFT reinforced tested columns.
7. The plastic strains of the FRP-reinforced CFFT columns is linearly proportional to the envelop unloading strains. The relationship is depended little on level of confinement but strongly on the longitudinal reinforcement amount and type, particularly when $\varepsilon_{un,env} > 0.0035$.
8. Using FRP bars instead of conventional steel bars in the CFFT columns can provide a step forward to develop a totally corrosion-free new structural system.
9. For the GFRP-reinforced control specimens, the ACI 440.R1 (2015), CSA S806 (2012), and CSA S6-06 (2010) predication values were an average (P_{test}/P_{pred}) of 1.45±0.02, 1.57±0.02, and 1.67±0.02 and COVs of 1.38%, respectively. The ACI 440.R1 (2015) was the closest predication values to the experimental results. However,

10. The ACI 440.R1 (2015), CSA S806 (2012), and CSA S6-06 (2010) design provisions provided higher conservative results for the GFRP-reinforced control specimens than that of steel-reinforced specimen. This might be due to neglecting the contribution of the compressive resistance of the GFRP bars to the axial carrying capacity.

11. For FRP-reinforced CFFT columns, the ACI 440.2R (2008), CSA S806 (2012), and CSA S6-06 (2010) predication values were 1.68±0.31, 1.57±0.18, and 1.72±0.35 with a COV of 18.4%, 11.3%, and 20.5%, respectively. By considering the confinement codes limits, the CSA S806 (2012) was better predication based on the average than that of the CSA S6-06 (2010) and ACI 440.2R (2008), particularly for specimens cast with tube Type B.

12. Removing the FRP hoop tensile strength limit to 0.006 its elastic modulus E_{FRP} by CAN/CSA S806 (2012) lead to less conservative predictions for the confined concrete compressive strength. While the CAN/CSA S6-06 (2010) and ACI 440.2R (2008) confinement models showed good yet conservative predictions.

Further experimental investigations are needed to better understand and model the behaviour of CFFT columns internally reinforced with FRP and steel bars subjected to cyclic axial compression loading.

5.3 Conclusions en Français

Les conclusions générales suivantes peuvent être émises sur la base des résultats des essais expérimentaux et des discussions de travaux de recherche présentés dans cette thèse:

1. Les colonnes CFFT renforcées avec de barres en PRFV présentaient des réponses similaires comparées à celles renforcées de barres d'acier avec la même quantité d'armature longitudinale. Aucune différence significative n'a été observée en termes de capacités ultimes de résistance axiale et de déformation.
2. Les colonnes CFFT testées montrent sensiblement différents modes de rupture par rapport à ceux obtenus avec des colonnes de contrôle. Le tube en PRF fournit un confinement significatif attribuant à changer le mode de rupture d'une rupture des matériaux axialement à une rupture au niveau de l'instabilité en flexion.

3. En général, les courbes d'enveloppe pour les échantillons testés ont montré des réponses bilinéaires avec une zone de transition proche de la pointe de la résistance du béton non confiné ($f_c^{'}$). La pente de la deuxième branche est fortement régie par la rigidité du tube PRFV plutôt que la quantité et le type d'armatures longitudinales.
4. La courbe de l'enveloppe des colonnes CFFT sous chargement cyclique est presque identique à la courbe charge axiale-déformation du même échantillon sous chargement monotone. Cependant, la déformation axiale et la rupture en déformation étaievt légèrement plus grandes lorsque l'échantillon est soumis à une charge cyclique.
5. Les chemins de déchargement pour les colonnes testées avec de l'acier ou des barres en PRF montrent un comportement non-linéaire. Le degré de la non-linéarité augmente à mesure que la déformation axiale de déchargement augmente. En outre, les chemins de rechargement pourraient ressembler à des lignes droites.
6. L'augmentation de l'épaisseur des tubes en PRFV augmente de manière significative les capacités uttimes de déformation et axiale des colonnes testées.
7. Les déformations plastiques des colonnes renforcées de PRF sont linéairement proportionnelles aux tensions d'enveloppe de déchargement. La relation dépend un peu du niveau de confinement mais fortement de la quantité et du type de renfort longitudinal, en particulier lorsque $\varepsilon_{de,env} > 0{,}0035$.
8. L'utilisation des barres en PRF au lieu de barres d'acier conventionnelles dans les colonnes CFFT peut fournir un pas en avant pour développer un nouveau système structural sans corrosion.
9. Pour les échantillons de contrôle renforcés de PRFV, les valeurs prédites de l'ACI 440.R1 (2015), du CSA S806 (2012), et du CSA S6-06 (2010) étaient en moyenne (P_{test} / P_{pred}) de 1,45 ± 0,02, 1,57 ± 0,02, et 1,67 ± 0,02 et 1,38% de COV, respectivement. Les valeurs prédites de l'ACI 440.R1 (2015) étaient plus proches des résultats expérimentaux.
10. Les prévisions de l'ACI 440.R1 (2015), CSA S806 (2012), et CSA S6-06 (2010) ont fourni des résultats conservateurs plus élevés pour les échantillons de contrôle en PRFV que celui de l'échantillon d'acier. Cela peut être dû à l'effet de la négligence de la contribution de la résistance à la compression des barres en PRFV à la capacité de la charge axiale.

11. Pour les colonnes renforcées de PRFV, les valeurs prédites de l'ACI 440.2R (2008), du CSA S806 (2012), et du CSA S6-06 (2010) étaient de 1,68 ± 0,31, 1,57 ± 0,18 et 1,72 ± 0,35 et un COV de 18,4%, 11,3%, et 20,5%, respectivement. En considérant les limites des codes de confinement, la prévision du CSA S806 (2012) était mieux basée sur la moyenne que celles du CSA S6-06 (2010) et de l'ACI 440.2R (2008), en particulier pour les échantillons testés avec le tube de type B.
12. La suppression de la limite de résistance à la traction du cerceau en PRF à 0,006 de son module d'élasticité E_{FRP} par le CAN/CSA S806 (2012) conduit à des prévisions moins prudentes pour la résistance à la compression du béton confiné. Alors que les modèles de confinement de la norme CAN/CSA S6-06 (2010) et de l'ACI 440.2R (2008) ont montré des bonnes prédictions encore conservatrices.

En outre, des études expérimentales sont nécessaires pour mieux comprendre et modéliser le comportement des colonnes CFFT renforcés avec des barres de PRF et de l'acier et soumises à des charges de compression axiale cycliques.

5.4 Recommendations for Future Work

This chapter presents the conclusions that can be drawn from the research conducted. However, more work in related areas still needs to be conducted. A few recommendations for future study are also made:

1. Examine the behaviour of FRP-reinforced CFFT columns under combined axial load and bending moment and establish interaction diagrams for the sections.
2. Examine the behaviour of FRP-reinforced CFFT columns under dynamic lateral loading.
3. Investigate the effect of cross-section (square and rectangular) on the behaviour of the FRP-reinforced CFFT columns.
4. Investigate the effect of slenderness ratio on the behaviour of the FRP-reinforced CFFT square and rectangular columns.

REFERENCES

Abbasnia, R., Ahmadi, R., Ziaadiny, H., (2012), "Effect of confinement level, aspect ratio and concrete strength on the cyclic stress–strain behaviour of FRP-confined concrete prisms", Composites: Part B 43 (2012) 825–831.

Abbasnia, R., Hosseinpour, F., Rostamian, M., Ziaadiny, H., (2013), "Cyclic and monotonic behaviour of FRP confined concrete rectangular prisms with different aspect ratios", Construction and Building Materials 40 (2013) 118–125.

American Concrete Institute (ACI), (2008), "Guide for the design and construction of externally bonded FRP systems for strengthening concrete structures." ACI 440.2R-08, Farmington Hills, Mich.

American Concrete Institute (ACI), (2014), "Building code requirements for structural concrete." ACI 318-11, Farmington Hills, Mich.

ASTM D638 - 10 (2010), "Standard test method for tensile properties of plastics" American National Standards Institute (ANSI), 25 W. 43rd St., 4th Floor, New York, NY 10036, http://www.ansi.org.

ASTM D3410/D3410M-03, (2008), "Standard test method for compressive properties of polymer matrix composite materials with unsupported gage section by shear loading", American National Standards Institute (ANSI), 25 W. 43rd St., 4th Floor, New York, NY 10036, http://www.ansi.org.

ASTM A615/A615M-09, ASTM (2009), "Standard specification for deformed and plain carbon steel bars for concrete reinforcement", West Conshohocken, Pa.

ASTM D2290 – 12, (2012), "Standard test method for apparent hoop tensile strength of plastic or reinforced plastic pipe", American National Standards Institute (ANSI), 25 W. 43rd St., 4th Floor, New York, NY 10036, http://www.ansi.org.

Bank, L. C., (2006), "Composite for construction: Structural design with FRP materials," John Wiley & Sons, Hoboken, NJ, Canada, ISBN-13: 978-0471-68126-7, pp. 560.

Benthelot J. (1995). "High mechanical performance composites and design of composite structures." Polymer and the Advanced Materials: Engineering Technologies and Business Opportunities. Edited by P.N. Prasad et al., Plenum Press, New York, pp. 7-20.

Binici, B. (2005). "An analytical model for stress–strain behaviour of confined concrete." Eng. Struct., 27(7), 1040–1051.

Burgueño, R., (1999), "System characterization and design of modular fiber reinforced polymer (FRP) Short- and Medium-Span Bridges," PhD thesis, University of California, San Diego, La Jolla, CA, 587 pp.

Canadian Standards Association (CAN/CSA), (2014), "Design of concrete structures." A23.3-14, Mississauga, Canada.

Canadian Standard Association (CSA), (2012), "Design and construction of building components with fibre-reinforced polymers." CSA-S806-12, Rexdale BD, Toronto.

Canadian Standard Association (CSA), (2010), "Canadian highway bridge design code." CAN/CSA-S6-06, Toronto.

Collins, M. P.; and Mitchell, D., (1997), "Prestressed concrete structures", Response publications, Toronto, Canada, 61-62 pp.

Considere, A., (1903), "Experimental research on reinforced concrete", Translated and Arranged by Leon S, Moisseiff, McGraw Publishing Co., New York, 188 pp.

Davol, A.; Burgueño, R.; and Seible, F., (2001), "Flexural behaviour of circular concrete filled FRP shell," Journal of Structural Engineering, V. 127, No. 7, pp. 810-817.

Fam, A., (2000), "Concrete-filled fiber reinforced polymer-reinforced tubes for axial and flexural structural members" *PhD thesis*, Department of Civil and Geological Engineering. The University of Manitoba, Winnipeg, Manitoba.

Fam, A. Z., and Rizkalla, S. H., (2001a), "Behaviour of axially loaded concrete-filled circular fiber reinforced polymer tubes," ACI Structural Journal, V. 98, No. 3, May- June, pp. 280-289.

Fam, A. Z., and Rizkalla, S. H., (2001b), "Confinement model for axially loaded concrete confined by FRP tubes," ACI Structural Journal, V. 98, No. 4, July-Aug., pp. 451-461.

Fam, A. Z., and Rizkalla, S. H., (2002), "Flexural behaviour of concrete-filled fiber-reinforced polymer circular tubes," Journal of Composites for Construction, ASCE, V. 6, No. 2, pp. 123-132.

Fam, A., Flisak, B., and Rizkalla, S., (2003a), "Experimental and analytical modeling of concrete-filled fiber-reinforced polymer tubes subjected to combined bending and axial loads", ACI Structural Journal, V. 100, No. 4.

Fam, A., Greene, R. and Rizkalla, S., (2003b), "Field Applications of Concrete-Filled FRP Tubes for Marine Piles", ACI Special Publication SP-215-9 (Field Application of FRP Reinforcement: Case Studies), pp.161-180.

Fam, A, Schnerch, D, and Rizkalla, S., (2005), "Rectangular filament-wound glass fiber reinforced polymer tubes filled with concrete under flexural and axial loading: Experimental Investigation", Journal of Composites for Construction, Vol. 9, No. 1, pp.25-33.

Fitzwilliam, J and Bisby, L., (2010), "Slenderness effects on circular CFRP confined reinforced concrete columns," Journal of Composites for Construction, Vol. 14, No. 3, pp.: 280-288.

Gardner, N. J., and Jacobson, E. R., (1967), "Structural behaviour of concrete filled steel tubes", ACI J., 64 (7), 404-413.

Hadi, M., and Le, T., (2014), "Behaviour of hollow core square reinforced concrete columns wrapped with CFRP with different fibre orientations," Construction and Building Materials, 50 (January), 62-73.

Hahn H. and Tsai, S. (1973). "Nonlinear elastic behaviour of unidirectional composite laminae." Journal of Composite Materials, Vol. 7, January, pp. 102-118.

Hahn H., (1973), "Nonlinear behaviour of laminated composites." Journal of Composite Materials, Vol. 7, April, pp. 257-271.

Haj-Ali, R. and Kilic, H., (2002), "Nonlinear behaviour of pultruded FRP composites." Composites Part B: Engineering, Elsevier, Vol. 33, pp. 173-191.

Han TH, Stallings JM, Cho SK, Kang YJ., (2010), " Behaviour of a hollow RC column with an internal tube", Magazine of Concrete Research, 62(1):25-38.

Harries, K., and Kharel, G., (2002), "Behaviour and modeling of concrete subject to variable Confining Pressure", ACI Materials Journal, V. 99, No. 2.

Hong, W. K., and Kim, H. C., (2004), "Behaviour of concrete columns confined by carbon composite tubes." Can. J. Civ. Eng., 31(2), 178–188.

Hollaway, L. (Ed.), (1990), "Polymers and polymer composites in construction". Thomas Telford Ltd., London.

Hu, H., (1993), "Buckling analyses of fiber-composite laminate shells with material nonlinearity." Journal of Composites Technology & Research, JCTRER, Vol. 15, No. 3, Fall 1993, pp. 202-208.

Idris, Y., and Ozbakkaloglu, T. (2013). "Seismic behaviour of square high-strength concrete-filled FRP tube columns." J. Compos. Constr., 10.1061/(ASCE)CC.1943-5614.0000388.

Jiang, T., and Teng, J. G., (2013), "Behaviour and Design of Slender FRP-Confined Circular RC Columns." Journal of Composites for Construction, Vol. 17, No. 4, pp: 443-453.

Jones, R. (1975). "Mechanics of composites materials". McGraw-Hill Book Co., New York, N.Y.

Karimi, K, Tait, M, and El-Dakhahkni, W., (2012), "Influence of Slenderness on the behaviour of a FRP-Enclosed Steel-Concrete Composite Column", Journal of Composites for Construction, ASCE, ISSN 1090-0268/2012/1-100–109.

Kent, D. C.; and Park, R., (1971), "Flexural members with confined concrete", Proceedings, ASCE, V. 97, ST7, July 1971, 1969- 1990 pp.

Kilpatrick, A. E., and Rangan, B. V., (1997), "Deformation-control analysis of composite concrete columns," Research Report No. 3/97, School of Civil Engineering, Curtin University of Technology, Perth, Australia, July.

Kloppel, Von K., and Goder, W., (1957), "Traglastversuche mit ausbetonierten Stahlrohren and Aufstellung einer Bemessungsformel", Der Stahlbau (Berlin), 26 (1).

Kusumawardaningsih, Y., Hadi, M., (2010), "Comparative behaviour of hollow columns confined with FRP composites. Composite Structures, 93(1):198-205.

Lam, L., and Teng, J. G. (2003). "Design-oriented stress-strain models for FRP confined concrete." Construct. Build. Mater., 17(6–7), 471–489.

Lam, L., and Teng, J. G. (2004). "Ultimate condition of FRP-confined concrete." J.Compos. Constr., 8(6), 539–548.

Lam, L., and Teng, J. G., (2009), "Stress-strain model for FRP-confined concrete under cyclic axial compression." Eng. Struct., 31(2), 308–321.

Lifshitz, J. (1988) "Determination of nonlinear shear modulus of a fiber-reinforced lamina from the axial behaviour of (±45) Specimens." Journal of Composites Technology & Research, JCTRER, Vol. 10, No. 4, pp. 146-150.

Lignola, G., Prota A., Manfredi G., and Cosenza E., (2007), " Experimental performance of RC hollow columns confined with CFRP". Journal of Composites for Construction, 11(1):42-49.

Lorenzis, L., and Tepfers, R., (2003), "Comparative study of models on confinement of concrete cylinders with fiber-reinforced polymer composites", Journal of Composites for Construction, Vol. 7, No.3.

Lyse, I., and Kreidler, C. L., (1932), "Fourth progress report on column tests at Lehigh University." ACI Structural Journal, V.28, 317–346.

Mandal, S., Hoskin, A., and Fam, A., (2005), "Influence of concrete strength on confinement effectiveness of fiber-reinforced polymer circular jackets", ACI Structural Journal, V. 102, No. 3.

Masmoudi, R. and Mohamed, H., (2011), "Axial behaviour of slender-concrete-filled FRP tube columns reinforced with steel and carbon FRP bars". 10th International Symposium on Fiber-Reinforced Polymer Reinforcement for Concrete Structures, Tampa, Florida, April 2011, ACI-SP-275.

Matthys, S., Taerwe, L., and Audenaert, K., (1999), ''Tests on axially loaded concrete columns confined by fiber reinforced polymer sheet wrapping.'' Proc., FRPRCS-4, Baltimore, 217–228.

Mirmiran, A., (1995), "Concrete composite construction for durability and strength," Symposium on Extending Life Span of Structures, International Association for Bridge and Structural Engineering (IABSE), San Francisco, Calif., Aug., pp. 1155-1160.

Mirmiran, A., Shahawy, M., Samaan, M., El Echary, H., Mastrapa, J. C., and Pico, O., (1998), "Effect of column parameters on FRP-confined concrete." J.Compos.Constr.,10.1061/(ASCE)1090-0268(1998)2:4(175), pp.175–185.

Mirmiran, A.; Shahawy, M.; and Beitleman, T., (2001), "Slenderness Limit for Hybrid FRP Concrete Columns," Journal of Composites for Construction, ASCE, V. 5, No.1, pp. 26-34.

Mohamed, H., and Masmoudi, R., (2008), "Behaviour concrete filled GFRP tube columns under eccentric loading" MESC-5, the fifth Middle East Symposium on structural composites for infrastructure applications. Innovations &Applications, proceedings on CD-Rom, Hurghada, Egypt, 23-25th May, 10p.

Mohamed, H., Abdel Baky, H.M., and Masmoudi, R., (2010), "Nonlinear stability analysis of CFFT columns: Experimental and Theoretical Investigations", ACI Structural Journal, V. 107, No. 6, pp. 699-708.

Mohamed, H., and Masmoudi, R., (2010), "Axial load capacity of concrete-filled FRP tube columns: Experimental versus Theoretical Predictions." J. Compos. Constr., 14(2), pp. 231-243.

Mohamed, (2010), "Axial and flexural behaviour of reinforced concrete-filled FRP tubes: experimental and theoretical studies", PhD thesis, Civil engineering Department, University of Sherbrooke, 296 pp.

Mohamed, H.; Afifi, M.; and Benmokrane, B., (2014), "Performance Evaluation of Concrete Columns Reinforced Longitudinally with FRP Bars and Confined with FRP Hoops and Spirals under Axial Load", the Journal of Bridge Engineering, © ASCE, ISSN 1084-0702/04014020(12).

Ozbakkaloglu, T., and Saatcioglu, M., (2006), "Seismic behaviour of high strength concrete columns confined by fiber reinforced polymer tubes." J. Compos. Constr., 10.1061/(ASCE)1090-0268(2006)10:6(538), pp. 538–549.

Ozbakkaloglu, T., and Saatcioglu, M., (2007), "Seismic performance of square high-strength concrete columns in FRP stay-in-place formwork." J. Struct. Eng., 10.1061/(ASCE)0733-9445(2007)133:1(44), pp. 44–56.

Ozbakkaloglu, T., and Akin, E., (2012), "Behaviour of FRP-confined normal- and high-strength concrete under cyclic axial compression," J. Compos. Constr. 2012.16:451-463.

Ozbakkaloglu, T, and Vincent, T., (2013), "Axial compressive behaviour of circular high strength concrete-filled FRP tubes" Journal of Composites for Construction, © ASCE, ISSN 1090-0268/04013037(11).

Ozbakkaloglu, T. (2013a). "Axial compressive behaviour of square and rectangular high-strength concrete-filled FRP tubes." J. Compos. Constr., 10.1061/(ASCE)CC.1943-5614.0000321, 151–161.

Ozbakkaloglu, T. (2013b). "Compressive behaviour of concrete-filled FRP tube columns: Assessment of critical column parameters." Eng. Struct., 51, 151–161.

Ozbakkaloglu, T. (2013c). "Concrete-filled FRP tubes: Manufacture and testing of new forms designed for improved performance." J. Compos. Constr., 10.1061/(ASCE)CC.1943-5614.0000334, pp. 280–291.

Ozbakkaloglu, T, Lim, J, Vincent, T., (2013), "FRP-confined concrete in circular sections: Review and assessment of stress–strain models", Engineering Structures 49 (2013) 1068–1088, http://dx.doi.org/10.1016/j.engstruct.2012.06.010.

Park, R.; and Paulay, T., (1975), "Reinforced concrete structures", John Wiley and Sons, New York, N.Y, 1975,2 1-23 pp.

Park, J. H., Jo, B. W., Yoon, S. J., and Park, S. K. (2011). "Experimental investigation on the structural behaviour of concrete filled FRP tubes with/without steel re-bar." KSCE J. Civ. Eng., 15(2), pp. 337–345.

Pessiki, S., Harries, K. A., Kestner, J. T., Sause, R., and Ricles, J. M., (2001), "Axial behaviour of reinforced concrete columns confined with FRP jackets." J. Compos. Constr., 5(4), 237–245.

Prion, H. G. L., and Boehme, J., (1994), "Beam-column behaviour of steel tubes filled with high-strength concrete," Canadian Journal of Civil Engineering, V. 21, pp. 207-218.

Pultrall, Inc., (2007), "V-ROD Composite Reinforcing Rods Technical Data Sheet", Thetford Mines, Canada, www.pultrall.com.

Richart, F. E.; Brandtzaeg, A.; and Brown, R. L., (1928), "A Study of the failure of concrete under combined compressive stresses", Engineering Experimental Station Bulletin No- 1 85, University of Illinious, Urbana, 1928, 1 O4 pp.

Rizkalla, S. and Fam, A., (2002), "State of the art of concrete-filled FRP tubular structural members", 3rd Middle East Symp. On Structural Composites for Infrastructure Applications, MESC-3, Aswan, Dec. 17-20.

Rochette P., (1996), "Confinement of short square and rectangular columns with composite materials", MS thesis, University of sherbooke, Quebec, Canada.

Saatcioglu, M. and Razvi, R., (1992), "Strength and ductility of confined concrete", J. Struct. Eng., 118(6), 1590-1607.

Saatcioglu, M., Ozbakkaloglu, T., and Elnabelsy, G., (2008), "Seismic behaviour and design of reinforced concrete columns confined with FRP stay-in-place formwork." ACI Special Publications, 257, 149–170.

Sakino, K., (2006), Confined concrete in concrete-filled steel tubular columns. American Concrete Institute, ACI, 238 (Special Publication), pp.267-287.

Samaan, M.; Miamian, A.; and Seahawk, M., (1998), "Model of concrete confined by fiber composites." Journal of Structural Engineering, ASCE, V. 124, No. 9, pp. 1025-1031.

Shahawy, M., and Mirmiran, A., (1998), "Hybrid FRP-concrete beam- columns," Proceedings of ICCE/5 Fifth International Conference on Composites Engineering, Las Vegas, Nev., July 5-11, pp. 619-620.

Seible, F., (1996), "Advanced composite materials for bridges in the 21st century," Proceedings of the ddvanced composite materials in bridges and structures, M. El-Badry, ed., CSCE, Montreal, Canada, pp. 17-30.

Seible, F., Burgueño, R., Abdallah, M. G., and Nuismer, R. (1996). "Development of advanced composite carbon shell systems for concrete columns in seismic zones." Proc., 11th World conference on earthquake Engineering, Elsevier Science, Oxford, UK, Paper No. 1375.

Shao, Y., Zhu, Z., and Mirmiran, A., (2006), "Cyclic modeling of FRP confined concrete with improved ductility." Cem. Concr. Compos., 28(10), 959–968.

Sheikh, S. A., (1978), "Effectiveness of rectangular ties as confinement steel in reinforced concrete columns", Ph.D. Thesis, 1978, University of Toronto, Canada.

Sheikh, S. A.; and Uzumeri, S. M., (1980), "Strength and ductility of tied concrete columns", Journal of the Structural Division, ASCE, Vol. 106, No ST5, May 1980, 1079-1 102 pp.

Spoelstra, M. R., and Monti, G., (1999), ''FRP-confined concrete model.'' J. Compos. Constr., 3(3), pp. 143–150.

Theodoros R., (2001), "Experimental investigation of concrete cylinders confined by carbon FRP sheets, under monotonic and cyclic axial compression load", Research Report. Publication 01: 2, Division of Building Technology, Chalmers University of Technology.

Tobbi, H., Farghaly, A., and Benmokrane, B., (2012), "Strength model for concrete columns reinforced with fiber-reinforced polymer bars and ties", ACI Structural Journal, V. 111, No. 1-6.

Vincent, T., and Ozbakkaloglu, T., (2013a), "Influence of concrete strength and confinement method on axial compressive behaviour of FRP confined high- and ultra-high-strength concrete," Composites: Part B 50, 413–428.

Vincent, T. and Ozbakkaloglu, T., (2013b), "Influence of fiber orientation and specimen end condition on axial compressive behaviour of FRP-confined concrete," Construction and Building Materials 47, 814–826.

Vincent, T. and Ozbakkaloglu T., (2014), "Influence of Slenderness on Stress-Strain Behaviour of Concrete-Filled FRP Tubes: Experimental Study", Journal of Composites for Construction, © ASCE, ISSN 1090-0268/04014029(13).

Wang, Z; Wang, D.; Smith, S., Lu, D., (2012), "CFRP-Confined Square RC Columns. II: Experimental Investigation", the Journal of Composites for Construction, Vol. 16, No. 2, April 1, 2012. ©ASCE, ISSN 1090-0268/2012/2- 150–160.

Wei, S.; Mau, S. T.; and Mantrala, S. K., (1995), "Performance of new sandwich tube under axial loading: experiment," Journal of Structural Engineering, V. 121, No. 12, Dec., pp. 1806-1821.

Wong,Y., Yu,T., Teng, J., and Dong, S., (2008), "Behaviour of FRP confined concrete in annular section columns", Composites: Part B 39, 451–466.

Yamakawa, T., Zhong, P., and Ohama, A. (2003). "Seismic performance of aramid fiber square tubed concrete columns with metallic and/or nonmetallic reinforcement." J. Reinf. Plast. Compos., 22(13), pp. 1221–1237.

Yuan, W., Mirmiran, A., (2001), "Buckling analysis of concrete filled FRP tubes", International Journal of Structural Stability and Dynamics Vol. 1, No. 3 (2001) 367–383 © World Scientific Publishing Company.

Zhishen W., Xin W., Gang W., (2012), "Advancement of structural safety and sustainability with basalt fiber reinforced polymers." A Proceedings of CICE, 6th International Conference on FRP Composites in Civil Engineering, Rome, Italy, 13-15 June.

Zhu, Z., Ahmad, I., and Mirmiran, A., (2006), "Seismic performance of concrete-filled FRP tube columns for bridge substructure." J. Bridge Eng., 10.1061/ (ASCE) 1084-0702(2006)11:3(359), 359–370.